SCANNING STOPPED-FLOW STUDIES OF AMP-AMINOHYDROLASE AND TRYPTOPHANASE

By

Sami Victor Elias

A DISSERTATION

Submitted to
Michigan State University
in partial fulfillment of the requirements
for the degree of

DOCTOR OF PHILOSOPHY

Department of Chemistry

1983

ABSTRACT

SCANNING STOPPED-FLOW STUDIES OF
AMP-AMINOHYDROLASE AND TRYPTOPHANASE

By

Sami Victor Elias

Scanning stopped-flow studies were performed on AMP-aminohydrolase and tryptophanase. Both enzymes are activated by monovalent cations, such as K^+. In the absence of monovalent cation activators, AMP-aminohydrolase can also be activated by its own substrate, 5'-AMP. Tryptophanase however, absolutely requires monovalent cations for activity.

AMP-aminohydrolase catalyzes the conversion of 5'-AMP to IMP and ammonia. In the presence of monovalent cation activators the enzyme follows the Michaelis-Menten scheme, while in their absence it displays sigmoidal kinetics. The homotropic activation of the K^+-free enzyme by 5'-AMP was studied at pH 6.5. The full time progress curves were analyzed with a generalized non-linear curve fitting program, KINFIT4 (18). Three models were tested, of which the most successful was a phenomenological model, which included apparent cooperativity effects in its scheme. The data

when analyzed in terms of this model, suggested dissociation of the tetrameric enzyme at temperatures below 20°C. Sedimentation velocity experiments indicated that AMP-aminohydrolase maintains its tetrameric configuration, at 20°C, even in the absence of monovalent cation activators.

Tryptophanase catalyzes α,β-elimination reactions of several amino acids. In addition to requiring monovalent cations for activity, tryptophanase also requires a prosthetic group, pyridoxal-5-phosphate (PLP), with which it covalently bonds to form a Schiff base, and which results in a pH and cation dependent absorption bands, with maxima at 337 and 420 nm. Upon addition of an amino acid, the α-elimination step results in a quinonoid intermediate between PLP and substrate, with an intense maximum at 508 nm. This is then followed by the β-elimination step, in which the quinonoid decays to yield the final products of ammonia, pyruvate, and the α,β-elimination product of the amino acid.

The reaction of tryptophanase with one substrate, S-benzyl cysteine, was investigated at pH 8.0. Analysis of the data indicated that: (1) the rate constant for disappearance of the 420-nm absorbance (44.2±0.3 sec^{-1}) was the same as that of the fast phase of the biphasic growth of quinonoid at 508 nm (45±2 sec^{-1}); (2) the rate of disappearance of the 337-nm absorbance (0.48±0.01 sec^{-1}) was the same as the rate of the slow phase of quinonoid formation (0.47±0.02 sec^{-1}); (3) the average rate constant for the slow phase obtained with S-benzyl-cysteine (0.40±0.12 sec^{-1})

agreed closely with the rate constant (0.43 ± 0.03 sec^{-1}) for the conversion of the 337-nm form to the 420-nm form, following a rapid decrease in pH (193).

The results obtained with the substrate, S-benzyl-cysteine, are in accord with those of June *et al.* (197) who investigated the interaction of the amino acid inhibitors, ethionine and L-alanine, with tryptophanase.

I humbly dedicate this dissertation

to my brother Freddy

ACKNOWLEDGMENTS

I wish to sincerely thank Professor J. L. Dye for his assistance and expert advice throughout the course of this work.

My thanks are due to Professor C. H. Suelter who acted as my second reader. I extend my gratitude to Professor F. Horne who furnished advice and assistance during difficult times. I wish to express my appreciation to Professor G. J. Karabatsos for his professional help and advice, and also for his interesting and enlightening discussions. Financial support in the form of research and teaching assistantships from Michigan State University, as well as research support from the National Science Foundation are also acknowledged.

My special and warmest appreciations to Dr. Elizabeth Kauffmann, who even though across the seas, offered a listening ear, and provided mental support when such support was needed.

Finally, no words can express my feelings and love for my brother, Freddy, who stood by me constantly and never hesitated to assist in my hours of need; this work would not have been completed without his support and devotion.

TABLE OF CONTENTS

LIST OF TABLES

Table | Page

LIST OF FIGURES

CHAPTER 1

INTRODUCTION

An existing computer-interfaced rapid scanning stopped-flow system (9) was used to study the full time course kinetics of the catalytic reactions of two enzymes, AMP-aminohydrolase and tryptophanese. Results from these studies were analyzed in terms of new and existing models, consistent with the observed data, for AMP-aminohydrolase and tryptophanese respectively.

Both enzymes can be activated by monovalent cations (50, 144,145,175). In the absence of monovalent cation activators, AMP-aminohydrolase can also be activated by its substrate, 5'-AMP (50,146), while tryptophanase absolutely requires monovalent cations for activity (175).

The first part of this work (Part A) describes stopped-flow studies of the activation of AMP-aminohydrolase by the substrate, 5'-AMP; while the second (Part B) describes such studies of the reaction of S-benzyl-L-cysteine with tryptophanase.

PART A: AMP-AMINOHYDROLASE

Non-linear steady state kinetics are often observed in enzyme systems (25,27-31,39,40,45,141). The Michaelis-Menten model alone is unable to account for the behavior of such kinetic patterns. Several more complex theoretical models have been proposed to explain such patterns (20-31, 34,44,45,126), and most of those have been interpreted in terms of allosteric and/or hysteretic interactions (20-31, 39,40,45,126,127,141).

In recent years, interest has been focused on the mode of action of regulatory enzymes (27-29,31,127,141), the majority of which have been shown to exhibit both allosteric and hysteretic phenomena (31,127). Of interest among these metabolically relevant group of enzymes is AMP-aminohydrolase (EC3.5.4.6), which catalyzes a simple reaction, namely, the irreversible deamination of 5'-AMP to IMP.

The interest in AMP-aminohydrolase stems from the fact that in the presence of a monovalent cation activator, such as K^+, the enzyme follows the Michaelis-Menten scheme; whereas, in the absence of any effectors except the substrate, 5'-AMP, this enzyme can display both allosteric (146) and hysteretic (27) phenomena in its deamination reaction, with the substrate doubling as a homotropic activator. Such a simple system, with only enzyme and substrate, which can display allosteric and hysteretic behavior, both

of which are removable in the presence of a monovalent cation activator, could be said to represent a most basic form of non-linear interactions in enzyme catalysis.

Several mechanisms (27-29) were proposed to describe the homotropic activation of AMP-aminohydrolase by substrate, in the absence of monovalent cation activators, but none were reported to consistently fit the full time course data as a function of different initial substrate concentrations.

The present study was undertaken in order to investigate for a mechanism(s) that would not only consistently fit the full time course data over a wide range of initial enzyme and substrate concentrations, at various temperatures, but also account for substrate depletion throughout the course used for measuring the kinetic behavior.

The initial part of the study consisted of a search for spectrophotometrically observable intermediates. The search, however, was unsuccessful. Later, sedimentation velocity experiments showed that the enzyme maintained its tetrameric configuration even in the absence of monovalent cation activators. This eliminated the possibility that polymerization or depolymerization effects were a cause for the observed allosteric and hysteretic phenomena.

Preincubation studies of the product, IMP, with the enzyme indicated that while the product, at high concentrations, was able to partially remove the hysteretic lag, it

was not substantially activating the enzyme as evidenced by the steady state regions of the full time course progress curves.

Finally, a systematic stopped-flow study of the kinetics of deamination of 5'-AMP, in the absence of monovalent cation activators, was performed over a wide range of enzyme and substrate concentrations, at 2°, 12° and 22°C, and at pH 6.5.

As a precursory step to simulation and modelling, lag times in the pre-steady state regions, as well as the shut-off behavior of the progress curves were examined as functions of initial substrate and enzyme concentrations. The activation energy of the catalytic reaction was also determined, using data at the different temperatures used in the study.

Three models were proposed and fitted to the full time course data curves, at the three temperatures, using the generalized non-linear curvefitting program KINFIT4 (18). Substrate depletion over the time course used for measuring the kinetic behavior was incorporated in the three models tested. One common feature embodied in the mechanisms of these models involved an isomerization step(s).

The first model which assumes the existence of an isomerization step from an inactive enzyme-substrate complex, to an active enzyme-substrate complex, without invoking cooperative interaction phenomena in its scheme, is an extension of the Suelter et al. model (27). The second was

the Monod et al. model (20). While both models were able to describe the general behavior of the full time course data, they were unable to consistently fit all the progress curves as a function of initial enzyme and substrate concentrations.

The third model, which is a generalization of the mechanism proposed by Suelter et al. (27), is a phenomenological model with apparent cooperativity effects in its scheme. This model was able to consistently fit the data as a function of the different initial enzyme and substrate concentrations at the three temperatures. Further analysis of the results indicated that subunit dissociation was occurring in the enzyme at temperatures below 20°C.

PART B: TRYPTOPHANESE

Tryptophanase (EC4.1.99.1), a pyridoxal 5'-phosphate (PLP) dependent enzyme, catalyzes α,β-elimination reactions of amino acid substrates, and requires monovalent cations for optimum catalytic activity (175). The binding of PLP to the enzyme results in a pH-dependent absorption maxima at 337 and 420 nm (184). When tryptophanase interacts with competitive inhibitors, a stable, dead end quinonoid complex, characterized by an intense absorption band centered at 508 nm, is produced (184,197,198).

A mechanism of quinonoid formation was proposed by June et al. (197) based on their studies on the interaction

of two competitive inhibitors, ethionine and alanine, with tryptophanase. Their stopped-flow studies (197) of the kinetics of formation of the quinonoid with the inhibitor ethionine showed that the 420 nm form of the enzyme was the active form. Their assignment was supported by the following observations: (1) the rate constant for disappearance of the 420 nm absorbance was the same as that of the fast phase of the biphasic growth of quinonoid at 508 nm; (2) the rate of disappearance of the 337 nm absorbance was the same as the rate of the slow phase of quinonoid formation and was essentially unaffected by the inhibitor concentration or the nature of the inhibitor, ethionine or alanine; (3) the average rate constant for the slow phase obtained with ethionine agreed closely with the rate constant for the conversion of the 337 nm form, conformation γ, to the 420 nm form, conformation β, following a rapid decrease in pH (195). Thus the authors (197) concluded that the 337 nm form did not form quinonoid directly, but was first converted to the 420 nm form before the α-proton of an amino acid inhibitor was removed to form quinonoid.

It could be argued however that the interaction of tryptophanase with competitive inhibitors, which leads to a stable dead end quinonoid, may not represent the same interaction as with a substrate, where the quinonoid appears only as a transient intermediate.

The present work describes a stopped-flow study of the

changes in absorbance at 337, 420 and 508 nm following the interaction of a substrate, S-benzyl-L-cysteine, with tryptophanase. The objective was that if the time progress at these wavelengths, for this substrate, could be interpreted in the same fashion as was done with the inhibitors, ethionine and alanine (197), then this should confirm the scheme for the mechanism of quinonoid formation proposed by June et al. (197).

Analysis of the data established the correspondence between the present results to those obtained by June et al. (197). Preliminary principal component analysis [M-analysis] (17,201-203) indicated that a minimum of six independent absorbers were necessary to reconstruct the experimental surface to within its random error. This was in agreement with the experimental data which showed the presence of six absorbers.

Non-Michaelis-Menten Enzyme Models

Plots of initial velocity versus substrate concentration are non-hyperbolic for a large number of enzymes, particularly those termed regulatory (31,45,141). For such enzymes it is necessary to devise models more complex than the Michaelis-Menten scheme. These non-Michaelis-Menten models are frequently defined in terms of allosteric and hysteretic interactions. Recall that AMP-aminohydrolase is a regulatory enzyme which displays both allosteric and hysteretic behavior.

The following is a brief introduction to some proposed allosteric and hysteretic enzyme models:

Allosteric Enzyme Models

Allosterism has been defined in terms of deviations of the reaction velocity from the predictions of the Michaelis-Menten Scheme (128).

Two "classical" limiting molecular models have been proposed to account for allosteric control mechanisms. One is due to Monod, Wyman and Changeux (20), the MWC model; the other is due to Adair, Koshland, Nemethy and Filmer (21-23), the AKNF model.

Both models are based on the subunit structure of proteins and alterations in conformation coupled to ligand binding. Both are illustrated in Figure (1.1).

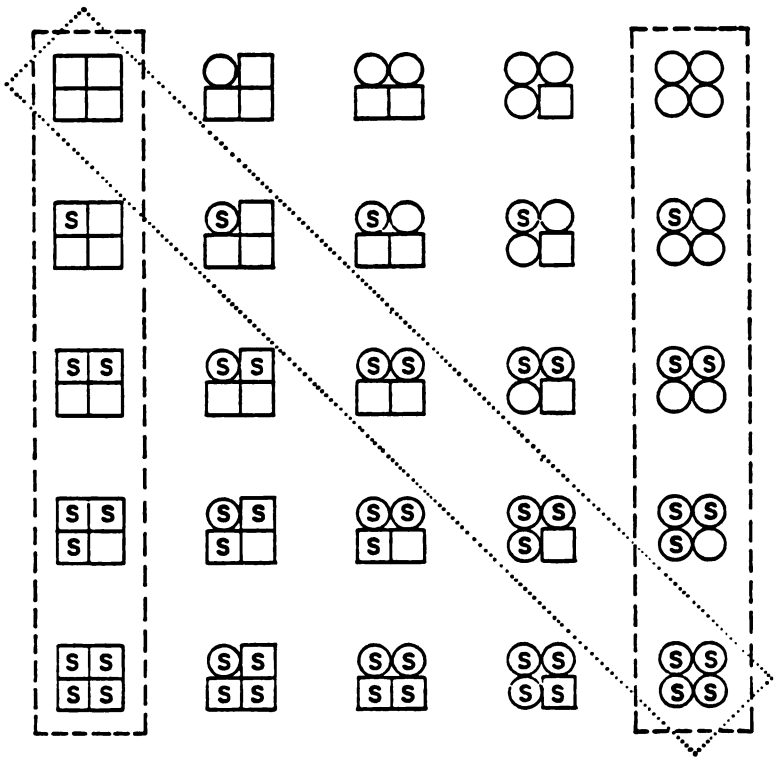

Figure 1.1. A General Allosteric Model From Hammes and Wu (25) and Eigen (24).

(Note: The figure illustrates a general allosteric model for the binding of substrate (S) to a four subunit enzyme. The squares and circles are different conformations of the subunits. The MWC model is shown by dashed vertical lines, and the AKNF model by dotted diagonal lines. The free substrate and arrows between the states are omitted for the sake of clarity. Some of the intermediates in which (S) can bind to either the square or the circle are presented by one state.)

The MWC model predicts a concerted conformational change (all or nothing), while the AKNF model predicts a sequential conformational change for each subunit.

The homotropic cooperative effects are always positive for the MWC model (i.e., the binding of the first molecule enhances the binding of the second, etc.), whereas they may be positive or negative in the AKNF model. The MWC model assumes the same conformational state is stabilized by a variety of ligands, whereas the AKNF model predicts that different ligands may induce different conformational changes.

Both the MWC and AKNF models are limiting cases of a more general scheme, as shown in Figure (1.1), initially proposed by Eigen (24). This is because states with more than a single ligand bound can take up different geometrical configurations; for example:

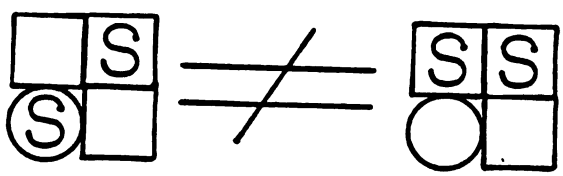

Finally, a complete solution based on experimental evidence, to any of these models without any simplifying assumptions is quite difficult, as the number of unknown parameters becomes unrealistically large. The general model combining both the MWC and AKNF extremes, along with dissociation of the subunits, etc., has been analyzed (26), but the results are too complex for general use, and it is far more convenient to interpret experiments in terms of the MWC or AKNF limiting schemes.

The MWC and AKNF models, which assume the existence of interactions among the enzyme subunits are not unique in describing allosteric behavior. Several other models have been proposed (27,29-31,34,44,45,126,127) and some of these are shown in Table (1.1).

A common feature among these models is the existence of at least one slow step in their scheme Table (1.1), which appears to be sufficient in order for allosterism to be manifested even when cooperative interactions are not considered. The slow step(s) normally describes a conformational change, such as an isomerization of the enzyme and/or enzyme-substrate complex, from an inactive to an active form, with the active form having higher affinity for substrate. Allosterism then results from this interconversion of configurations, which are assumed to be slow relative to other catalytic steps, such that the different configurations are no longer in equilibrium with each other

Table 1.1. Non-Michaelis-Menten Enzyme Models.

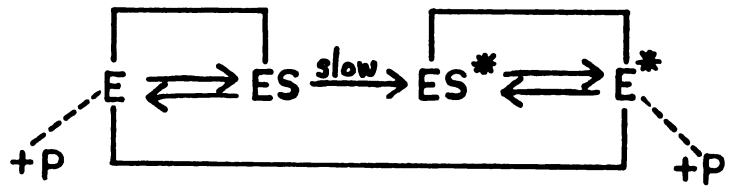

Blum (34)

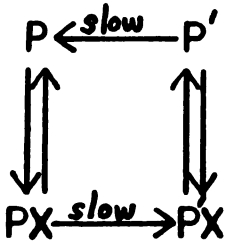

Weber (126)

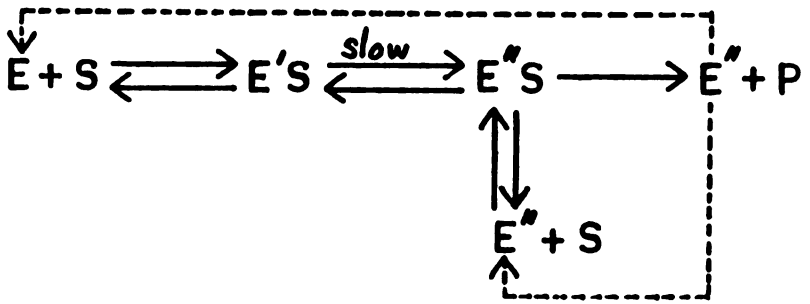

Rabin (44)

Table 1.1. Continued.

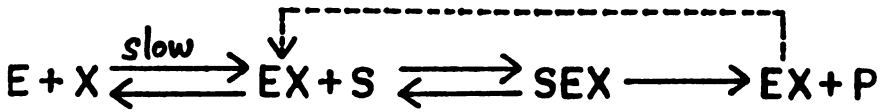

Suelter et al. (27)

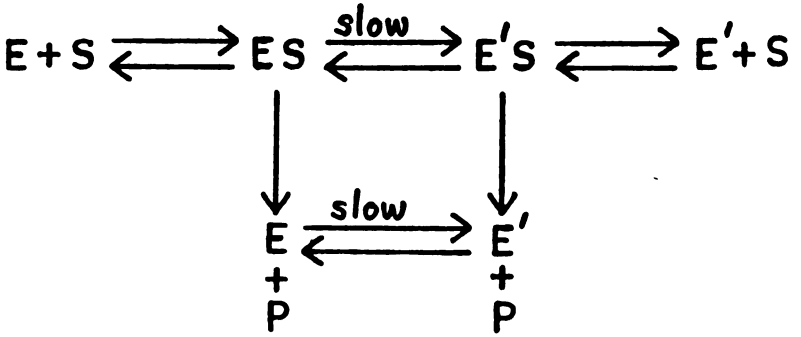

Frieden (29) and Ho (14)

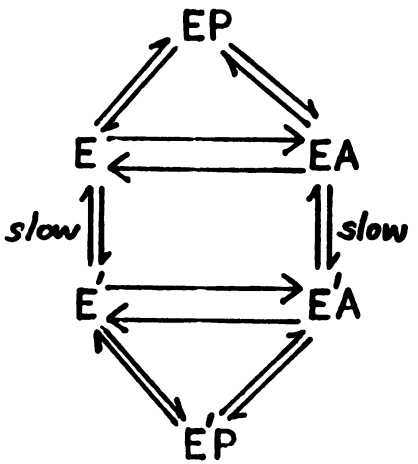

Ainslie et al. (30)

during catalysis. The extensive reviews by Whitehead (45) and Citric (141) describe a large variety of models which illustrate this point as well as showing that no one mechanism proposed is the right one, but as Whitehead (45) pointed out, they are all true for some cases in their description of allosterism.

Hysteretic Enzyme Models

Frieden (29) defined hysteretic enzymes as those which respond slowly to rapid changes in ligand concentration. Hence, unlike those enzymes which obey the Michaelis-Menten scheme, where product formation is always linear with time, hysteretic enzymes exhibit an initial lag or burst in product formation as a function of time. Frieden (29) suggested that mechanisms which may be responsible for slow processes in hysteretic enzymes include: (1) isomerization processes; (2) displacement of a tightly bound ligand by another with a different effect on activity; and (3) polymerization or depolymerization processes. The majority of regulatory enzymes have been shown to be hysteretic (27-31,34,44,45,126,127,141).

Blum (34) was the first to describe such systems (Table 1.1). Later, Weber (126), Suelter *et al.* (27), Rabin (44), Ainslie *et al.* (30), and Ho (14) also presented schemes describing hysteresis (Table 1.1). For extensive reviews of hysteretic models see Citri (141), Whitehead (45),

Frieden (31) and Kurganov (127).

It is interesting to note that models proposed for hysteretic enzymes (27-31,45,127,141), including the Frieden model as analyzed by Pierce (32), not only include a slow step(s) in their scheme, but are also able to display (or were initially proposed to account for) allosterism. Only recently, with the availability of computers, which facilitate numerical analysis of models by simulations (18) and other techniques (32,33), has it been possible to show that with proper choice of rate constants, many schemes can be shown to display not only allosteric as well as hysteretic phenomena, but that it is also possible to reduce complex schemes to simpler ones which display similar behavior to the full model. For example, Pierce (32) using non-linear sensitivity analysis (33), analyzed the Frieden (29) and Ainslie et al. (30) models in terms of bursts, lags, and cooperativity. He found that with judicious choice of rate constant values, both models can display several different combinations of bursts, lags, positive and negative cooperativity. Furthermore, he was able to show that the Ainslie et al. model can be reduced to one which exhibits essentially the same behavior as their full model.

While it will always be both interesting and necessary to examine theoretical models, the challenge still remains in finding a model(s) which can account for what is observed

experimentally. In his review article, Whitehead (45) summed it up as follows:

> "In light of the above discussion, the various models on offer will perhaps not be seen as a set of rival and exclusive orthodoxies, but are all closely related. The simpler ones are special cases of more general ones. Choice between them amounts to asking which equilibria, which interactions, which rates can for practical purposes be forgotten as a determining factor in the overall effect? Thus not only may different models be applicable to different enzymes, but different models may be applicable to <u>one</u> enzyme."

In conclusion, the <u>true</u> mechanism for an enzyme may never be discerned, and one can only hope to provide plausible models to help explain that which is observed. But this is not a strange phenomena to one who studies kinetics. The oft quoted phrase that "one can always disprove a mechanism", may in the end, prove to be the <u>only true</u> mechanism.

PART A

STOPPED-FLOW STUDIES OF THE ACTIVATION OF AMP-AMINOHYDROLASE BY 5'-AMP

CHAPTER 2

AMP-AMINOHYDROLASE - AN INTRODUCTION

This chapter introduces the background, physiological significance, chemical and physical properties of AMP-aminohydrolase; after which the reaction of the enzyme with 5'-AMP is explored in light of the work of previous authors.

A. Background

AMP-aminohydrolase (EC 3.5.4.6; 5'-adenylic acid aminohydrolase; adenylate deaminase) catalyzes the irreversible deamination of 5'-AMP (5'-adenosine monophosphate; adenylic acid) to form IMP (5'-inosine monophosphate; inosinic acid) and ammonia: (page 18)

It was first described by Schmidt (46-48), who separated it from adenosine deaminase from rabbit skeletal muscle, and demonstrated its specificity for 5'-AMP. The enzyme is widely distributed in animal tissues, and has been isolated from a variety of sources (49-54), including muscle (55-64), calf brain (65), guinea pig and human epidermis (66), pig kidney (67), bakers yeast (68), marine bacteria (69), human erythrocyte (70), and rabbit cardiac

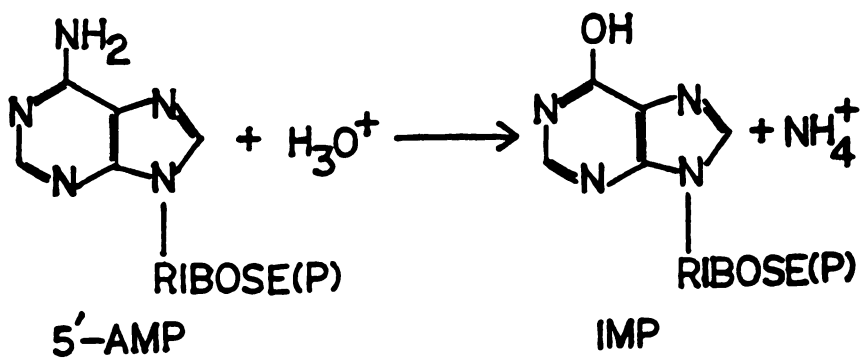

muscle (71). Lowenstein (72) reported that the specific activity of the skeletal muscle enzyme is more than ten times higher than that found in other tissues. The highest concentration of the enzyme is also found in skeletal muscle (49,56,72), where it is reported to be closely associated with myosin (49,51,57,58,73-77).

Ashby and Frieden (76) reported that in rabbit skeletal muscle, binding of the enzyme to myosin in vitro appears to be specific, in the sense that there are approximately two moles of enzyme bound per mole of myosin, and that the interaction may be affected by the presence of certain ligands. Shiraki et al (74,75) reported that in rat muscle, in vitro, AMP-aminohydrolase is bound to the myosin

molecule in a ratio of one mole of enzyme to three moles of myosin.

Sections (B) through (F) present additional information on AMP-aminohydrolase, which in the author's opinion is complimentary to the present study of the enzyme; however, a reader may gloss over these sections without loss in continuity.

B. Physiological Role

Although the physiological role of AMP-aminohydrolase remains obscure, it has long been recognized that the reaction catalyzed by this enzyme is the major source of ammonia in muscle (78,79), and that ammonia production is proportional to the work done by the muscle (80). The levels of AMP-aminohydrolase in skeletal muscle from humans suffering Duchenne muscular dystrophy have been shown (54) to be lower than in normal patients. Pennington (81) earlier reported similar findings in mice.

Recently, Suelter et al. (82) and others (82-85) have studied the activity of AMP-aminohydrolase in normal and dystrophic chicken. They reported that the activity of the enzyme was lower in dystrophic chicken muscle, as compared to normal chicken muscle. Raggi et al. (86,87) reported that in the rat, white muscles have a higher AMP-aminohydrolase content than red muscles; that different types of AMP-aminohydrolase exist in white and red muscles, and that

the higher enzyme activity in white muscles is accounted for by an enzyme form which is present in much lower amounts in red muscle. The activity of AMP-aminohydrolase in muscle contraction (88) and as related to muscle fatigue (89-91) has also been reported.

Setlow et al. (61) proposed a scheme for the regulation by AMP-aminohydrolase, in the interconversion of purine nucleotides in mammalian organs, where adenosine triphosphate (ATP) acts as an activator and quanosine triphosphate (GTP) as an inhibitor. The levels of (ATP) and (GTP) necessary for activation and inhibition respectively, are in themselves complicated and further modulated by other nucleotides, as well as monovalent and divalent ions. Hence, a proposed control mechanism based upon observed changes in vitro, is subject to still undefined in vivo effects by other factors.

In the cyclic scheme of purine nucleotide interconversions described by Lowenstein (61), the deamination of aspartate in muscle tissue also serves important regulatory functions where (5'-AMP) is generated as (IMP) is depleted. The net effect of the cycle is the deamination of aspartate to yield ammonia in skeletal muscle.

$$\text{aspartate} + \text{GTP} + H_2O \rightarrow \text{fumarate} + NH_3 + \text{GDP} + P_i$$

Lowenstein (72) also proposed that the purine nucleotide

cycle consists of AMP-aminohydrolase, adenylosuccinate synthetase, and adenylosuccinatelyase, and that these enzymes operate in the ammoniagenesis from amino acids in skeletal muscle. He also suggested that this cycle was closely linked to glycolytic oscillation (96).

An interesting physiological role for AMP-aminohydrolase is in the biochemical pathway of the purine catabolism cycle, whose major end product in humans and the higher apes is uric acid. The production of above normal levels of uric acid can lead to gout. Those afflicted with this disease have markedly elevated levels of uric acid in their blood and other body fluid systems. Hers et al. (103) have proposed that primary gout is caused by the presence of an abnormal AMP-aminohydrolase which is less sensitive to its physiological inhibitors, thus the degradation of adenine nucleotides in the liver is increased resulting in excess uric acid formation.

C. On the Regulation of AMP-Aminohydrolase by ATP, ADP and GTP as a Function of pH

Ranieri-Raggi et al. (104), Ronca-Testoni et al. (105), and Raggi et al. (106) studied AMP-aminohydrolase (isolated from rat skeletal muscle) in order to clarify the effects of pH and salt on the activity of the enzyme and its sensitivity to modifiers. While they confirmed the general activatory and inhibitory effects of (ATP) and (GTP)

respectively, their results further indicated the modulation of the effects of these modifiers on the enzyme activity as a function of pH.

They reported that whereas at acidic pH values, a hyperbolic substrate saturation curve is obtained at optimal KCl concentration, the curve is always sigmoidal at pH 7.1 regardless of the concentration of KCl employed. Similar observations have been reported by Wheeler and Lowenstein (107,108). The former authors (104-106) further pointed out that the study of the kinetic properties of the enzyme has mainly been restricted to the optimal pH value of 6.5; a rather distant one from the physiological pH of 7.1. They interpreted their results by tentatively assuming the existence of two kinetically distinct states of AMP-aminohydrolase whose ratio is pH dependent. State (I), which corresponds to the active conformation of the enzyme and present at acidic pH, is characterized by the familiar hyperbolic substrate saturation curve at optimal KCl concentration. State (II), whose induction is triggered by an elevation of the pH above neutrality is a less active conformation of AMP-aminohydrolase showing sigmoidal kinetics even at optimal salt concentration.

Relevant deductions for the in vivo activation pattern of the skeletal muscle enzyme can be inferred from the above for the enzyme regulation. In view of the alkaline pH in resting muscle, State (II) is likely to be the primary

conformation of the enzyme. Therefore, the activity of AMP-aminohydrolase should be very low under these conditions, and also because of the low 5'-AMP (0.1 mM) content of tissue (109), and the effective inhibition excreted by (ATP) at low concentrations (10 μM), whereas at concentrations higher than 50 μM (ATP) acts as an activator. This possibility is supported by the reported inability to detect ammonia formation in resting muscle (110).

During sustained contractile activity the decrease of tissue pH may be the cause of activation of AMP-aminohydrolase, causing a shift in the equilibrium towards State (I) which characteristically has a much higher affinity for 5'-AMP and a low sensitivity to inhibitors. The activation pattern of the enzyme is again confirmed by the circumstances of ammonia production in muscle (105,110).

Barasacchi, et al. (71) reported that the affinity of AMP-aminohydrolase for 5'-AMP, in rabbit cardiac muscle, was low in the absence of activators (K_m = 3.1 mM), but in the presence of (ATP), it became as high as that of the skeletal muscle enzyme (K_m = 0.4 mM). At pH 7.5-8.0, the cardiac muscle enzyme was maximally activated, whereas the skeletal muscle enzyme was maximally inhibited by (ATP). Thus the cardiac muscle enzyme may always be in the activated state (State I), whereas the skeletal muscle enzyme was active only during exhaustive contractions.

Coffee and Solano (111) also reported that in rat

skeletal muscle, the activity of AMP-aminohydrolase is very stringently controlled as evidenced by the fact that the enzyme is operating at only 10 to 15% of its capacity. The results of Coffee and Solano are in complete agreement with the suggestions of Ronca-Testoni et al. (105) who reported that the enzyme activity in resting muscle (or in muscle undergoing moderate contractions) may be inhibited to a great extent. They suggested that maximal activity may be approached only under conditions of extreme stress.

Chung and Bridger (112) present yet another complimentary view for the activation sensitivity of the rabbit cardiac muscle AMP-aminohydrolase towards (ADP) and (ATP). They reported that both nucleotides activate the cardiac enzyme, but much higher concentrations of ATP (10 mM) than ADP (1.3 mM), are required to produce a demonstrable effect. The authors estimated that at 0.1 mM AMP, K'_as for ADP and ATP are approximately 0.65 mM and 0.9 mM respectively. Their results suggest that ADP may be an important physiological regulator for the activity of AMP-aminohydrolase in cardiac muscle.

Tornheim and Lowenstein (113) have suggested that 5'-AMP deamination might protect indirectly against ATP depletion, by virtue of the fact that removal of 5'-AMP would cause net conversion of ADP to ATP via readjustment of the adenylate kinase system:

$$2\ ADP \rightleftarrows ATP + 5'\text{-}AMP$$

Hence AMP-aminohydrolase may play the regulatory role in the adenylate kinase system, as a buffer against ADP accumulation in the contracting muscle.

The allosteric properties of AMP-aminohydrolase thus provide for negligible activity at the physiological concentrations of 5'-AMP until ADP has accumulated. High rates of conversion of ATP to ADP resulting from prolonged strong contraction of muscle will result in, activation of AMP-aminohydrolase, reduction of 5'-AMP, and readjustment of the adenylate kinase equilibrium with net conversion of ADP to ATP at the expense of the overall pool of adenine nucleotides.

Such activation might be regarded as an emergency measure providing short term but immediate rescue from conditions favoring ADP accumulation. Uncontrolled enzyme activity would not be beneficial because of the eventual net consumption of energy required for the regeneration of 5'-AMP from IMP via the purine nucleotide cycle.

Ranieri-Raggi *et al.* (104) have concluded that the correspondence in the modulatory effects of both ATP and pH on muscle AMP-aminohydrolase can thus play an important role in protecting the muscle cell against the danger of unrestrained activity of the enzyme, which would ultimately lead to depletion of the adenine nucleotide stores.

It has also been suggested by Mockrin et al. (114) that negative cooperativity (which ATP has with AMP-aminohydrolase) with its inherent difficulty of saturating the active sites of the enzyme, can be a very advantageous solution for limiting the catalytic activity at high substrate levels.

The connection between the mechanism of regulation suggested above for AMP-aminohydrolase from skeletal muscle, and the specialized metabolism of this tissue is underlined by the remarkable differences in kinetic properties of the cardiac muscle enzyme (71).

D. Structure and Composition

Any realistic crystallographic structural determination for an enzyme as complex as AMP-aminohydrolase must begin with homogenous and highly active single crystals. In this regard Smiley et al. (115) reported on the preparation of homogenous, highly active, hexagonal bipyramidal crystals of the enzyme. Earlier, Lee (55) was the first to report on the crystallization of AMP-aminohydrolase. Although Lee presented evidence that his preparation was homogenous, the ratio of the optical densities at 280 and 260 mμ (nm) of about 1.2 indicated the presence of nucleic acid contaminants, whereas Smiley, et al. had a ratio of 1.8 or higher, indicating little or no contamination by nucleic acids. However, no crystallographic

studies have been reported so far.

Depending on the animal source and the tissue from which the enzyme was extracted, AMP-aminohydrolase has an average molecular weight close to 280,000 and is composed of four identical subunits (60,68,111,116-124).

The amino acid composition of the enzyme from a variety of sources has been reported (60,62,117,120,125). The rabbit skeletal muscle enzyme has a normal amino acid content, i.e., no unusually small or large amounts of a particular amino acid was found.

Zielke and Suelter (116) characterized AMP-aminohydrolase, isolated from rabbit skeletal muscle, as a zinc metalloenzyme. They reported that the apo-enzyme binds 4 gram atoms of zinc per mole of enzyme, while the native enzyme as isolated contains 2.6 to 3.2 gram atoms of zinc per molecule. Although the addition of the fourth zinc atom increased V_{max}, this increase was only 28% of that expected, assuming that a linear correspondence exists between V_{max} and gram atoms of zinc per mole of enzyme up to 4 gram atoms of zinc. They concluded that the fourth zinc atom does not appear to be directly associated with activity. They further suggested that the problem of assigning a precise integral stoichiometry for the zinc to protein ratio in vivo resides with the difficulty in defining the similarity of the isolated enzyme in vitro to that in vivo. Raggi et al. (129) reported that the

rat muscle enzyme contains 2 gram atoms of zinc per mole when isolated by the procedure of Smiley et al. (115).

Isoenzymes having the same catalytic reaction as AMP-aminohydrolase, but differing in activity on the basis of differences in relative substrate specificities have been reported (74,122,130-132).

E. Substrates

AMP-aminohydrolase is a highly specific enzyme towards its native substrate 5'-AMP. Other naturally occurring nucleotides, and synthetic analogs either have very low V_{max} or very high K_m values when compared to 5'-AMP (133-138). Zielke and Suelter (138) examined a total of 24 nucleotides as substrates for rabbit muscle AMP-aminohydrolase. Their results showed that 5'-AMP is the preferred substrate, having the largest V_{max} and the lowest K_m values. They also found that while adenosine and ADP were deaminated, albeit poorly, ATP with three phosphoryl groups was not. Substitution in the ribose moiety have marked effects on deamination. Indications that the phosphate group may be important for binding of substrate are obvious.

F. Activators and Inhibitors

F.1. Inorganic

The enzyme from many sources is activated by monovalent cations such as K^+, Na^+, Li^+, NH_4^+, Rb^+, and Cs^+ (50, 105,139,140). Campbell and Suelter (147) reported that AMP-aminohydrolase from rabbit skeletal muscle is also activated by H^+. They presented evidence which indicated that the binding of H^+ and K^+ was linked, in that the dissociation constant K_A for K^+ activation was reduced as the pH was lowered. Smiley et al. (115) reported that K^+, Na^+ and Li^+ are the most effective activators, with K^+ being the best for the rabbit muscle enzyme. However, the relative order of effectiveness is dependent upon the source of enzyme. For example Setlow and Lowenstein (65) reported that in the calf brain, Li^+ is the most effective alkali metal ion. Smiley et al. (115) studied the stability of AMP-aminohydrolase in various concentrations of K^+. The general role of monovalent cations in enzyme activation has been explored by Suelter (144,145). The same V_{max} was observed at high concentrations of 5'-AMP in either the presence or absence of activating cations (50). The V_{max} values in the presence of K^+, Na^+ or $(CH_3)_4N^+$ are identical (146).

The demonstration that the V_{max} of the reaction is the same in the presence and absence of K^+ eliminates the

possibility that the mechanism of activation involves a direct role of K^+ in catalysis. Rather, the binding of K^+ affects the active site indirectly (allosteric heterotropic activation), such that the apparent affinity for 5'-AMP is increased, presumably through a change in the protein conformation. Coffee and Solano (111) reported that for the rat muscle enzyme K_m and V_{max} appear to be independent of K^+ concentration, in the absence of other effectors in the reaction.

Many divalent cations are known to inhibit the enzyme. These include Cu^{2+} (65,148), Zn^{2+}, Fe^{3+} and Ag^+ (148), Cd^{2+} and Ni^{2+} (65), and Hg^{2+} (149). A variety of anions such as inorganic phosphate (148,150-153), sulfate and nitrate (154), pyrophosphate (148,155), tripolyphosphate (155), and F^- (148,152,153,156-158) inhibit the enzyme to various degrees.

F.2. Organic

In the absence of monovalent cations, AMP-aminohydrolase can be activated by its own native substrate 5'-AMP (27,28,65). Thus the substrate acts as an allosteric homotropic activator. Smiley and Suelter (146) reported that in the absence of K^+ or Na^+ and at pH 6.5, the enzyme from rabbit skeletal muscle can also be activated by ADP or ATP, and inhibited by GDP and GTP. Their data suggested that ADP was a better activator than ATP. Chung and Bridger

(112) reported the same finding for the rabbit cardiac AMP-aminohydrolase, except that much higher concentrations of ADP and ATP were required to demonstrate the activation effect in the cardiac enzyme. ADP activation is inhibited by GDP and GTP, while the ATP activation is inhibited only by GTP. Inorganic phosphates also strongly inhibit the activation by nucleotides

Setlow et al. (61) reported that in the absence of monovalent cations and at a pH of 7.2, AMP-aminohydrolase isolated from a variety of rat tissues was activated by ATP and strongly inhibited by GTP, and that the GTP inhibition was relieved by the addition of ATP. Setlow and Lowenstein (65) found that the calf brain enzyme is also activated by ATP, and reported (155) the effects of several nucleotide triphosphates on the calf brain enzyme. They found (155) that ATP was the most effective activator, and GTP the most effective inhibitor. The inhibition by GTP was reversed by raising the concentration of ATP. The activation of ATP was reversed by raising the concentration of GTP, and both ATP and GTP were very effective in protecting the enzyme against heat inactivation.

Tomozowa and Wolfenden (159) reported that in the enzyme from rabbit skeletal muscle, binding of ATP and GTP are mutually inhibitory, and proposed two binding sites for GTP and a minimum of four binding sites for ATP, and that both act as allosteric effectors towards AMP-aminohydrolase.

Yoshino et al. (123) reported that the chicken erythrocyte enzyme was inhibited by concentrations of ATP and GTP below 100 μM and 250 μM respectively, but was activated at concentrations of ATP and GTP above 400 μM and 1500 μM respectively. They suggested that these unusual kinetics with respect to ATP and GTP could be explained by assuming two inhibitory and four activatory sites for each ligand.

Ashby and Frieden (64) reported that for the rabbit skeletal muscle enzyme, in 0.15 M K^+ and pH 6.5, ATP was an inhibitor at low concentrations (10 μM) and an activator at high concentrations (200 μM). GTP also inhibits at levels below (20 μM) but the inhibition is decreased at its level is increased above (20 μM) and, at (100 μM), the initial rate is almost the same as that in the absence of GTP. Wheeler and Lowenstein (107) reported similar findings for the rat muscle enzyme. Barsacchi et al. (71) reported that AMP-aminohydrolase from rabbit heart was activated by ATP, and less efficiently by ADP.

Ronca-Testoni et al. (105) studied the enzyme isolated from the skeletal muscle of frog, pigeon, guinea pig, rabbit and rat. Coffee and Solano (111) studied the rat muscle enzyme. Both groups attempted to focus more specifically on the role of K^+ ions in the expression of the regulatory properties of the enzyme, and on the specific effects of ADP, ATP, GTP, P_i (inorganic phosphate) and creatine-P, on the kinetic parameters K_m and V_{max}. For instance, both

teams suggested that at physiologically significant levels of these metabolites, and as pH 6.5, (25 μM) ATP and (10 μM) GTP inhibit the enzyme by reducing its affinity for 5'-AMP; i.e., they increase K_m from 0.35 mM to about 0.6 mM, without significantly affecting the V_{max} of the reaction. But at K^+ concentrations of 5 mM (approximately twenty times less than the average in vivo levels in muscle, ADP and ATP both cause a dramatic increase in K_m to about 1.0 mM; and a decrease of about 40% in the value of V_{max}.

Skladanowski et al. (160) reported a different view on the K^+ dependent regulation by ATP and ADP of AMP-aminohydrolase from beef heart. Their results showed that ATP was a much more efficient activator than ADP, both at low and high K^+ concentration.

Melander (161) reported that IMP and NH_4^+ both inhibit rabbit skeletal muscle AMP-aminohydrolase; however Ashby and Frieden (64) reported that IMP substantially activates the enzyme, and found that when 0.5 mM IMP was preincubated with the enzyme at 20°C, pH 6.5, and 0.15 M KCl, the activity increased by about 8% over that with no IMP added. Suelter et al. (27) reported that products of the reaction have no activating or inhibiting effect.

Zielke and Suelter (116) reported that the rabbit skeletal muscle enzyme was sensitive to inhibition by di- and tricarboxylic acids such as succinate, maleate, fumarate and citrate. The ADP activated enzyme was more sensitive

to these inhibitors than enzyme assayed in the presence of activator K^+.

A more complete list of activators and inhibitors for AMP-aminohydrolase is found in Zielke's dissertation (162) and reference (50).

G. Reactions with 5'-AMP

In the presence of monovalent cation activators, such as K^+, and at pH 6.5, AMP-aminohydrolase displays normal Michaelis-Menten kinetics (27,28,50,64,146). At 30°C, calculated values for K_m range from 0.16 mM to 0.7 mM; V_{max} values from 1000 to 1500 µmoles 5'-AMP deaminated per minute per milligram enzyme (28,64,104,111,115,140,146,163). The Hill slope (19,164) is equal to 1.1, as reported by Smiley and Suelter (146).

Smiley and Suelter (146) investigated the allosteric properties of AMP-aminohydrolase prepared from rabbit skeletal muscle. Their results showed that a univalent cation can act as an allosteric activator for the enzyme, but that K^+ is not absolutely required for the catalysis. The same authors (146) also demonstrated that the enzyme had homotropic effects with its substrate 5'-AMP.

In the absence of monovalent cation activators, a lag phase in the deamination reaction, which occurs on the stopped-flow time scale (27,28) clearly indicates activation by the substrate, 5'-AMP. Suelter *et al.* (27), using

stopped-flow techniques, studied the time dependence of activation of muscle AMP-aminohydrolase by substrate and K^+. They observed (27) that when substrate or substrate plus activator K^+ were mixed with the enzyme, there was an initial increase in the rate of deamination of the substrate, 5'-AMP. They interpreted the time course of this change in rate to reflect the progress of activation by substrate or K^+, in that the enzyme is initially inactive, and that the rate-limiting step in the reaction was the activation of the enzyme by substrate or K^+, i.e., the activation process involves a slow conformational transition from an inactive to an active form. The same authors (27) proposed a scheme consistent with their data and capable of explaining the sigmoid dependence of initial velocities versus substrate concentrations observed in steady state kinetics, without involving the concept of cooperative interaction between catalytic sites. Their scheme is represented as follows:

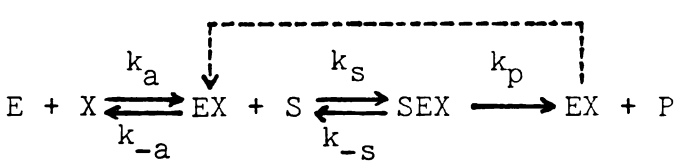

where X is 5'-AMP, H^+, K^+ or other activators; k_s, k_{-s} and k_p are assumed to be fast compared to k_a and k_{-a}. They further proposed that their scheme, like the schemes proposed by Rabin (44) and Weber (126) [see Table 1.1], might

explain sigmoid velocity-substrate curves, even with only one catalytic site per enzyme molecule, and that the scheme is able to account for the time course of product formation even under conditions far from steady-state situations, as observed with AMP-aminohydrolase at high concentrations.

The authors (27) analyzed data via their proposed scheme when K^+-free enzyme was mixed with substrate containing saturating levels of K^+. Hence both substrate and K^+ were simultaneously activating the enzyme, and activation effects due to substrate alone were not analyzed via the scheme.

Later, Ellis and Sturtevant (28), also using stopped-flow methods, studied the activation of AMP-aminohydrolase by 5'-AMP in the absence of monovalent cation activators. They reported that it was possible to interpret their data in terms of the Monod et al. model (20). Although they employed a wide range of initial substrate concentrations, including levels well above K_m, their conclusions were probably incorrect, since they did not take into account substrate depletion in their analysis. Furthermore, they fitted their data to the Monod et al. model with the assumption that the enzyme was composed of six identical subunits; whereas in fact the enzyme has been shown to be tetrameric (60,116).

Ashby and Frieden (64) attempted to analyze the full time course of the catalytic reaction, in the absence of

monovalent cation activators, by computer simulation, using mechanisms which assumed substrate depletion. They reported (64) that none of the mechanisms attempted would consistently fit the data as a function of different initial substrate concentrations. The reason for this, they explained, was that in the absence of K^+, their data indicated that one of the products of the reaction, IMP, was substantially activating the enzyme.

No further studies on the mechanism of homotropic activation of AMP-aminohydrolase, in the absence of monovalent cation activators, have been reported so far in the literature.

CHAPTER 3

INSTRUMENTATION AND DATA ANALYSIS

A. Stopped-Flow Studies

The stopped-flow method was introduced by Roughton (1) in 1934, and greatly improved by Chance (2) some six years later. Further modifications were made by Gibson (3), Sturtevant (4), Dye (5), Dye and Feldman (6), Dewald *et al.* (7), and others (8-13). The technique is one of several fast kinetic methods available to investigators involved in the study of enzyme mechanisms. Essentially the method involves the rapid (a few milliseconds) and efficient mixing of two reactants, stopping the flow, and at a convenient point after mixing, the progress of the reaction is monitored spectrophotometrically.

Modern stopped-flow systems are generally computer, interfaced for data acquisition. Whether data are collected in a scanning or fixed wavelength mode, instrumentation can be complex. In order to extract useful as well as accurate information from such a system, several characteristics have to be either known, or calibrated prior to each experiment performed.

A thermostated, computer-interfaced, double beam

scanning stopped-flow system built by Guan-Huei Ho (14) was used in this research. The entire flow system is made up of inert material such that reagents contact only Kel-F, quartz (mixing and observation cell), polypropylene and Teflon tubing.

The entire flow system, including reagent reservoirs and pushing syringes, is housed inside a water-tight five gallon bath which permits circulating water to be pumped from the bottom to the top of the bath, and allowing for temperature controlled experiments.

In absorbance measurements, flexible quartz fiber optics transmit light dispersed from the scanning monochromator through the water bath, to the observation cell window, and out to the photomultiplier tubes. The use of heavy-walled precision bore pushing and stopping syringes, with a small cross section (Trubore, I.D. = 0.396 inch, ACE Glass Inc., Vineland, NJ) helps reduce the volume of solutions required per push to about 0.25 ml for each of the two reactants. To insure complete mixing of reagents prior to observation, a quartz double four-jet mixing chamber is used. The sample and reference cells are constructed from precision bore quartz capillary tubing, and each provided with two path length options (0.2 cm and 1.86 cm). The mixing chamber is fused directly to the entrance of the sample cell. Details on the construction of the observation cells and the mixing system are found in Guan-Huei Ho's dissertation (14).

Some of the essential characteristics of this stopped-flow system are as follows:

A.1. Scanning Mode

A Perkin-Elmer Model 108 Scanning Monochromator is able to repeatedly scan from 3 to 150 complete spectra per second, in the 220 to 1200 nanometer (nm) range, using the appropriate photomultiplier tubes (PMT). The scanning mode advantages are three-fold. First, precious enzyme is conserved, since a complete spectrum is scanned repeatedly in one push. The need for several fixed-wavelength mode pushes at different wavelengths is thus eliminated. Second, it minimizes reproducibility problems associated with performance of the same experiment at different wavelengths. Third, the problems of long-time baseline drift are minimized. The disadvantages in the scanning mode include noise introduced by the rotating (nutating) mirror of the monochromator, and the inability to follow reactions whose half-lives are less than about 15 milliseconds.

A.2. Fixed Wavelength Mode

Both the disadvantages associated with the scanning mode are eliminated in the fixed wavelength mode. The study of reactions whose half-lives are in the order of 5 milliseconds is possible. In this mode, the progress

of a reaction can be followed at any desired wavelength simply by setting the scanning monochromator to that particular wavelength. The absence of noise introduced by the rotating mirror results in the enhancement of the signal-to-noise ratio (S/N).

A.3. Flow Velocity

The flow of solutions should be fast enough to insure turbulence which is necessary for efficient mixing. The flow velocity can be calculated by measuring the flow time, which is the time required for the stopping syringe to travel the distance between the start flag and the stop flag. A measure of turbulent flow is the Reynold's number (R):

$$R = (d)(v)(\frac{\rho}{\eta})$$

where (d) is the diameter of the tube in (cm); (v), the flow velocity in (cm sec^{-1}); (ρ), the density of the medium, and (η), the viscosity of the medium, for water (η) is 1.002 poise (gm cm^{-1} sec^{-1}).

Figure (3.1) shows the velocity profile of the aqueous solution as a function of time, at 35 pounds per square inch (psi). For the 2 mm I.D. tubes used, the calculated value of 556.4 cm/sec (corresponding to 17.48 ml/sec) is

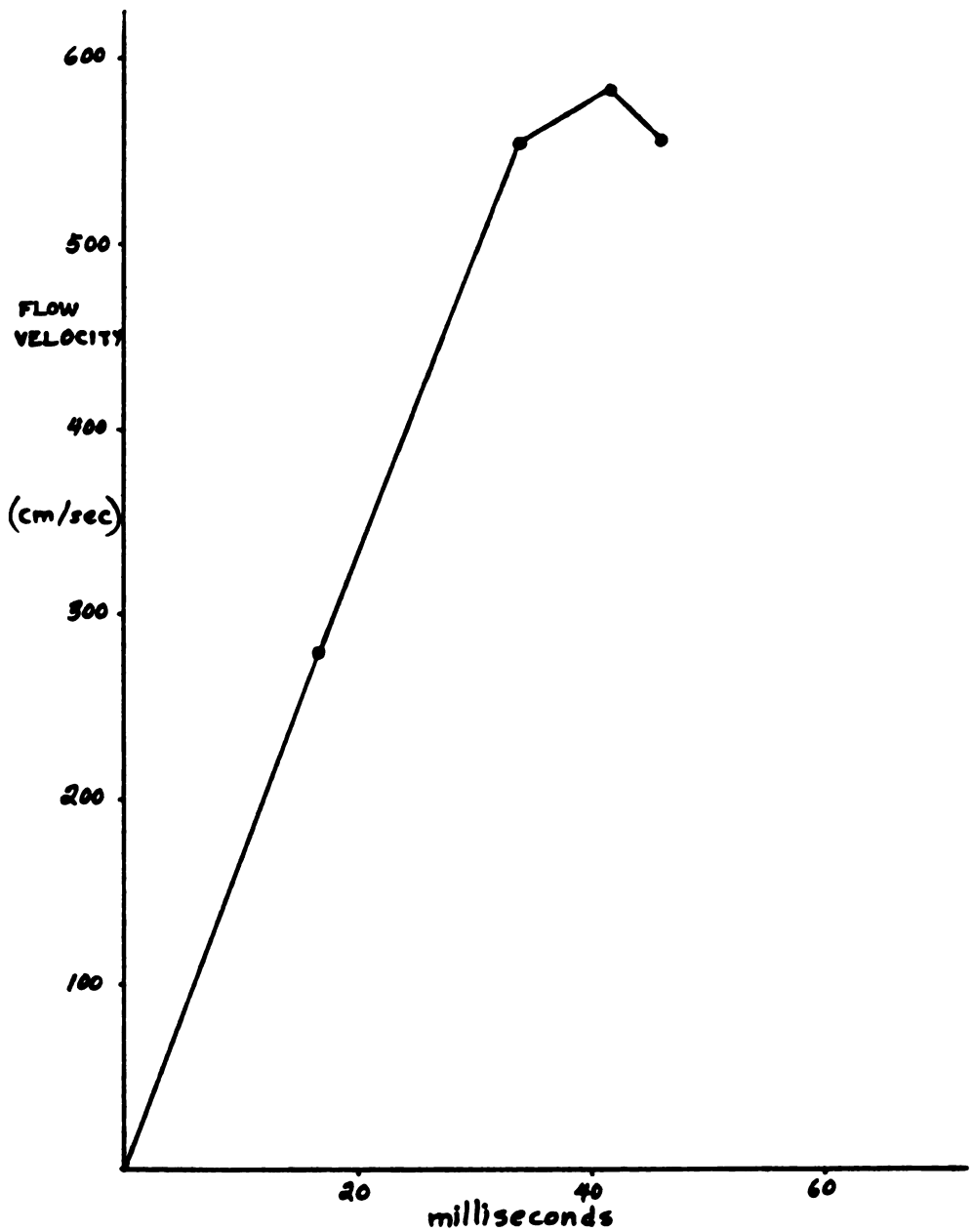

Figure 3.1. Flow Velocity Profile.

well above the velocity of 200 cm/sec required for turbulent flow.

A.4. Dead Time (t_d)

The dead time of a stopped-flow system is defined as the time required for a solution to be transferred from the mixing point to the observation point. It can be estimated by the equation,

$$t_d = \frac{V}{v}$$

where (V), the dead volume in (ml), is the volume from the mixing point to the end of the observation cell window; and (v), is the average flow velocity in ml/sec. The dead volume was computed by Ho (14) to be 0.059 ml for the short path length, and 0.146 ml for the long path length. This resulted in a dead time of 3.38 msec and 8.35 msec for the short and long path lengths respectively.

A.5. Mixing Efficiency

The mixing efficiency of the double four-jet mixer was tested by using stoichiometric amounts of NaOH and HCl. 0.01 M NaOH with phenolphthalein, and an absorbance of 0.83 at 536 nm, was pushed against 0.01 M HCl (colorless). Data collection was triggered with the start flag, which initiates

data collection before the flow stops. The resultant solution had a constant absorbance of 0.25 at 536 nm, during and after the flow had stopped. Since protonation reactions of acid-base indicators are diffusion-controlled, the color change of the phenolphthalein should be complete within the 8.35 msec dead time of the system. Figure (3.2a) shows the spectral changes which occurred upon mixing the acid and base solutions with phenolphthalein as the indicator. Figure (3.2.b) shows the time progress of the absorbance at 536 nm collected in the fixed wavelength mode. Figure (3.2c) is a 100-fold expansion of Figure (3.2b). The constancy of the absorbance as shown in the last two figures clearly indicates complete mixing was achieved before the arrival of the solutions at the observation point.

A.6. Stopping Time

Stopping time is defined as the time required for the mixed solutions to come to complete rest, after the flow has been stopped. It was obtained by Ho (14) who determined its value by studying the fast reaction,

$$(0.02M)Fe^{3+} + (0.02M)CNS^{-} \rightarrow FeNCS^{2+}$$

in 0.2M $HClO_4$, and monitoring the absorbance changes at 456 nm. He found the stopping time to be reproducible

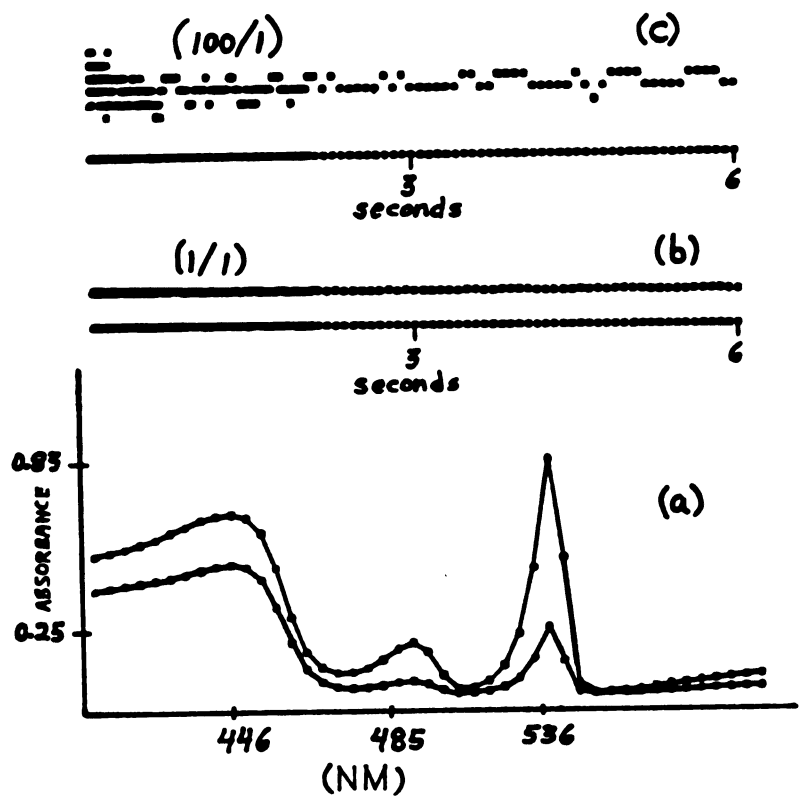

(a) Spectral changes upon mixing 0.01 M HCl and 0.01 M NaOH with phenolphthalein as indicator.

(b) Time progress of absorbance at 536 nm collected in the fixed wavelength mode.

(c) 100-Fold expansion of (3.2b).

Figure 3.2. Mixing Efficiency Spectra.

and less than 0.5 msec under a pushing pressure of 50 psi.

More complete mechanical, electronic, and computer-interfacing details are found in the doctoral dissertations of Guan-Huei Ho (14), Nicholas Papadakis (15), and Richard B. Coolen (16).

B. Data Collection and Calibration

A PDP8/I computer interfaced to the stopped-flow system was used for data acquisition. The raw data collected were subsequently stored on floppy disks for later calibration and analysis. Data stored on floppy disks can also be retrieved and displayed on a Tektronix Model 610 storage display scope, connected to a Tektronix Model 4601 hard-copy unit. Figures (3.2a, b and c) are photocopies of output from the hard copy unit. This capability in the system allows for great flexibility during the performance of experiments, in that it gives the advantage for one to examine results from an experiment immediately after data collection is ended, or anytime thereafter.

Data stored on floppy disks were then transferred to the Michigan State University CYBER7000 computer. Calibration of raw data was performed as described in the Ph.D. dissertation of Robert N. Cochran (17).

C. Data Analysis

An existing general non-linear curvefitting computer program KINFIT4 was used for all data calculations. KINFIT4 is a modified version of program KINFIT originally developed by Dye and Nicely (18). Individual or multiple progress curves were fitted to derived equations in order to extract rate and equilibrium constants. Models proposed for a reaction were first tested by simulation with KINFIT4. When the simulated progress curves followed the progress of the experimental data, the program was then used to fit the actual data to the derived rate equations, in order to find the "best" parameters to fit the experimental results.

D. Computer Graphics

Two dimensional computer plots were obtained from two sources; the plotting subroutine of KINFIT4 on the CYBER 7000, and the Program MULPLT on a PDP-11 computer in the Department of Chemistry. The latter program was developed by Dr. Tom Atkinson at Michigan State University.

Three dimensional plots were obtained using Program GEOSYS. It is available on the Michigan State University CYBER 7000.

CHAPTER 4

EXPERIMENTAL METHODS - AMP-AMINOHYDROLASE

A. Materials

Frozen rabbit skeletal muscle, Type 1, deboned, was purchased from Pel-Freez Biological, Inc., Rogers, Arkansas 72756. 5'-AMP, IMP, MES (anhydrous, 2[N-morpholino]ethane sulfonic acid), TRIS (TRIZMA base, TRIS (Hydroxymethyl) aminoethane), 2-mercaptoethanol(2-hydroxyethyl-mercaptan; -mercaptoethanol), SDS (sodium dodecylsulfate), acrylamide, and ammonium persulfate were all purchased from the Sigma Chemical Company, St. Louis, Missouri. Bisacrylamide (N,N'-methylenebisacrylamide) was purchased from Canalco. Cellulose phosphate was purchased from Whatman, and $(CH_3)_4NCl$ (Tetramethylammonium chloride) from Aldrich Chemicals. Distilled water was passed through a mixed ion exchange resin bed prior to use.

B. Preparation of AMP-aminohydrolase

The enzyme was prepared according to the method of Smiley et al. (115). Five hundred grams of partially thawed rabbit skeletal muscle were cut into small pieces

and placed, along with 2 liters of phosphate buffer at pH 6.5, in a large Waring Blendor. The mixture was homogenized for 15 seconds at high speeds, and the process repeated every 15 minutes for a total of one hour. The resulting slurry was transferred to polyethylene bottles and centrifuged at high speeds (about 7000 x g) for 15 minutes, in a refrigerated (4°C) centrifuge. The supernatant fraction from each bottle was poured through two layers of cheese cloth to remove lipid particles. All succeeding steps were performed at room temperature.

About 5 grams (dry weight) of treated cellulose phosphate was added to the pooled extract. The suspension was stirred for 30 minutes after the cellulose phosphate was allowed to settle. At least 90% of the enzyme was bound to the cellulose phosphate at this stage. The reddish supernatant solution was siphoned off and discarded. The remaining cellulose phosphate slurry was then transferred to a sintered glass suction filter where it was washed repeatedly with approximately two liters of extraction buffer in 200-300 ml portions. During this process, the cellulose phosphate pad was not allowed to become dry. It was then washed with 1 liter of 0.45 M KCl adjusted to pH 6.5 with 50 mM MES-TRIS buffer, again in 200-300 ml portions. This salt solution and all following solutions contained 1 mM 2-mercaptoethanol. The cellulose phosphate was transferred to a (2 x 10 cm) polyethylene column, and

the enzyme eluted with 1 M KCl adjusted to pH 6.5 with 50 mM MES-TRIS buffer.

Each fraction was assayed for protein at 280 nm; ε (280 nm) = 0.913 ml/cm·mg, [from Zielke and Suelter (165)]. Fractions with readings below one absorbance unit were discarded. Those with readings higher than one absorbance unit were pooled into a screw-capped polyethylene tube, and purged with nitrogen gas prior to closure.

About 50 milligrams (mg) of pure enzyme were obtained per 500 grams of muscle, with an average enzyme concentration of between 2.5 and 3.5 mg/ml. An average value of 1350 micromoles 5'-AMP deaminated per minute per milligram of enzyme was obtained for the specific activity.

The difference in the extinction coefficient of 5'-AMP and IMP, $\Delta\varepsilon$, is equal to 0.12 x $10^3 M^{-1} cm^{-1}$ at 290 nm, 30°C and pH 6.5 (27).

Related to the specific activity, S.A., the turnover number, T.N., is defined here as the number of 5'-AMP molecules deaminated per active site of enzyme per second. Hence, at saturation conditions ($S >> K_m$) for AMP-aminohydrolase, with a molecular weight of 278,000 (116) and four subunits, one S.A. unit is equivalent to 1.16 T.N. units.

To remove K^+ ions, the enzyme solution was routinely dialyzed against 0.5 M $(CH_3)_4NCl$, which contained 50 mM MES-TRIS buffer at pH 6.5 and 1 mM 2-mercaptoethanol. The

final solution, designated as K^+-free enzyme throughout this present work, contained 10 μM or less K^+.

C. SDS Gel Electrophoresis

In order to investigate the purity of the enzyme prepared according to the method described above, SDS gel electrophoresis experiments were conducted on several enzyme preparations.

Enzyme isolated from newly purchased (one month or less) frozen rabbit muscle gave only one band when analyzed in 7% SDS gel electrophoresis. This confirms the findings of Smiley *et al.* (115). However, enzyme isolated from frozen rabbit muscle which was about six months old, yielded two additional minor bands. Both minor bands constituted about 10% of the total absorbance. However, the S.A. of the enzyme remained high, ranging from 1250-1400.

Several enzyme preparations from this same muscle were treated via a modified process (as recommended by Professor C. H. Suelter, Department of Biochemistry, Michigan State University, East Lansing, Michigan) in order to remove these minor impurities.

Instead of eluting the enzyme from cellulose phosphate with 1 M KCl, it was eluted with a linear gradient between 0.45 M and 1 M KCl. However, the contaminants were not removed.

Another batch was processed through two cellulose phosphate columns. 1 M KCl was used to elute the enzyme from the first column, and then a linear gradient between 0.45 M to 1.0 M KCl was used to elute it from the second column. The contaminating impurities were still evident, but to a lesser degree.

Still another batch was processed through three columns of cellulose phosphate. The enzyme solutions from each column were eluted successively with 1 M KCl; a gradient between 0.45 M and 1.0 M KCl; and finally, a gradient between 0.45 M KCl and 0.45 M KCl with 50 mM K^+ pyrophosphate. This process yielded one band in SDS gel electrophoresis.

D. Fluorescence Experiment

Two AMP-aminohydrolase solutions were prepared. One contained 0.97 mg/ml enzyme in 0.5 M KCl, the other 1.2 mg/ml enzyme in 0.5 M $(CH_3)_4NCl$. Both solutions also contained 50 mM MES-TRIS buffer at pH 6.5. After adjusting the spectrofluorometer for maximum emission, the spectrum of 1 ml of each sample was recorded. Both samples were maximally excited at 305±2 nm, and emitted at 364±2 nm. 0.5 ml of 5 mM 5'-AMP was added to each of the above enzyme samples, and their spectra recorded.

E. Analytical Ultracentrifuge Experiments

Sedimentation velocity experiments were performed on samples of enzyme which contained either KCl or $(CH_3)_4NCl$. Prior to these experiments, SDS gel electrophoresis performed on the same enzyme batch indicated the presence of one band. The specific activity of the enzyme in KCl was 1504, and that in $(CH_3)_4NCl$ was 1452.

Three different enzyme concentrations (1.8, 0.9 and 0.7 μM) were examined. At each concentration, two samples were run in parallel, one contained 0.5 M KCl, the other 0.5 M $(CH_3)_4NCl$. Both contained 50 mM MES-TRIS buffer at pH 6.5.

The ultracentrifuge was run at 32,000 rpm and 20°C. Two wavelengths, 260 and 280 nm were used to monitor the progress of the sedimentation velocity profile.

F. Stopped-Flow Experiments

Unless otherwise indicated, all stopped-flow experiments on AMP-aminohydrolase were conducted in the presence of 0.5 M $(CH_3)_4NCl$, 50mM MES-TRIS at pH 6.5, and 22°C. It is also important to note here that in all the stopped-flow experiments, concentrations of enzyme and substrate reported are the final values after mixing. This is because upon pushing enzyme against substrate, the final volume of the solution exactly doubles.

F.1. Scanning Experiments

Scanning experiments were performed to determine if intermediates could be detected during the reaction of K^+-free enzyme with 5'-AMP. The wavelength region scanned was from about 230 to 330 nm.

Several combinations of enzyme and substrate concentrations were used. For the long path cell (1.86 cm), concentrations of enzyme ranged from 0.36 to 4.3 μM, while substrate values ranged from 0.05 to 5 mM. At 0.5 to 5 mM levels of 5'-AMP, only the region from about 285 to 330 nm was scanned, due to the high absorbances of 5'-AMP and IMP at the lower wavelengths. For the short path cell (0.2 cm), concentrations of enzyme ranged from 1.8 to 5 micromolar, and substrate levels from 0.05 to 0.5 mM. At these levels of 5'-AMP it was possible to record the complete spectrum from about 230 to 330 nm. Scanning pushes were performed at 2°, 12° and 22°C.

F.2. Fixed Wavelength Experiments

F.2.1. Temperature Studies

Experiments were performed at 2°, 12° and 22°C. All initial enzyme solutions contained 1 M $(CH_3)_4NCl$, and 50 mM MES-TRIS buffer at pH 6.5. All initial substrate solutions contained 50 mM MES-TRIS buffer at pH 6.5.

Upon mixing the enzyme and substrate solutions in the stopped-flow system, the final $(CH_3)_4NCl$ concentration was 0.5 M, whereas the MES-TRIS concentration remained unchanged. The resultant final enzyme and substrate concentrations were hence half the initial.

In each of the reactions performed at the three temperatures, five final enzyme concentrations were employed: 3.6, 1.8, 0.9, 0.45, and 0.225 μM; while the final substrate concentrations used were: 5.0, 2.5, 1.25, 0.63 and 0.31 mM. Each of the enzyme concentrations was pushed against all the five substrate concentrations.

The highest and lowest concentrations of enzyme and substrate were chosen such that the preinduction time lags were completely covered, with minimal loss in signal to noise ratio (S/N). In other words, the maximum enzyme concentration (3.6 μM) when pushed against 5 mM substrate, displayed no detectable lag; whereas the minimum enzyme concentration (0.225 μM) versus the minimum substrate concentration of 0.3125 mM, produced a very large lag, but also resulted in a total absorbance change (substrate converted to product), that still had a high signal to noise ratio of more than 30. Obviously, the combination of lowest enzyme and substrate concentrations should present the lowest S/N ratios. This is because the rate of product formation, and the total absorbance change would be at their lowest values.

F.2.2. Preincubation Studies

Unless otherwise indicated, all experiments were conducted in 0.5 M $(CH_3)_4NCl$, 50 mM MES-TRIS (pH 6.5), and at 22°C.

Enzyme at a concentration of 0.45 μM was preincubated with either 5'-AMP, IMP or NH_4^+ (each at either 2.5 mM or 0.625 mM), prior to reaction with 1.25 mM 5'-AMP. For comparison, two additional enzyme samples were pushed against 1.25 mM 5'-AMP; one sample had no preincubated material, while the other had 0.5 M KCl instead of 0.5 M $(CH_3)_4NCl$.

CHAPTER 5

RESULTS AND DISCUSSION - AMP-AMINOHYDROLASE

A. Intermediates

The Michaelis-Menten (M-M) rate law is often used to describe the overall rate of an enzyme catalyzed reaction. However, the detailed mechanism of an enzymatic reaction is generally quite complex. Steady state methods are frequently employed, and are often helpful in predicting the general pathway of the reaction. But as the number of independent rate constants increases in a proposed mechanism, it becomes increasingly difficult to verify reliably the magnitudes of these constants without additional experimental evidence. A good "handle" often used to verify a mechanism, or part of a mechanism, is the study of transient intermediates detected during the course of a catalytic reaction.

Detecting intermediates in enzyme catalyzed reactions involves the premise that during the course of a reaction, some groups on the enzyme, enzyme-substrate complex, or substrate, undergo changes in their environment in going from one form to the next. Techniques which can be used to monitor such changes include stopped-flow, UV-VIS

difference spectra, luminescence, ORD and CD.

Transient intermediates fall into one of two categories, on or off enzyme. Off-enzyme intermediates have kinetics that are independent of enzyme concentration, and while they may yield some information about the reaction, they generally do not provide useful data in predicting a mechanism for the formation and interaction of the enzyme-substrate complex. On the other hand, on-enzyme intermediates are dependent on enzyme concentration, and are thus useful in mapping a more detailed and verifiable mechanism for the catalytic action of an enzyme.

In order to detect such on-enzyme intermediates for enzymatic reactions which involve only enzyme and substrate, with no added cofactors, as with AMP-aminohydrolase, several factors should generally be satisfied. Among them are: (1) high concentrations of enzyme should be used, since the enzyme spectrum must be recorded, (2) the enzyme-substrate complex should have a low dissociation constant, generally in the order of a fraction of millimolar or less, (3) the substrate concentration should be high enough to insure as complete a saturation of the enzymatic sites as possible, and (4) the spectrum of the enzyme, or the enzyme-substrate complex must be at wavelengths other than those of either substrate or product. Figure (5.1) shows the spectra of AMP-aminohydrolase, 5'-AMP and IMP, and Figure (5.2) shows a scanning spectrum of 3.4 μM AMP-aminohydrolase versus 0.5 mM 5'-AMP.

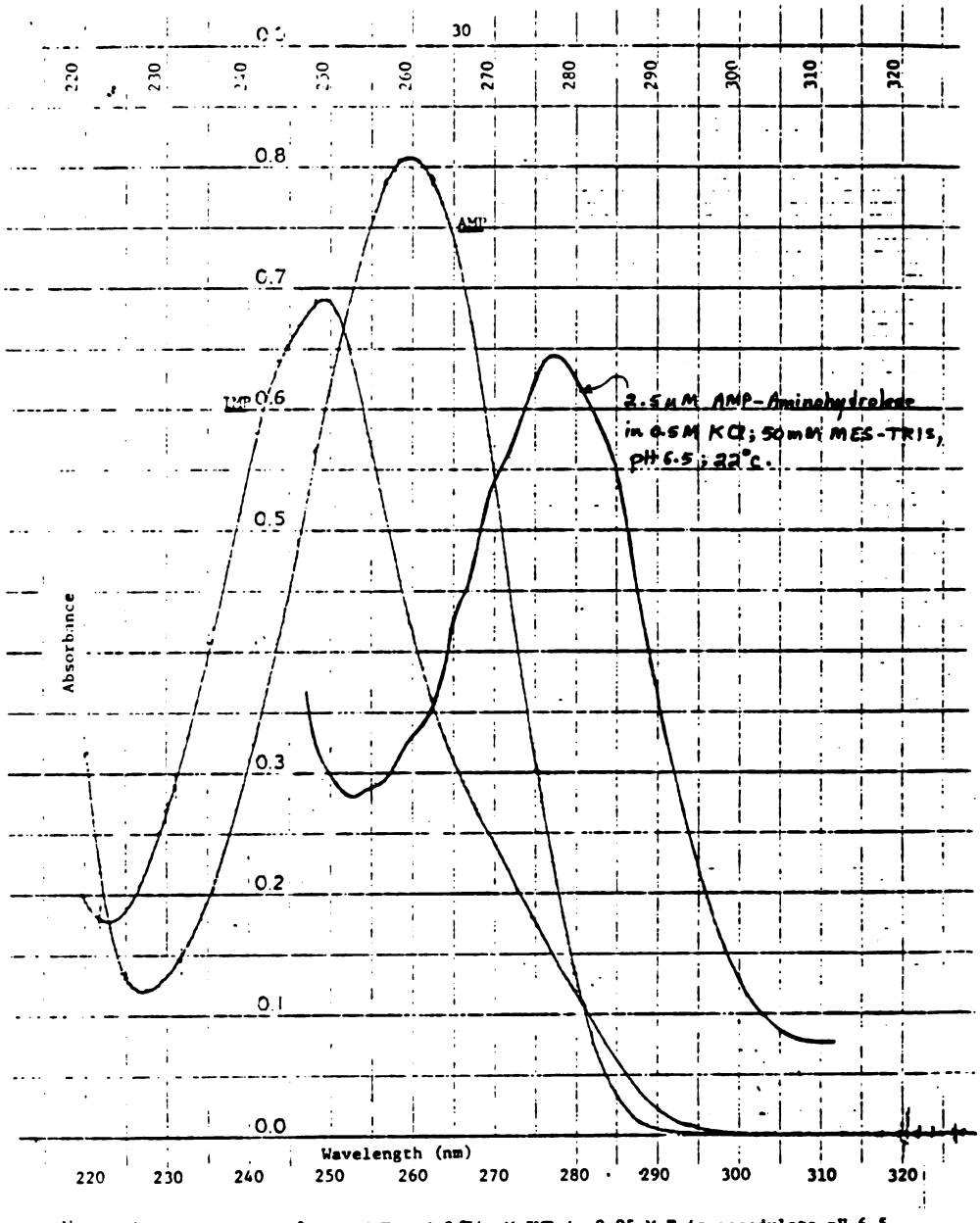

Absorption spectra of 0.053 mM AMP and 0.054 mM IMP in 0.05 M Tris-cacodylate pH 6.5.

Figure 5.1. Static Spectra of 5'-AMP, IMP and AMP-Aminohydrolase.

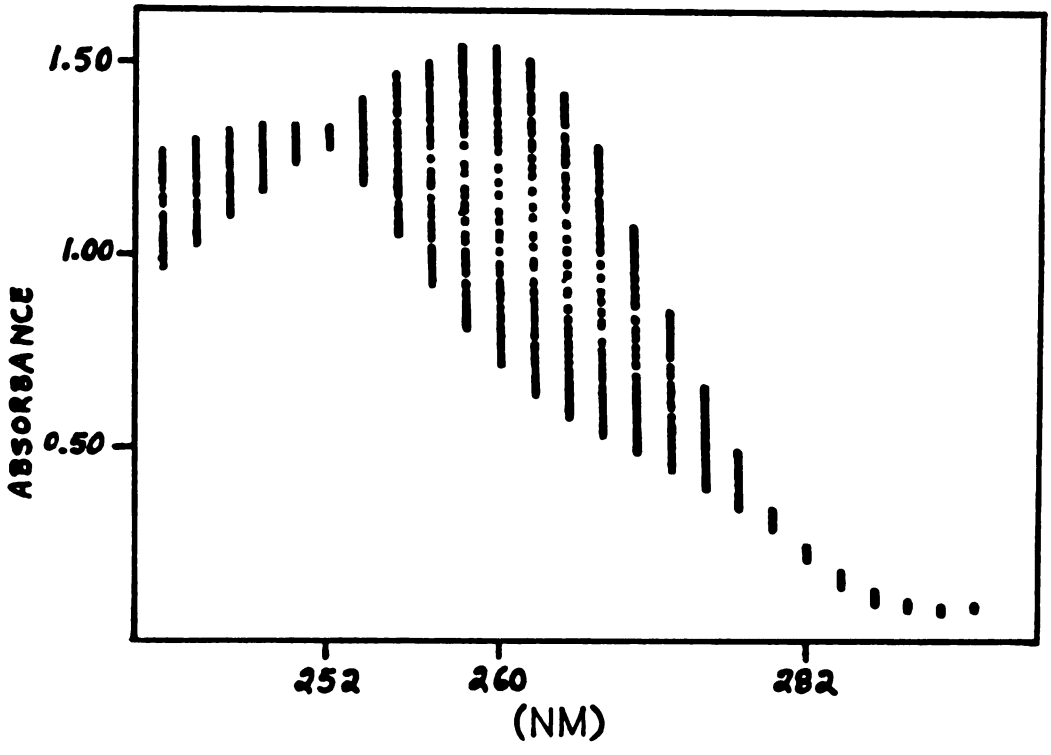

(Reaction medium: 0.5 M $(CH_3)_4NCl$; 50 mM MES-TRIS, pH 6.5; 22°C.)

Figure 5.2. Scanning Spectrum of 3.4 μM AMP-Aminohydrolase with 0.5 mM 5'-AMP.

A.1. Fluorescence Study

Since neither 5'-AMP nor IMP, possesses a fluorescence spectrum whereas AMP-aminohydrolase does, an experiment was performed to investigate the fluorescence properties of the enzyme in the presence and absence of K^+ and 5'-AMP, in order to assess the feasibility of conducting stopped-flow studies in the fluorescence mode. The two enzyme samples both contained 50 mM MES-TRIS buffer at pH 6.5, except that one sample was in 0.5 M KCl and the other in 0.5 M $(CH_3)_4NCl$. As can be seen in Figure 5.3, the overall shapes of both emission spectra are the same. Figure 5.4 shows the excitation and emission spectra of the enzyme in 0.5 M $(CH_3)_4NCl$. The difference in the absolute intensity is due to the difference in the enzyme concentration of the samples. The results clearly indicate that the fluorescence characteristics of active and inactive AMP-aminohydrolase are the same; hence, it appeared unlikely that any fluorescent intermediates would be detected during the course of the reaction.

A.2. UV-VIS Scanning Experiments

Scanning stopped-flow experiments for the reaction of K^+-free AMP-aminohydrolase with 5'-AMP were performed in order to determine if any transient intermediates could be detected during the course of enzyme activation

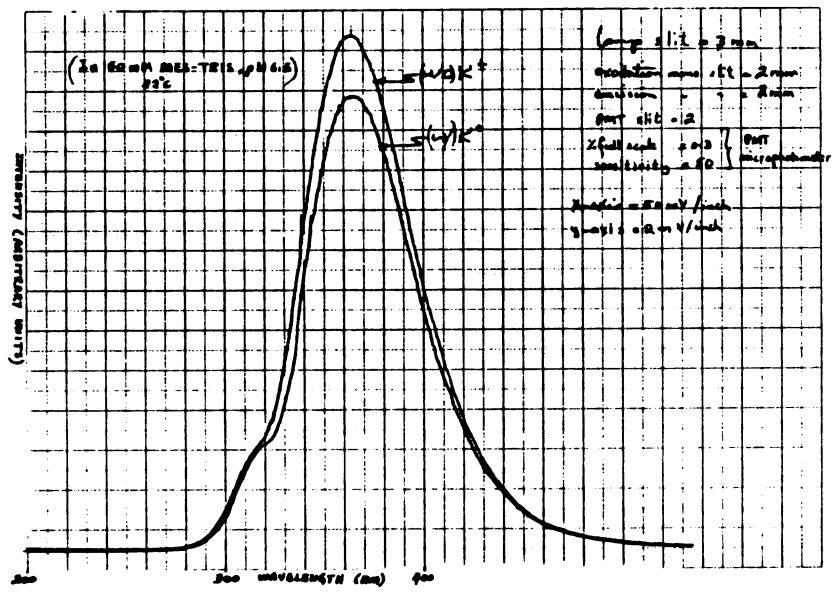

Figure 5.3. Fluorescence Spectra of AMP-Aminohydrolase in 0.5 M $(CH_3)_4NCl$ and 0.5 M KCl.

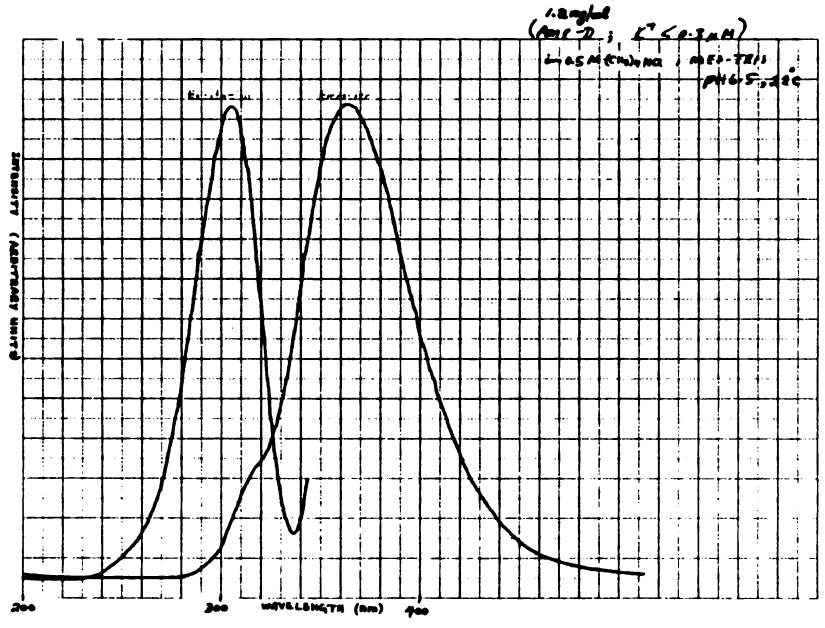

Figure 5.4. Excitation and Emission Spectra of AMP-Aminohydrolase in 0.5 M $(CH_3)_4NCl$.

by substrate. Each subunit of the enzyme contains 33 residues of phenylalanine, 5 residues of tryptophan and 30 residues of tyrosine. All three amino acids absorb in the UV, with phenylalanine having a maximum around 260 nm; tryptophan and tyrosine around 280 nm. Hence these amino acids are probably the major constituents responsible for the enzyme spectrum at these wavelengths.

The assumption was that if any spectral changes occur around these wavelengths, during the activation of the enzyme, they should be due to changes in the environment around these three amino acid residues. This would then indicate changes in the enzyme conformation from the inactive to the active form, during the course of activation. More specifically, one or more of these amino acids would then have to be present in the vicinity of the active and/or activator sites of the enzyme, since these sites should undergo the most changes when the enzyme undergoes a conformational change.

In all cases examined, as described in Chapter 4, Section (F.1), the only spectral changes observed were those due to substrate depletion with concurrent product growth (Figure 5.2). No further attempts were made to search for intermediates.

B. Analytical Ultracentrifuge Studies

Sedimentation velocity studies were conducted in order to investigate three points. The first was to ascertain the purity of the K^+ activated enzyme, the results of which would complement those obtained from gel electrophoresis measurements conducted earlier on the same enzyme preparation which showed only one band. The second was to determine if the K^+-free enzyme, present in $(CH_3)_4NCl$, undergoes any subunit dissociation, and if so, to measure the extent of this dissociation, and thus answer the question as to whether activation of the enzyme by monovalent cations might be associated with a change in the aggregation state of the enzyme. The third was to examine whether the constitution of the enzyme is concentration dependent. Results from the last two points would then be used in the formulation of a full-time course model, which would encompass activation of the enzyme by substrate, and include or preclude subunit association-dissociation phenomena. Three different enzyme concentrations (1.8, 0.9 and 0.7 μM) were used to determine if subunit dissociation was concentration dependent.

Examination of the spectra revealed that the sedimentation velocity profiles were similar in all cases, and indicate no major variations from one sample to the next. The spectra for the K^+-activated enzyme showed one moving boundary, which indicated the absence of contaminants,

and also that the active enzyme existed in the tetrameric configuration, as expected, in the presence of monovalent cation activators (115). Figures 5.5 and 5.6 show the sedimentation velocity spectra of 1.8 μM AMP-aminohydrolase in 0.5 M KCl, at 280 and 260 nm, respectively.

When the K^+-free enzyme results were compared to those of enzyme with K^+, it was found that all the spectra were quite similar in their profiles for all the three concentrations, except that the spectra for the K^+-free samples had a slightly broader boundary than those for the enzyme samples with K^+. For example, compare Figure 5.5 to 5.7, and Figure 5.6 to 5.8. This slightly broader boundary may be the result of one or two factors. The first factor could be a viscosity effect on the sedimentation, since the viscosity of 0.5 M KCl at 20°C is about 0.99 poise (relative to water at 1.00), while the viscosity of 0.5 M $(CH_3)_4NCl$ at 20°C is about 1.15 poise (gm $cm^{-1}sec^{-1}$). Thus, the protein molecules in the 0.5 M $(CH_3)_4NCl$ solution would experience slightly greater drag in their migration, which would then result in a slightly broader boundary than that manifested by those in the 0.5 M KCl solution. The second factor for the broadening in the 0.5 M $(CH_3)_4NCl$ solution could be the result of some minor subunit dissociation of the enzyme, but not to the extent that one could readily measure for these conditions at 20°C.

Sedimentation coefficients at 20°C in aqueous solution

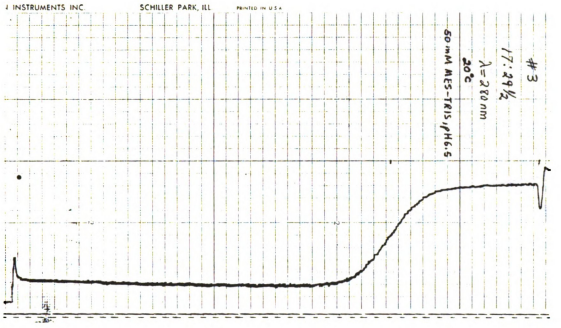

Figure 5.5. Sedimentation Velocity Spectrum of 1.8 μM AMP-Aminohydrolase in 0.5 M KCl at 280 nm.

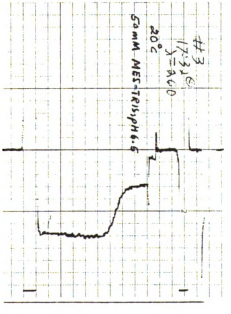

Figure 5.6. Sedimentation Velocity Spectrum of 1.8 μM AMP-Aminohydrolase in 0.5 M KCl at 260 nm.

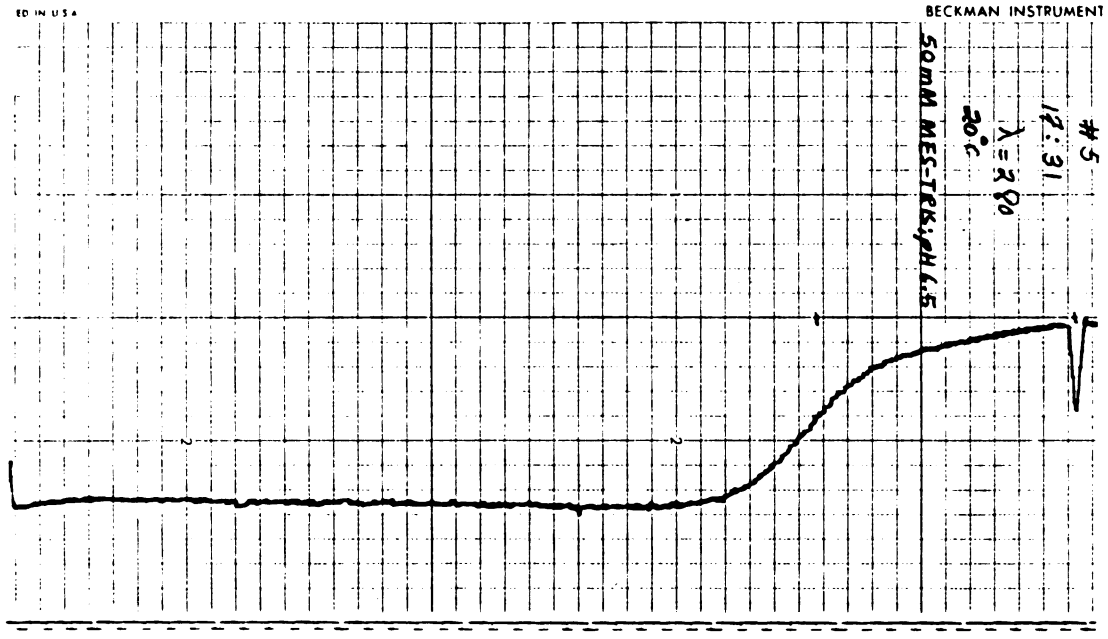

Figure 5.7. Sedimentation Velocity Spectrum of 1.8 μM AMP-Aminohydrolase in 0.5 M $(CH_3)_4NCl$ at 280 nm.

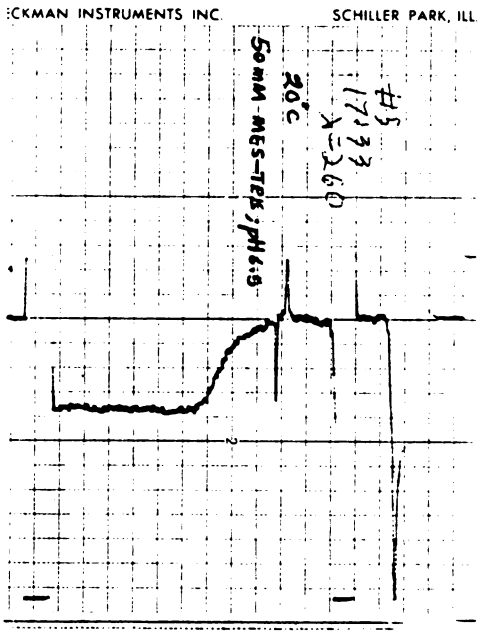

Figure 5.8. Sedimentation Velocity Spectrum of 1.8 μM AMP-Aminohydrolase in 0.5 M $(CH_3)_4NCl$ at 260 nm.

($S_{20,w}$) were calculated for all the samples, and the results are shown in Table 5.1. The $S_{20,w}$ values shown are in Svedberg units. Again the values of $S_{20,w}$ in the table clearly indicate that all samples were sedimenting in an equivalent fashion.

Table 5.1. Sedimentation Coefficients for AMP-Aminohydrolase at 20°C. $S_{20,w}$ values Calculated from Sedimentation Velocity Profiles at 280 nm. The Ultracentrifuge Velocity was 32,000 rpm.

Enzyme Conc. (μM)	$S_{20,w}$ (Svedbergs)	
	In 0.5M $(CH_3)_4NCl$	in 0.5M KCl
0.7	10.0	10.4
0.9	10.0	10.7
1.8	9.2	10.4

The $S_{20,w}$ values shown in Table 5.1 compare favorably with those obtained by Smiley et al. (115), who reported a value of 11.5 S for their enzyme preparation.

In summary, the sedimentation velocity results indicate that the composition of AMP-aminohydrolase is that of the tetramer, at 20°C, whether the enzyme is in 0.5 M KCl or 0.5 M $(CH_3)_4NCl$, and that this composition is not concentration dependent down to 0.7 μM.

C. Preincubation Studies

Stopped flow experiments were conducted to explore the effect of preincubating the components of the catalytic reaction with enzyme prior to reaction with substrate.

5'-AMP, IMP and NH_4^+, were each premixed with AMP-aminohydrolase, after which each mixture was reacted with 5'-AMP. The reactions were performed in 0.5 M $(CH_3)_4NCl$, 50 mM MES-TRIS buffer at pH 6.5, and at a temperature of 22°C. In addition, one enzyme sample contained no preincubating agent, while another contained 0.5 M KCl instead of 0.5 M $(CH_3)_4NCl$.

The effect of preincubating NH_4^+ with enzyme is shown in Figure 5.9. As can be seen from the figure, NH_4^+ at concentrations up to 2.5 mM has little or no inhibitory effect on the reaction progress. Calculated values of (dP/dt) for the steady-state region, corresponding to a maximum rate in product formation, are shown in Table 5.2.

The effects of IMP, 5'-AMP, and K^+, are shown in Figure 5.10. Table 5.2 shows the calculated values of (dP/dt) for the steady-state region. IMP with concentrations up to 2.5 mM has essentially no effect on the steady-state region. However, the lag is slightly removed by 0.625 mM IMP, and more so by 2.5 mM IMP. On the other hand, 0.625 mM 5'-AMP increases the rate of product release at the steady-state region by approximately 17%, and 2.5 mM 5'-AMP increases it by about 52%. Furthermore, the lag

Table 5.2. Preincubation Studies.[1]

0.45 μM Enzyme Preincubated With	(dP/dt), Steady-State Region (μM IMP/Second)
nothing	845
0.625 mM NH_4^+	777
2.5 mM NH_4^+	778
0.625 mM IMP	837
2.5 mM IMP	836
0.625 mM 5'-AMP	990
2.5 mM 5'-AMP	1283
0.5 M KCl (No $(CH_3)_4NCl$)	2121

[1]All samples contained 0.5 M $(CH_3)_4NCl$ (unless otherwise indicated), and 50 mM MES-TRIS buffer (pH 6.5). The reactions were conducted at 22°C. The AMP-aminohydrolase concentration is 0.45 μM; 5'-AMP concentration is 1.25 mM.

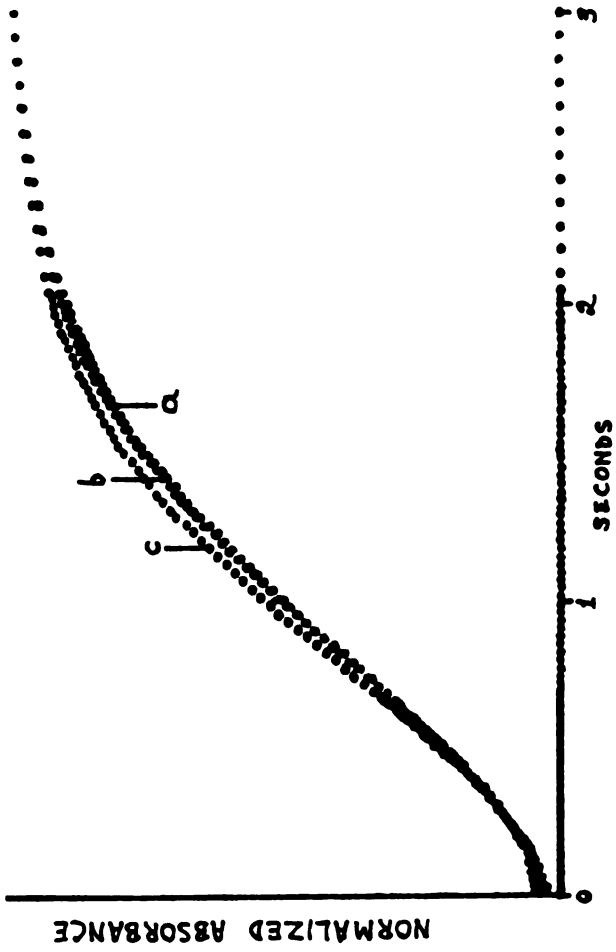

(Reaction: 0.45 μM AMP-Aminohydrolase + 1.25 mM 5'-AMP; in 0.5 M $(CH_3)_4NCl$; 50 mM MES-TRIS, pH 6.5; 22°C.)

(a) 2.5 mM NH_4^+; (b) 0.625 mM NH_4^+; (c) no preincubating material.

Figure 5.9. Preincubation of NH_4^+ with AMP-Aminohydrolase.

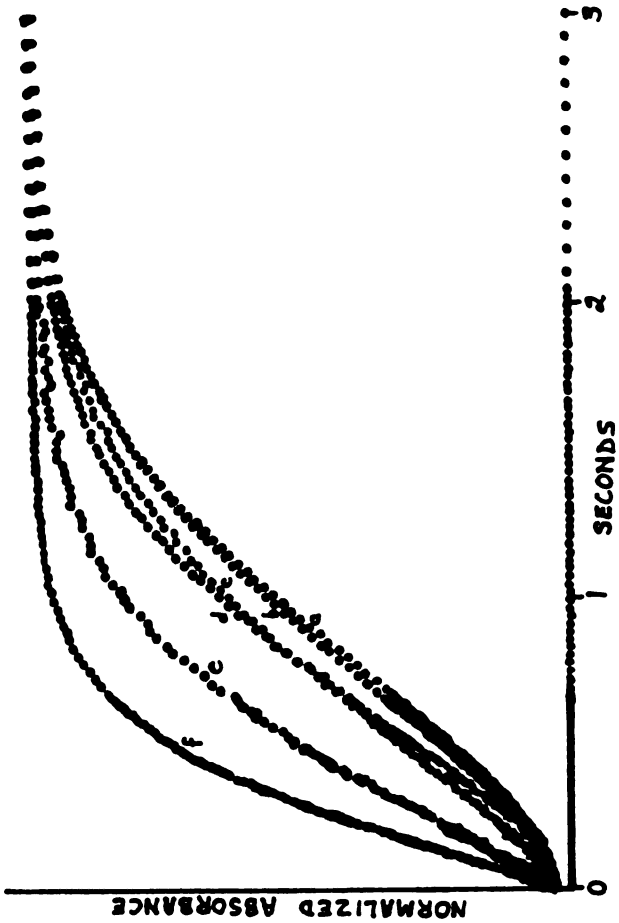

(Reaction: 0.45 μM AMP-Aminohydrolase + 1.25 mM 5'-AMP; in 0.5 M $(CH_3)_4NCl$; 50 mM MES-TRIS, pH 6.5, 22°C.)

(a) no preincubating material; (b) 0.625 mM IMP; (c) 2.5 mM IMP;
(d) 0.625 mM 5'-AMP; (e) 2.5 mM 5'-AMP; (f) 0.5 M KCl; no $(CH_3)_4NCl$.

Figure 5.10. Preincubation of IMP, 5'-AMP and K^+ with AMP-Aminohydrolase.

is substantially removed by 0.625 mM 5'-AMP, and completely removed by 2.5 mM 5'-AMP. In 0.5 M KCl, AMP-aminohydrolase is fully activated, and thus no lag is present. In addition, this gives the highest rate of product release for the steady-state region.

D. Temperature Studies

The objective of these studies was to systemitize the observed lags in product formation, along with the shut-off behavior, in the reactions of K^+-free AMP-aminohydrolase with 5'-AMP, and to propose a mechanism consistent with the data.

As explained in Section F.2.1, Chapter 4, the experiments performed provided progress curves for the reactions of five different enzyme concentrations, each pushed against five different substrate concentrations, at 2°, 12° and 22°C. All the reactions were conducted in 0.5 M $(CH_3)_4NCl$, 50 mM MES-TRIS buffer, at a pH of 6.5.

The progress ofthe reactions was monitored at wavelengths longer than 282 nm (an isosbestic point), due to the very high absorptivities of both 5'-AMP and IMP at shorter wavelengths. At wavelengths longer than 282 nm, the product IMP, uniformly has higher absorptivities than the substrate 5'-AMP (See Figure 5.1). Hence, all progress curves show a net effect of product growth.

No attempt was made to calibrate the exact wavelength at which each push (or a series of pushes) was performed. Rather, the scanning monochromator was manually adjusted for the maximum total final absorbance possible, and then kept at that wavelength (between 285-295 nm) for the duration of the push. The reason for this is that the catalytic reaction of AMP-aminohydrolase is a stoichiometrically "clean" reaction, with three isosbestics at 221, 250.5 and 281.5 nm; i.e., the only species whose absorbances are changing with time, at the wavelengths studied, are the substrate and the product, with a constant background and enzyme absorbance. For such conditions, and as shown in Appendix A, the ratio of the change in absorbance (ΔA), at any time (t), to the total absorbance (ΔA_∞), is independent of wavelength (λ); that is:

$$\frac{\Delta A}{\Delta A_\infty} = \frac{A_t - A_0}{A_\infty - A_0} = \frac{P}{S_0}$$

where (A_t) is the absorbance at time (t); (A_0), the absorbance at zero time; (A_∞), the absorbance at infinity; (P), the product concentration; and (S_0), the initial substrate concentration.

Rearranging the above equation yields

$$A_t = A_0 + \frac{(P)(A_\infty - A_0)}{(S_0)}$$

and A_t is the actual absorbance value derived from the stopped-flow.

For data collection, the existing stopped-flow system measures and stores data in progressive pairs of time points and their corresponding voltages. Through software programs described elsewhere (17), each voltage and time point pair is converted to a calibrated absorbance (A_t) and a corrected time. These constitute the final data used by KINFIT4, for all the simulations and data fittings.

D.1. Lag Times

In the absence of monovalent cation activators such as K^+, AMP-aminohydrolase exists in a catalytically inactive conformation. Upon mixing with 5'-AMP, the enzyme must combine, in some fashion, with 5'-AMP, to be transformed into an active conformation, after which product is formed. This time period, where the lag in product formation occurs, is often referred to as the activation period. It is for this reason that sigmoidal, rather than hyperbolic, progress curves result when K^+-free AMP-aminohydrolase is mixed with 5'-AMP.

In order to display the effect of enzyme and substrate concentrations on these lag times, experimentally observed lag times were plotted as a function of either enzyme or substrate concentration, at 2°, 12° and 22°C. The lag times were obtained from the calibrated absorbance values

(program ABCAL3 output). In each case, the lag time was chosen as the time during which the absorbance value had not risen beyond an average of about ±0.005 absorbance units, which in turn, was about the level of noise in the absorbance signal. Figures 5.11 through 5.16 show these plots.

Figure 5.17 shows an actual experimental hard copy output for the reaction of 3.6 μM AMP-aminohydrolase with 0.625 mM 5'-AMP at 22°C, while Figure 5.18 shows the first 500 milliseconds of the same reaction. Figure 5.19 shows the first 5000 milliseconds in the reaction of 0.90 μM AMP-aminohydrolase with 0.625 mM 5'-AMP at 2°C.

Figure 5.20 shows the first 1800 milliseconds in the reactions of 2.5 mM 5'-AMP versus 3.60, 1.80, 0.90, 0.45 and 0.225 μM AMP-aminohydrolase at 22°C. Each curve displayed is normalized to the same infinity absorbance value, and then divided by the enzyme concentration. So the curves display:

$$\left(\frac{1}{E_0}\right)\left(\frac{A - A_0}{A_\infty - A_0}\right) \text{ versus time}$$

Figure 5.21 shows the first 14 seconds of the full time progress curves of 2.5 mM 5'-AMP versus 3.60, 1.80, 0.90, 0.45 and 0.225 μM AMP-aminohydrolase, at 22°C. Each curve is normalized to the same infinity absorbance value, so the curves display $(A - A_\infty)$ versus time. It is evident from

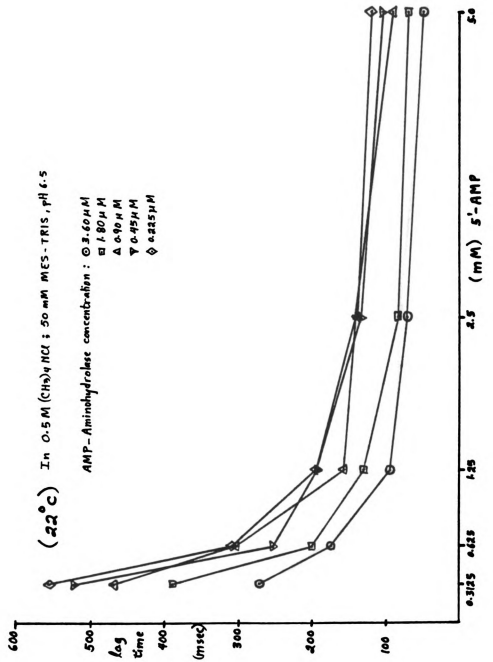

Figure 5.11. Lag Time as a Function of 5'-AMP at 22°C.

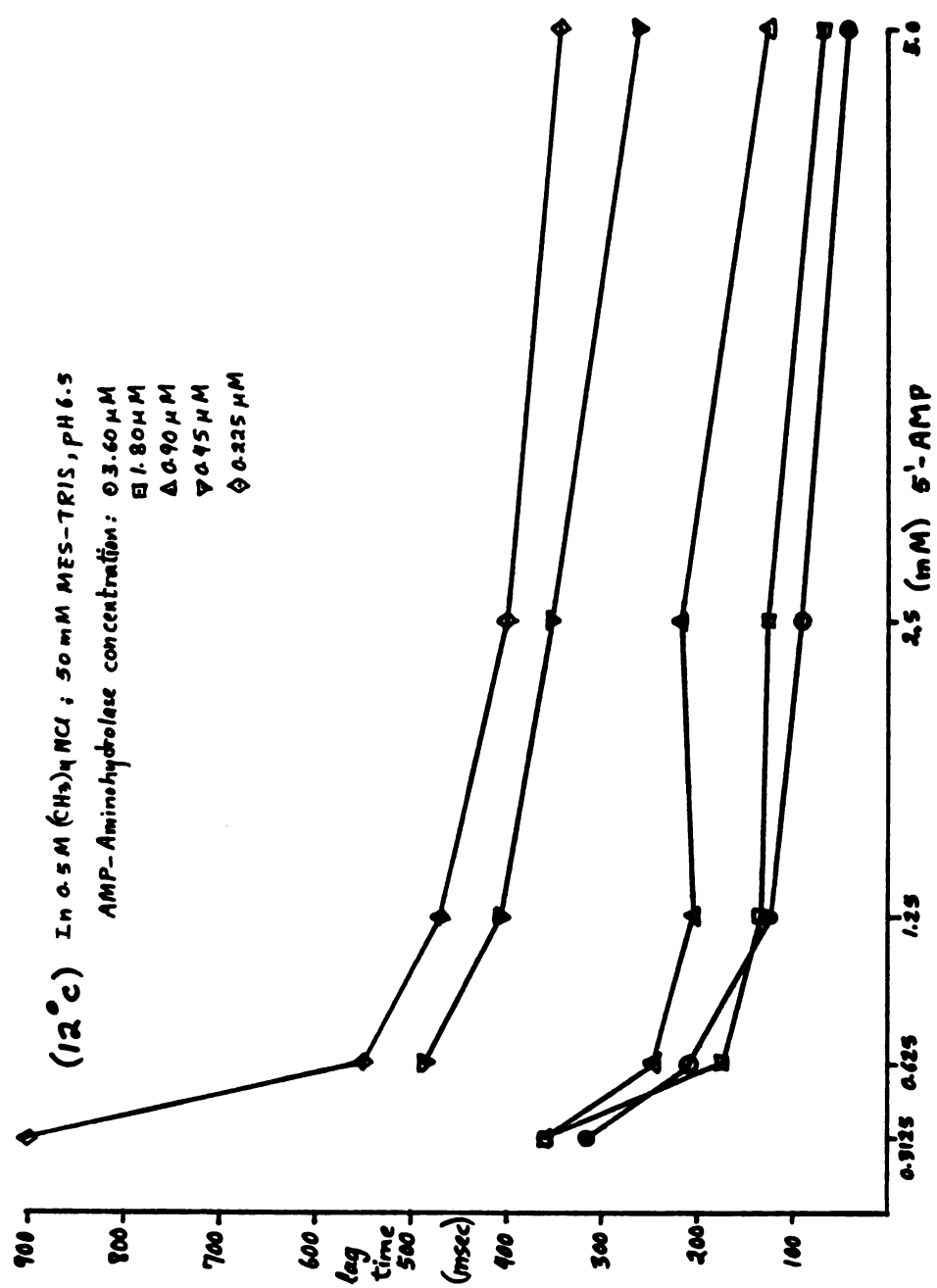

Figure 5.12. Lag Time as a Function of 5'-AMP at 12°C.

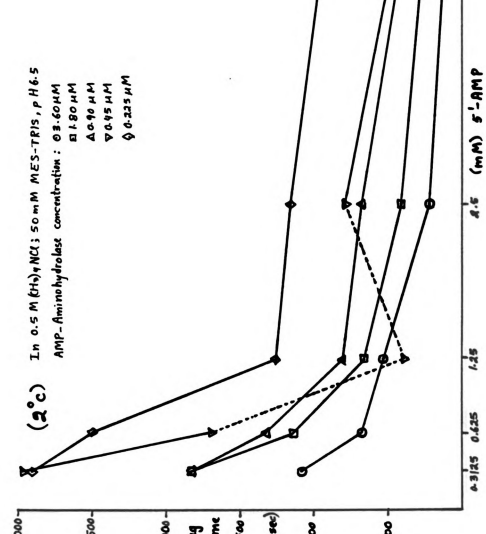

Figure 5.13. Lag Time as a Function of 5'-AMP at 2°C.

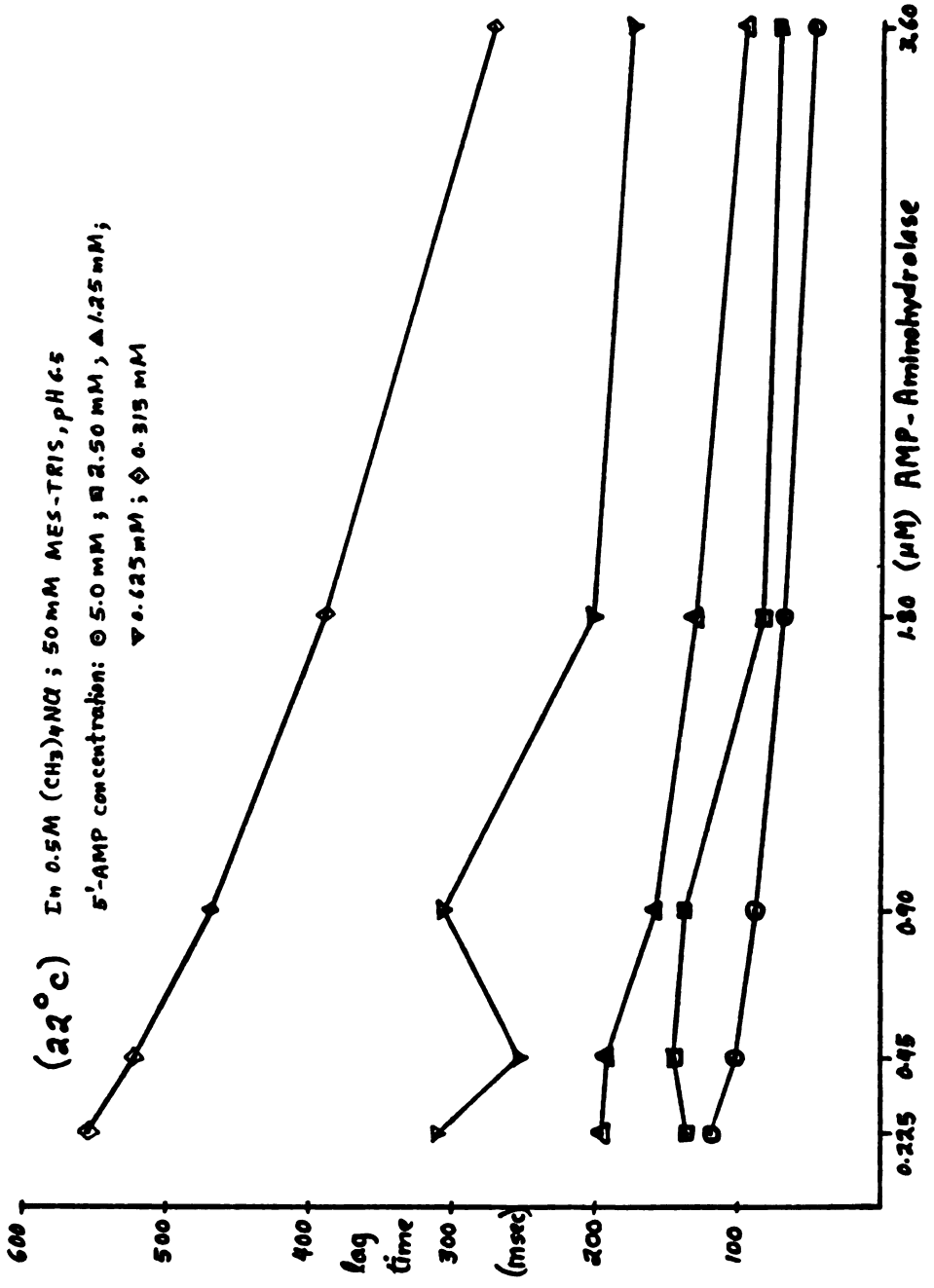

Figure 5.14. Lag Time as a Function of AMP-Aminohydrolase at 22°C.

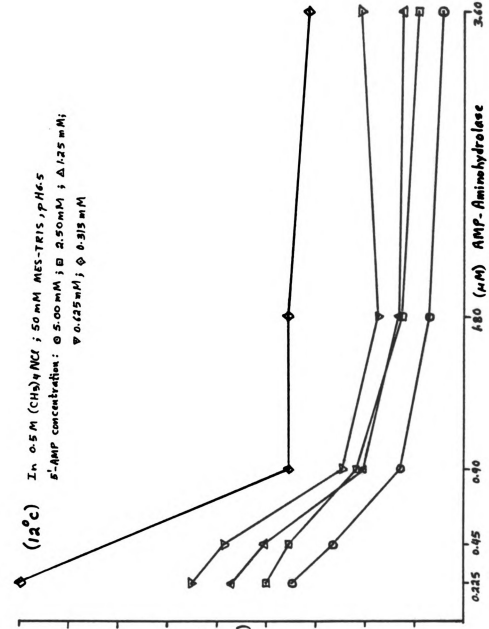

Figure 5.15. Lag Time as a Function of AMP-Aminohydrolase at 12°C.

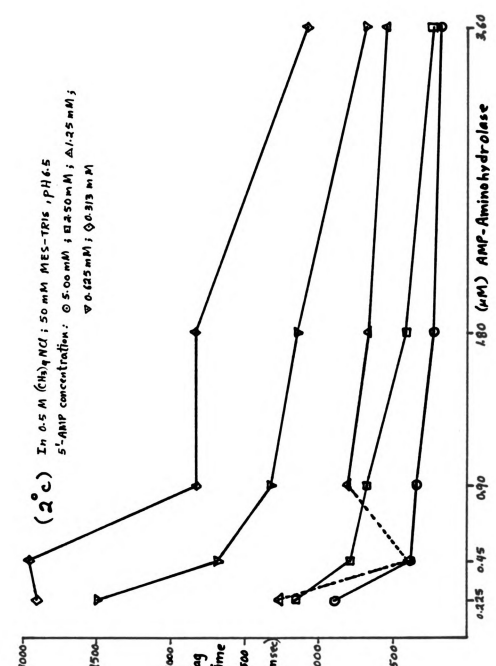

Figure 5.16. Lag Time as a Function of AMP-Aminohydrolase at 2°C.

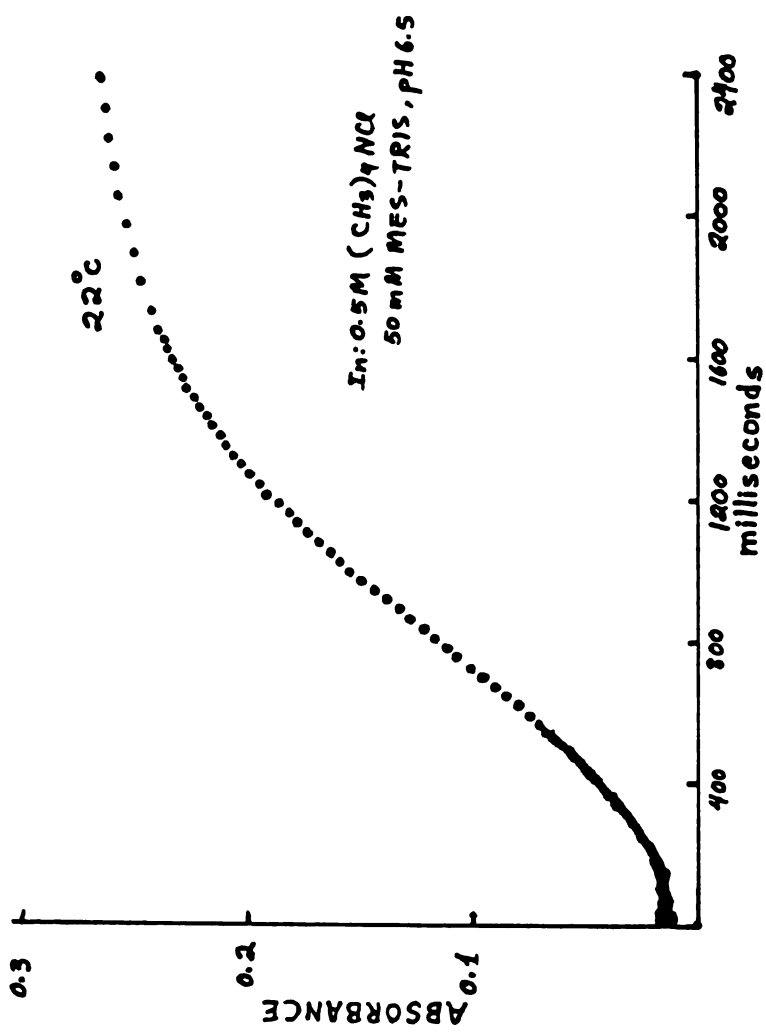

Figure 5.17. Hardcopy Output for the Reaction of 3.6 μM AMP-Aminohydrolase with 0.625 mM 5'-AMP, up to 2400 milliseconds, at 22°C.

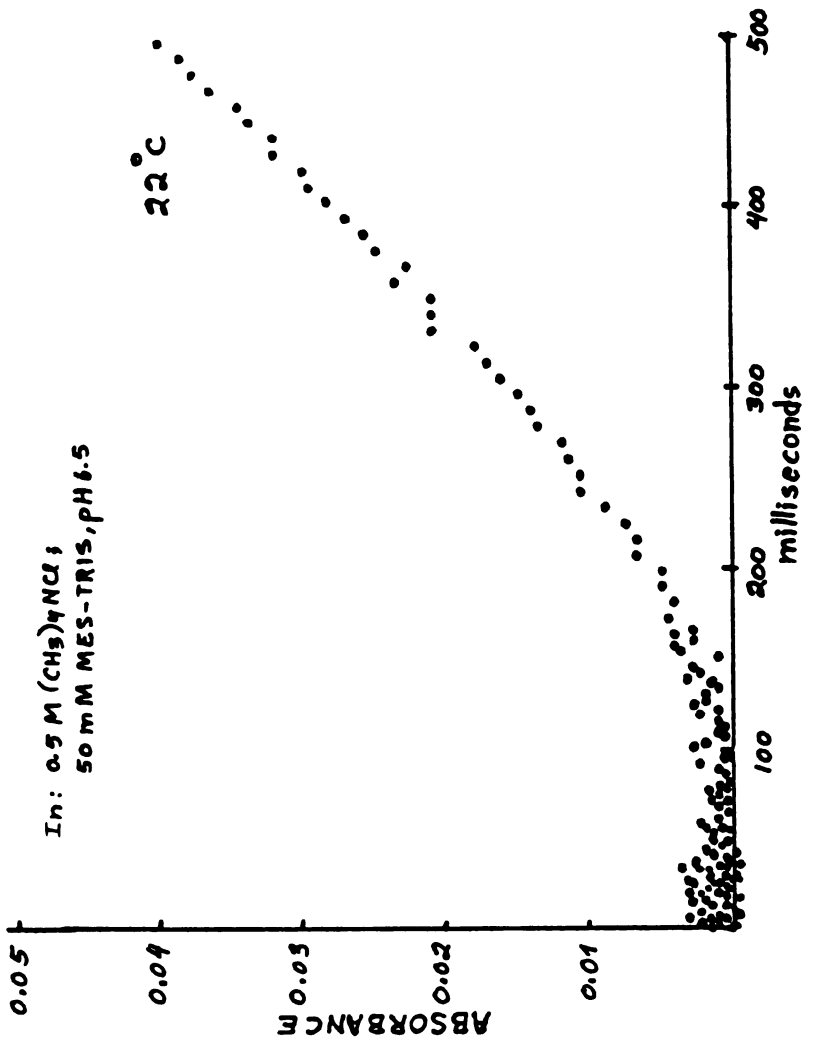

Figure 5.18. Hard copy Output for the Reaction of 3.6 μM AMP-Aminohydrolase with 0.625 mM 5'-AMP, up to 500 milliseconds, at 22°C.

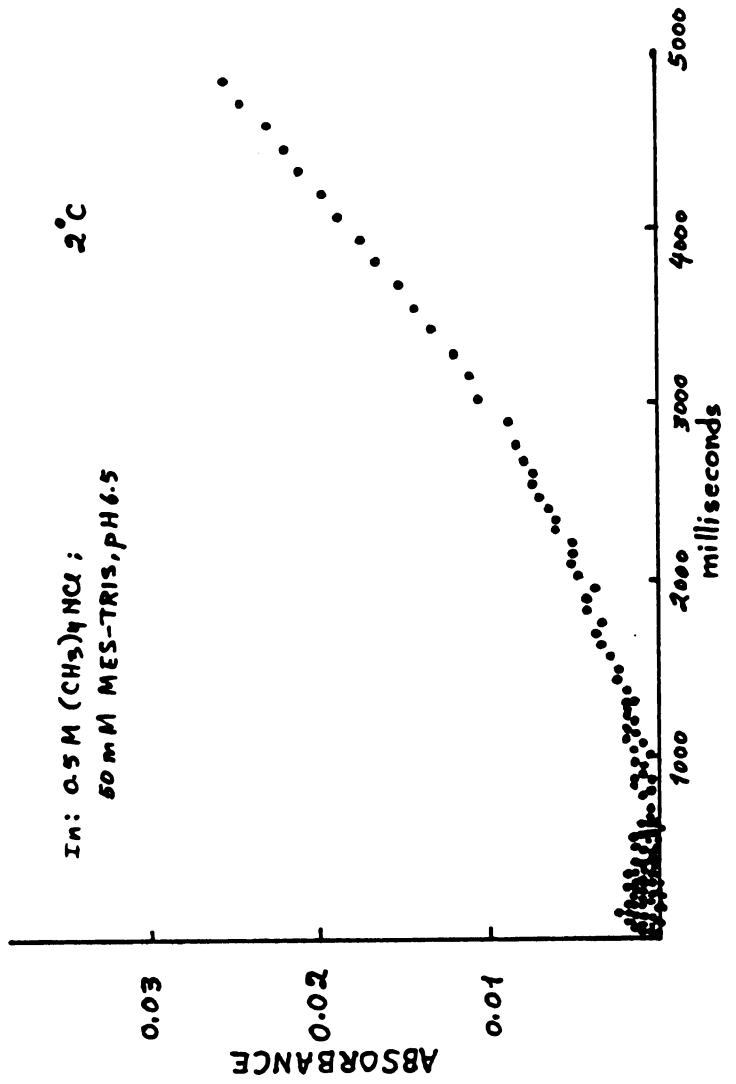

Figure 5.19. Hard Copy Output for the Reaction of 0.9 µM AMP-Aminohydrolase with 0.625 mM 5'-AMP, up to 5000 milliseconds, at 2°C.

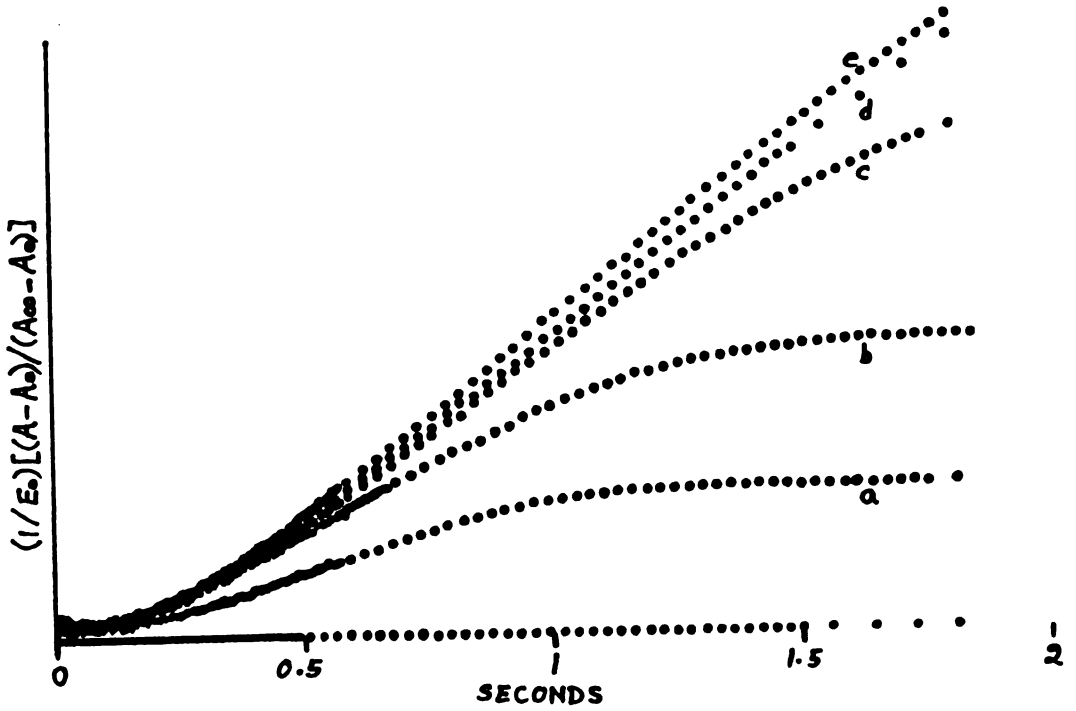

(In 0.5 M $(CH_3)_4NCl$; 50 mM MES-TRIS, pH 6.5) [AMP-Aminohydrolase concentration: (a) 3.60 μM; (b) 1.80 μM; (c) 0.90 μM; (d) 0.45 μM; (e) 0.225 μM]

Figure 5.20. Hard Copy Output for the Reactions of 2.5 mM 5'-AMP with 3.60, 1.80, 0.90, 0.45 and 0.225 μM AMP-Aminohydrolase; the Curves Display $(1/E_o)$-$[(A-A_o)/(A_\infty-A_o)]$ Versus Time.

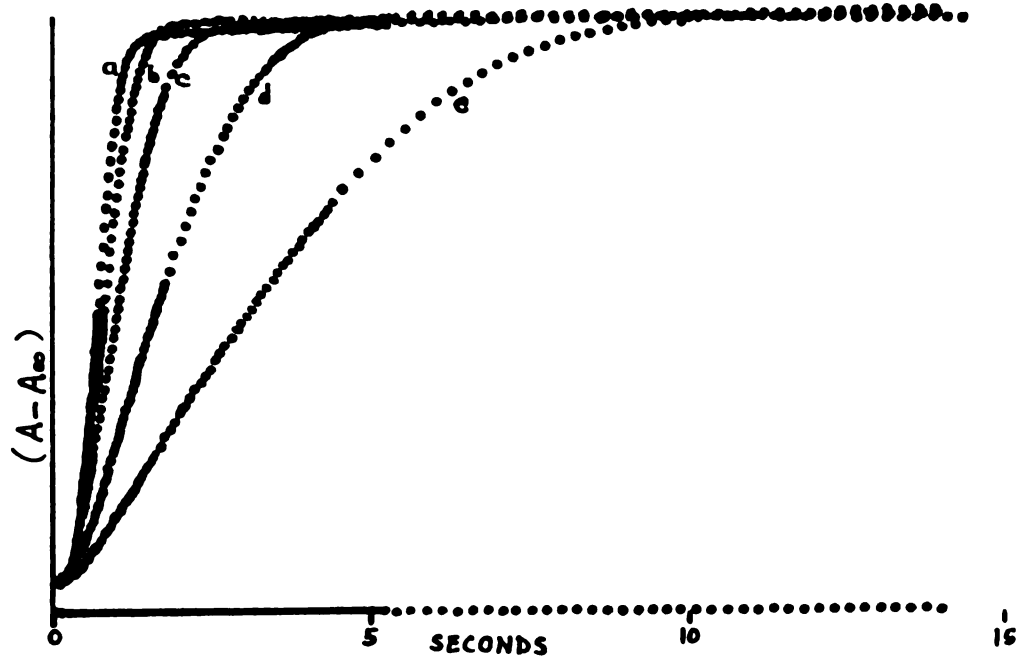

(In 0.5 M $(CH_3)_4NCl$; 50 mM MES-TRIS, pH 6.5) [AMP-Aminohydrolase concentration: (a) 3.6 μM; (b) 1.80 μM; (c) 0.90 μM; (d) 0.45 μM; (e) 0.225 μM]

Figure 5.21. Hard Copy Outputs for the Reactions of 2.5 mM 5'-AMP with 3.60, 1.80, 0.90, 0.45 and 0.225 μM AMP-Aminohydrolase; the Curves Display $(A-A_\infty)$ Versus Time.

these last two figures that the main effect of changing the enzyme concentration at constant substrate concentration is in changing the time scale of the reaction. The highest enzyme concentration (3.60 μM) requires the shortest time to completely turn-over 5'-AMP to IMP.

D.2. Shutoff Behavior

If the reaction kinetics follow the Michaelis-Menten law, after the initial activation of the enzyme, then it can be argued that, in essence, all the enzyme molecules are active. The extent of this activation should be a function of the initial enzyme and substrate concentration.

The reaction period extending from the time enzyme molecules are active (i.e., the end of the lag), at the steady state region, where product formation is proceeding at a maximum rate, and up to the end of the reaction, where substrate is completely depleted, is referred to here as the shutoff period. In the absence of other activators, as the substrate is depleted, the enzyme should return to its inactive confirmation, i.e., it shuts-off, and hence the Michaelis-Menten law should no longer hold.

The shutoff period for several enzyme and substrate concentrations were fitted to the Lineweaver-Burke plot. The results indicated that the Michaelis-Menten law was followed only when high (5 mM) concentrations of 5'-AMP were employed. Figure 5.22 shows one such plot, while Figure 5.23

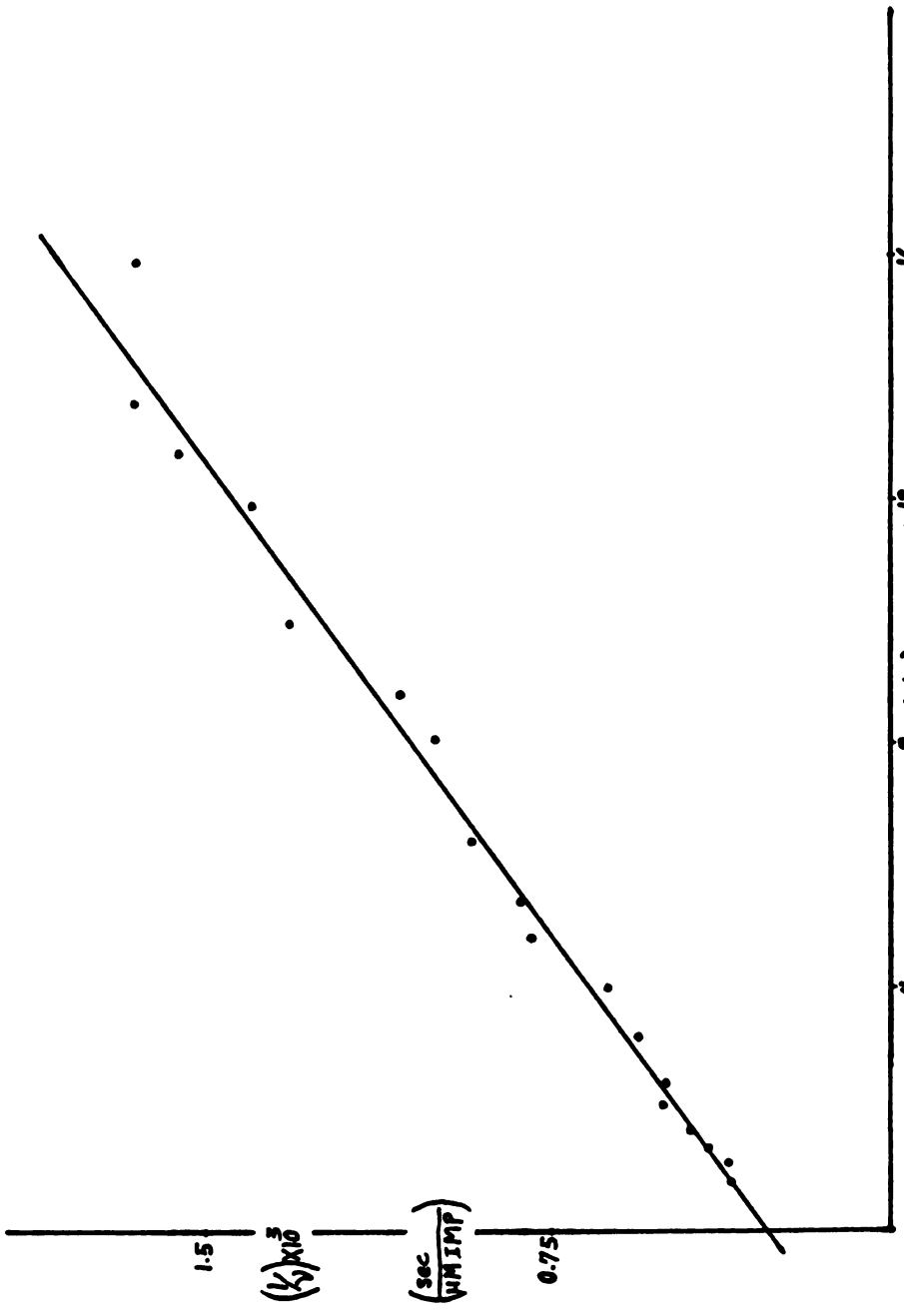

Figure 5.22. Lineweaver-Burke Plot for 0.9 μM AMP-Aminohydrolase Versus 5 mM 5'-AMP, in 0.5 M $(CH_3)_4NCl$, at 22°C and pH 6.5.

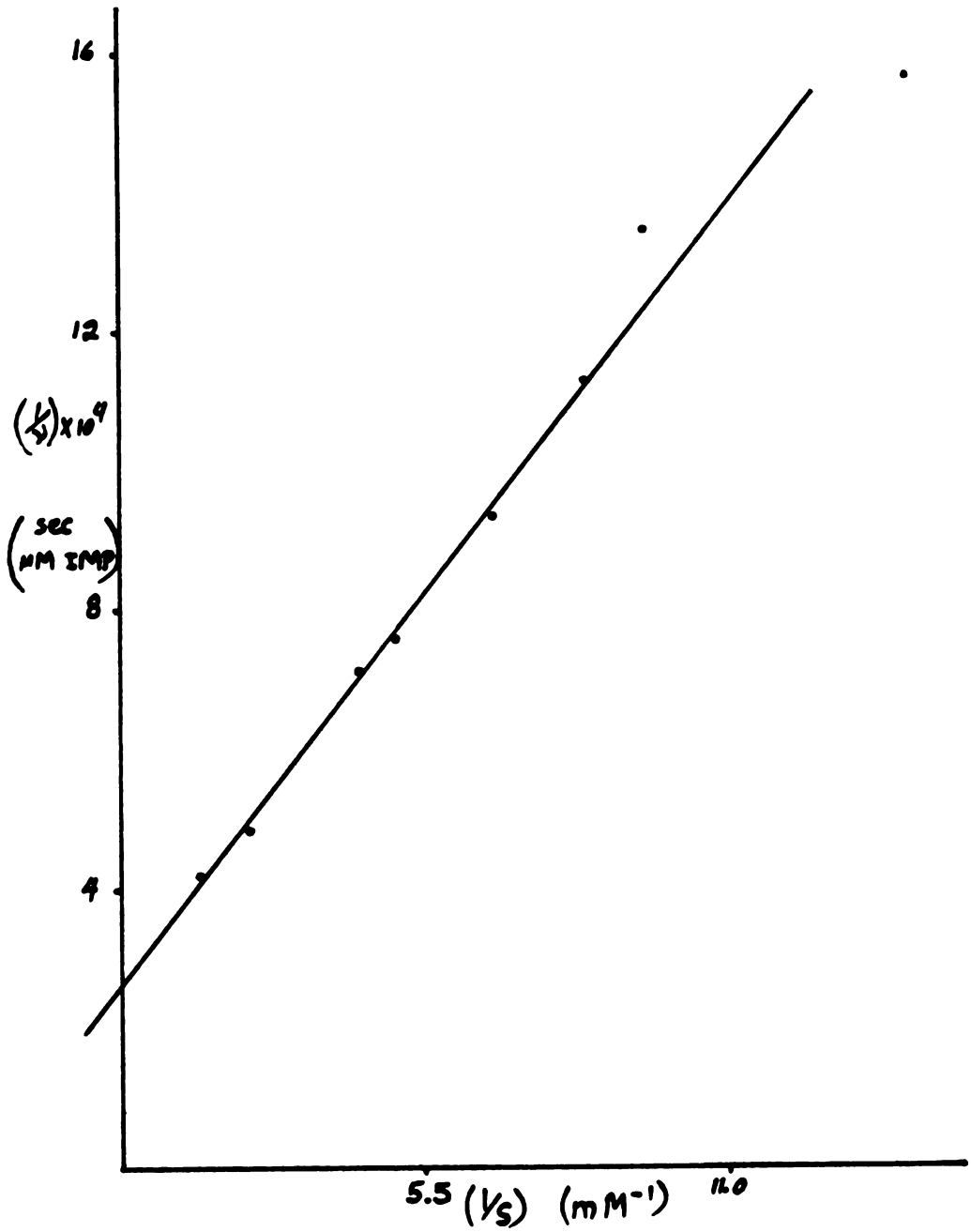

Figure 5.23. Lineweaver-Burke Plot for 0.9 µM AMP-Aminohydrolase versus 5 mM 5'-AMP, in 0.5 M KCl, at 22°C and pH 6.5.

shows the plot for a K^+ activated AMP-aminohydrolase. K_m was calculated from Figure 5.22 to be about 0.36 mM, while the turnover number was about 743 sec^{-1}, while from Figure 5.23, K_m was about 0.4 mM, and the turn-over number about 796 sec^{-1}.

D.3. Activation Energy

The Arrhenius relationship was used to calculate the activation energy (E_a) for the reaction of AMP-aminohydrolase with 5'-AMP. Turnover numbers calculated from four different temperatures (2°, 12°, 22° and 30°C) were used.

Figure 5.24, shows the Arrhenius plot of lnk versus 1/T. The calculated value of E_a was 16,500 calories per mole.

The turnover number at 30°C was calculated from an enzymatic reaction which contained 0.15 M KCl and 5 mM 5'-AMP, and assayed on a Beckman DU Spectrophotometer. The turnover numbers at the other three temperatures were calculated from the full time progress curves, obtained from the stopped-flow reactions of AMP-aminohydrolase pushed against 5 mM 5'-AMP, in 0.5 M $(CH_3)_4NCl$.

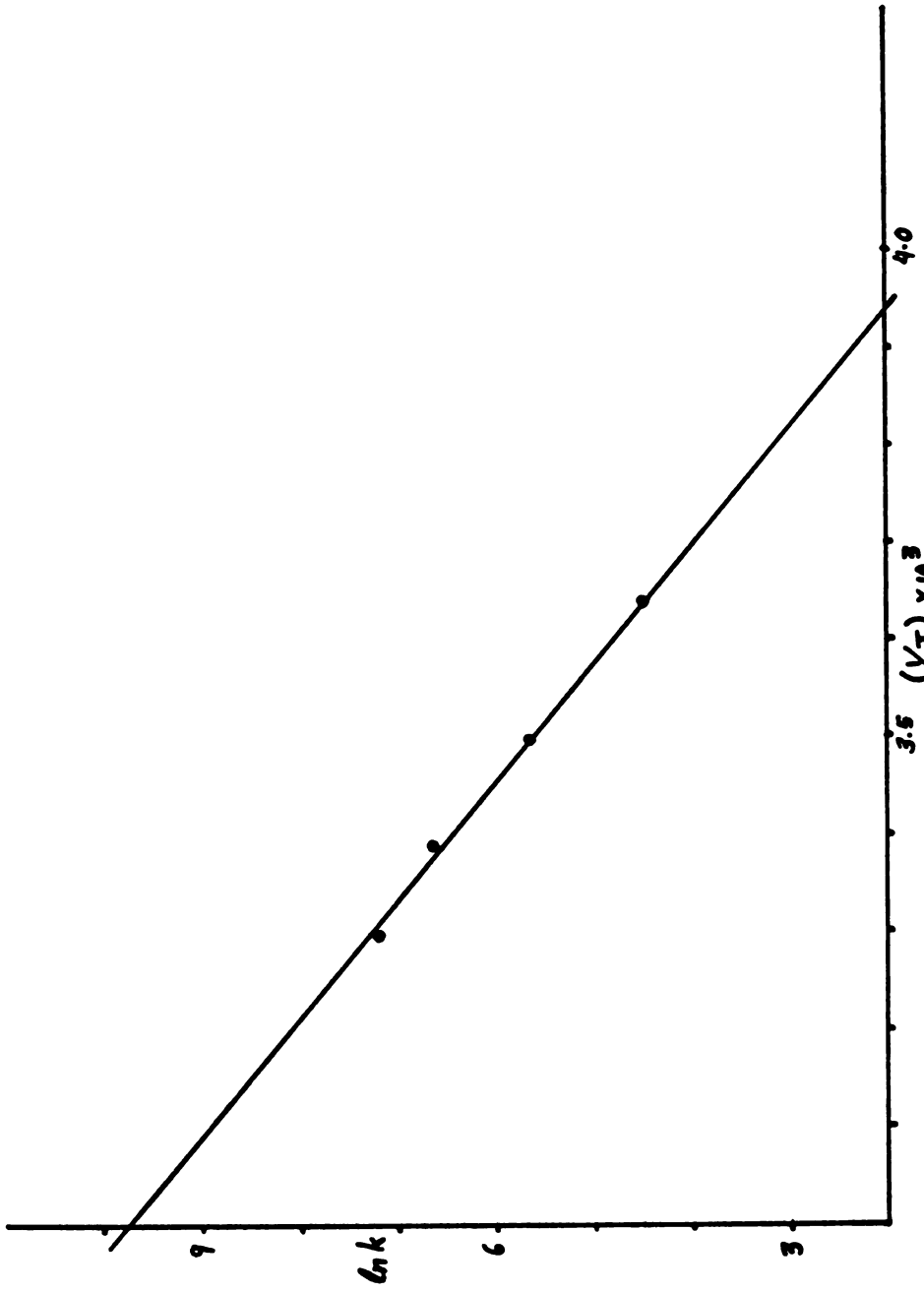

Figure 5.24. Arrhenius Plot for AMP-Aminohydrolase.

CHAPTER 6

MODELS FOR AMP-AMINOHYDROLASE

In order to propose mechanistic models for the catalytic reaction of K^+-free AMP-aminohydrolase with 5'-AMP, several points were taken into consideration, the essentials of which are as follows:

1. The dependence of lag times on both enzyme and substrate concentration,
2. In the presence and absence of monovalent cation activators, AMP-aminohydrolase exists in the tetramer configuration, at 20°C, as evidenced by sedimentation velocity experiments;
3. The effect of temperature on the enzyme constitution, and on the reaction progress;
4. The shutoff behavior is hyperbolic only for high substrate, and low enzyme concentration;
5. The product may be implicated as an effector in removing the lag, thus being an activator, but to a lesser extent than substrate;
6. The model must allow for substrate depletion throughout the course of the reaction.

A. Model A

This model assumes a nucleotide activator site(s) on the enzyme. This site is to be distinguished from a monovalent cation activator site. On a priori basis, it was assumed, that there exists one, and only one active conformation of AMP-aminohydrolase. This means that while the enzyme may exist in a variety of inactive conformations, each of these, has the potential of converting into one final active conformation, able to process substrate to product.

Evidence presented earlier in this work, showed that AMP-aminohydrolase activated by K^+ or 5'-AMP, has about the same turnover-number and K_m value. Smiley and Suelter (146), had earlier demonstrated that the V_{max} of the reaction is the same, in the presence and absence of KCl. Their findings were later confirmed by Coffee and Solano (111), who further reported that the K_m for the catalytic reaction is also the same, in the presence and absence of KCl.

Cooperativity between the subunits is not invoked in this model, as it had been shown by Pierce (32) and Suelter et al. (27) that enzymatic models can display sigmoidal kinetics even when cooperativity considerations are neglected.

This model represents an extension to the Suelter et al. (27) scheme with the inclusion of an isomerization step, from an inactive enzyme-substrate complex to an active

enzyme-substrate complex.

Model A is represented as follows:

$$\underline{\text{Step 1}} \quad - \quad E_i + S \overset{K_1}{\rightleftharpoons} E_iS \underset{k_2}{\overset{k_1}{\rightleftharpoons}} E_a$$

$$\underline{\text{Step 2}} \quad - \quad E_a + S \overset{K_m}{\rightleftharpoons} E_aS \xrightarrow{k_p} E_a + P$$

where (E_i), is the inactive enzyme; (S), the substrate; (E_a), the active enzyme; (P), the product; capital (K)'s are equilibrium constants, and small (k)'s are rate constants.

The first step in the model involves activation of the enzyme by substrate, while the second step is the Michaelis-Menten scheme for active enzyme. Thus K_m represents the Michaelis-Menten constant, and k_p the turnover-number. It was assumed that binding of substrate to inactive enzymes involves a fast equilibrium step. This is then followed by the slow conformational change of the enzyme, now bound to substrate, to its active conformation, after which Michaelis-Menten kinetics are followed.

The total concentration of active enzyme (E) is defined as:

$$E = E_a + E_aS$$

The working equations, used in KINFIT4, for this model

(see Appendix B) were as follows:

$$S = S_0 - P - E_0 - \frac{(S)(E)}{(K_m+S)} + \frac{K_1(E_0-E)}{(K_1+S)} \qquad (1)$$

$$\frac{dP}{dt} = k_p \frac{(S)(E)}{(K_m+S)} \qquad (2)$$

and,

$$\frac{dE}{dt} = k_1 \frac{(S)(E_0-E)}{(K_1+S)} - \frac{k_2(E)}{(1+S/K_m)} \qquad (3)$$

where (S_0) and (E_0) are the initial concentrations of substrate and enzyme respectively.

Initial estimates for KINFIT4 were as follows:

$k_p = 3000\ sec^{-1}$
$K_m = 0.3\ mM$
$K_1 = 0.6\ mM$
$k_1 = 1.0\ sec^{-1}$
$k_2 = 0.1\ sec^{-1}$

Simulation studies of this model were carried out, using the initial estimates of the equilibrium and rate constants, in addition to enzyme and substrate concentrations, as

input parameters into KINFIT4.

Full-time progress curves obtained from these simulations, indicated that the model is able to display both hyperbolic and sigmoidal behavior, depending on the initial estimates used.

Fitting of the simulated data was tested to determine how sensitive it was to the initial estimates. This was done by introducing initial estimates which were different (normally 5-10%) from the original input parameters used for simulation. Such procedure tested whether convergence to the original parameters was possible, and determined the standard error in the parameters which resulted from known amounts of noise on the data. Fitting of experimental data was attempted only when fitting of simulated data was successful. This procedure was routinely performed on all the models studied in this work.

The next step was to fit experimental data by using this model. Model A has five parameters (unknowns), and in order to adjust these simultaneously, KINFIT4 usually requires a large data base from which convergence tests are performed. However, in all such experimental (real) data fittings, the procedure adopted, as advised by Professor J. L. Dye, is to initially limit the number of unknowns. This is done by fixing one or more parameters, while allowing KINFIT4 to treat the remainder as unknowns. Following this procedure, one and two data sets were easily fitted with this model.

For example, a two-data set (the first containing 0.225 μM AMP-aminohydrolase, and 0.313 mM 5'-AMP; the second, 0.225 μM AMP-aminohydrolase and 5.0 mM 5'-AMP, both at 22°C) was fitted with only k_1, k_2 and k_p as unknowns, while holding K_1 and K_m fixed at 100.0 and 0.2 mM respectively. The values for K_1 and K_m were thus chosen, because they were found to give the best convergence (as evidenced by the randomness of the Residuals in KINFIT4) for this two-data set. The results were 96.3 ± 10.0 sec^{-1} for k_1; 5.8 ± 0.6 sec^{-1} for k_2; and 2614 ± 19 sec^{-1} for k_p.

Figures 6.1 and 6.2 show the KINFIT4 plots of the results for the first and second set respectively. As can be seen from the plots, the agreements of experimental points, marked by (x), and calculated points, marked by (o), are very good. The symbol (=) means an experimental and calculated point are within the same maximum relative change in any parameter during the last iteration for convergence to be assumed by KINFIT4.

However, the values 0.2 mM and 2614 sec^{-1} for K_m and k_p respectively, are lower than observed from experiment.

Next, nine-data sets were fitted simultaneously to the five parameters as unknowns. The nine-data sets included the initial concentrations of enzyme and substrate listed in Table 6.1. The reactions were those performed at 22°C.

Results for the best convergence were: 0.27 ± 0.013 M for K_1; 152.5 ± 19.4 sec^{-1} for k_1; 0.43 ± 0.071 sec^{-1}

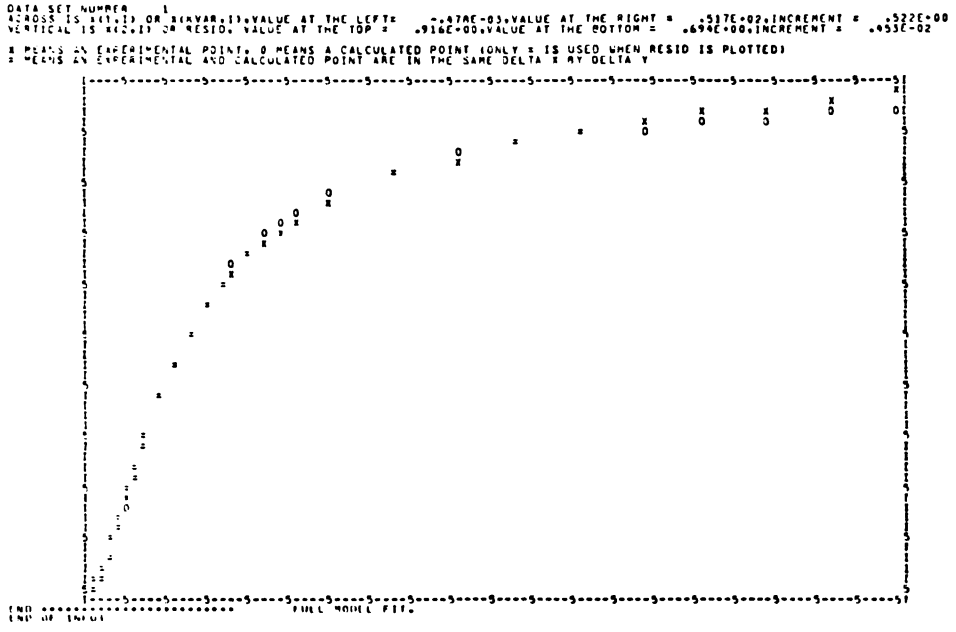

Figure 6.1. Model A, Two-Data Set Fitting; 0.225 μM AMP-Aminohydrolase with 0.3125 mM 5'-AMP, 22°C.

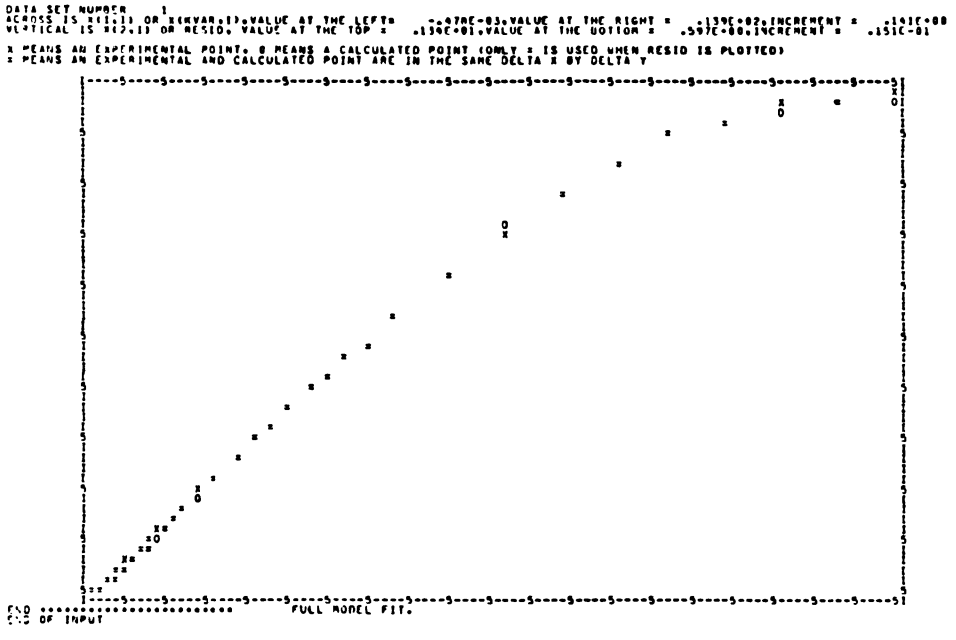

Figure 6.2. Model A, Two-Data Set Fitting; 0.225 μM AMP-Aminohydrolase with 5.0 mM 5'-AMP, 22°C.

Table 6.1. Nine-Data Sets Tested for Convergence by KINFIT4.

Data Set Number	Initial AMP-aminohydrolase Concentration (μM)	Initial 5'-AMP Conc. (mM)	Plot of KINFIT4 Results Shown in Figure:	
			Model A	MWC Model
1	0.225	0.31	6.3	6.13
2	0.225	1.25	6.4	6.14
3	0.225	5.0	6.5	6.15
4	0.90	0.31	6.6	6.16
5	0.90	1.25	6.7	6.17
6	0.90	5.0	6.8	6.18
7	3.60	0.31	6.9	6.19
8	3.60	1.25	6.10	6.20
9	3.60	5.0	6.11	6.21

All reactions were performed in 0.5 M $(CH_3)_4NCl$, 50 mM MES-TRIS buffer (pH 6.5), and at 22°C.

for k_2; 0.9 ± 0.19 mM for K_m; and 3649 ± 171 sec^{-1} for k_p. Figures 6.3 through 6.11 show the KINFIT4 plots of the final results. Values of 0.9 mM for K_m and 3649 sec^{-1} for k_p, are both higher than those calculated from experiment. With these nine-data sets, the "overall" fit is no longer as good as it was for the two data set. Compare Figure 6.1 with 6.3, and Figure 6.2 with 6.5. Such results are not unexpected if the model does not adequately describe the experimental behavior of the system. Further refinements of Model A were attempted. The primary one involved using the product as an additional activator for the enzyme; however, these attempts did not improve upon the original model, and were in fact less systematic than Model A.

B. The Monod, Wyman and Changeux Model (MWC)

The MWC model is an attractive "classical" model which has been shown to describe the action of many biological systems, of which the most notable is the allosteric binding of oxygen to the hemoglobin molecule (20).

This concerted (all or none) model accounts for positive cooperativity in a very simple and elegant manner. One of the assumptions made by the MWC model is that the same conformational state is stabilized by a variety of ligands. This point can further add to what was presented earlier in this chapter, where it was argued that whether activated

Figure 6.3. Model A, Nine-Data Set Fitting; 0.225 μM AMP-Aminohydrolase with 0.3125 mM 5'-AMP, 22°C.

Figure 6.4. Model A, Nine-Data Set Fitting; 0.225 μM AMP-Aminohydrolase with 1.25 mM 5'-AMP, 22°C.

Figure 6.5. Model A, Nine-Data Set Fitting; 0.225 μM AMP-Aminohydrolase with 5.0 mM 5'-AMP, 22°C.

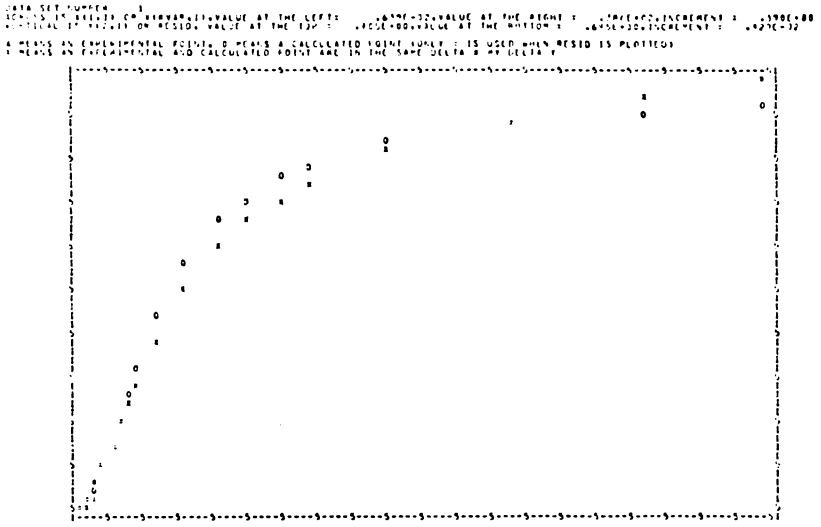

Figure 6.3

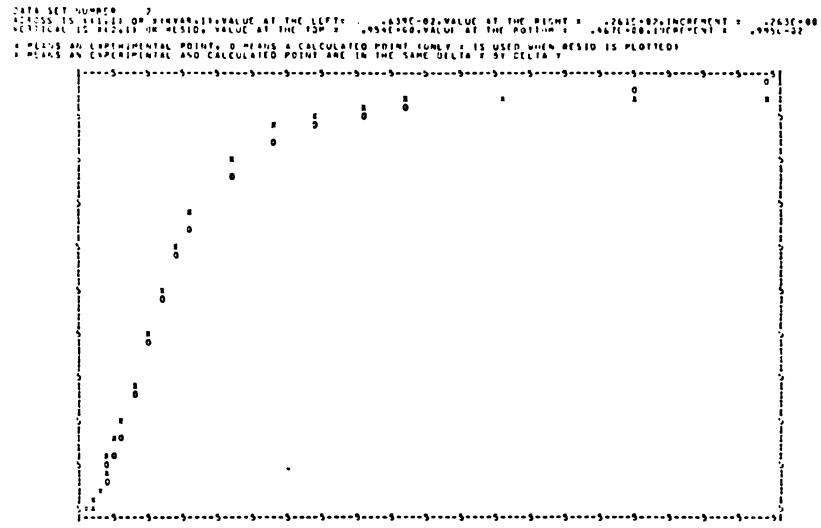

Figure 6.4

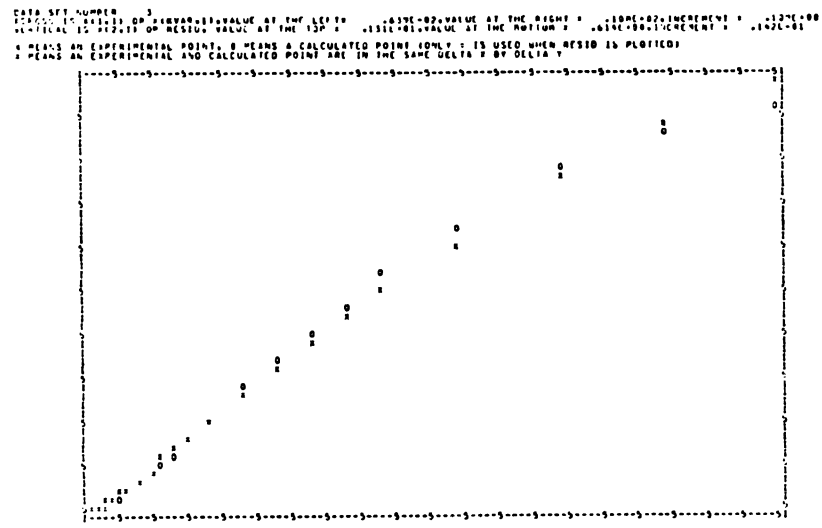

Figure 6.5

Figure 6.6. Model A, Nine-Data Set Fitting; 0.90 μM AMP-Aminohydrolase with 0.3125 mM 5'-AMP, 22°C.

Figure 6.7. Model A, Nine-Data Set Fitting; 0.9 μM AMP-Aminohydrolase with 1.25 mM 5'-AMP, 22°C.

Figure 6.8. Model A, Nine-Data Set Fitting; 0.9 μM AMP-Aminohydrolase with 5.0 mM 5'-AMP, 22°C.

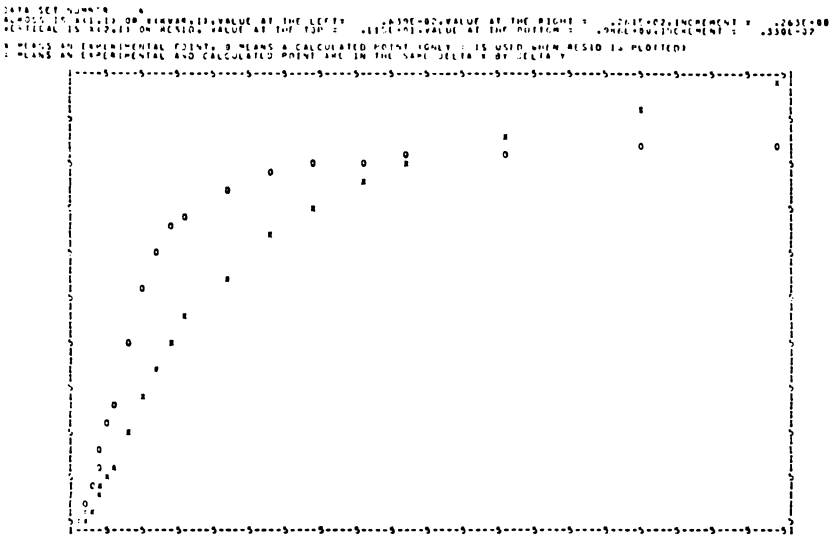

Figure 6.6

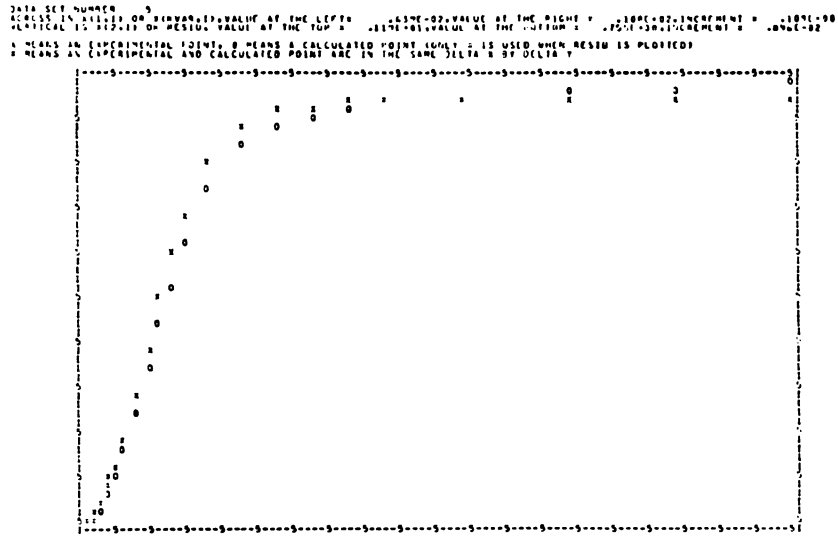

Figure 6.7

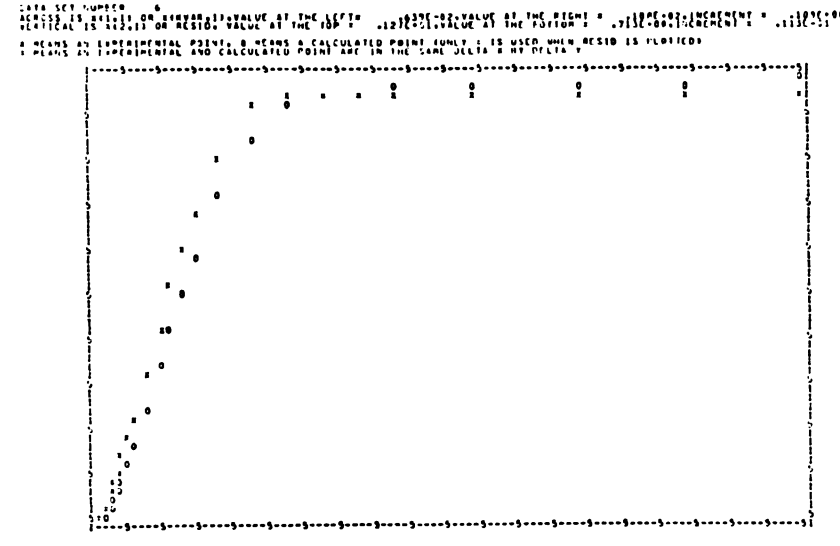

Figure 6.8

Figure 6.9. Model A, Nine-Data Set Fitting; 3.60 μM AMP-Aminohydrolase with 0.3125 mM 5'-AMP, 22°C.

Figure 6.10. Model A, Nine-Data Set Fitting; 3.60 μM AMP-Aminohydrolase with 1.25 mM 5'-AMP, 22°C.

Figure 6.11. Model A, Nine-Data Set Fitting; 3.60 μM AMP-Aminohydrolase with 5.0 mM 5'-AMP, 22°C.

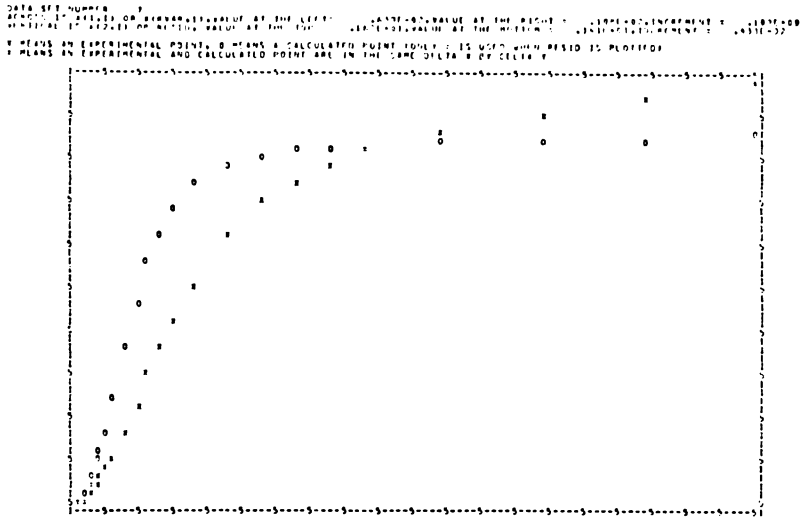

Figure 6.9

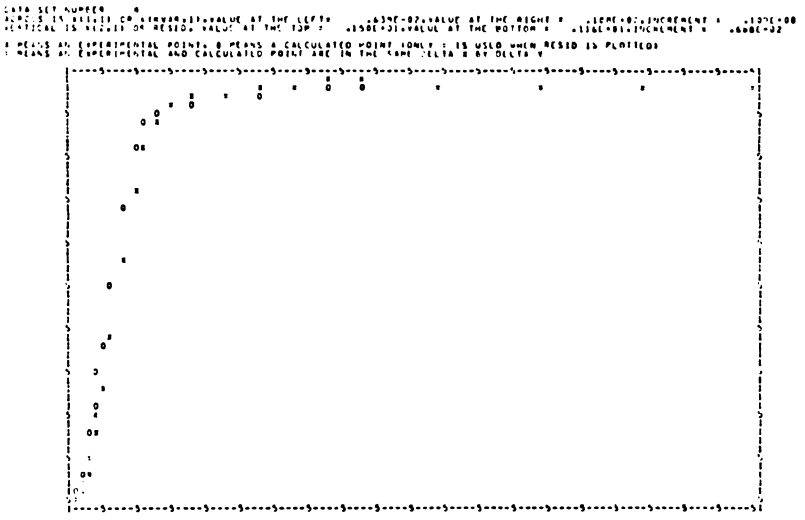

Figure 6.10

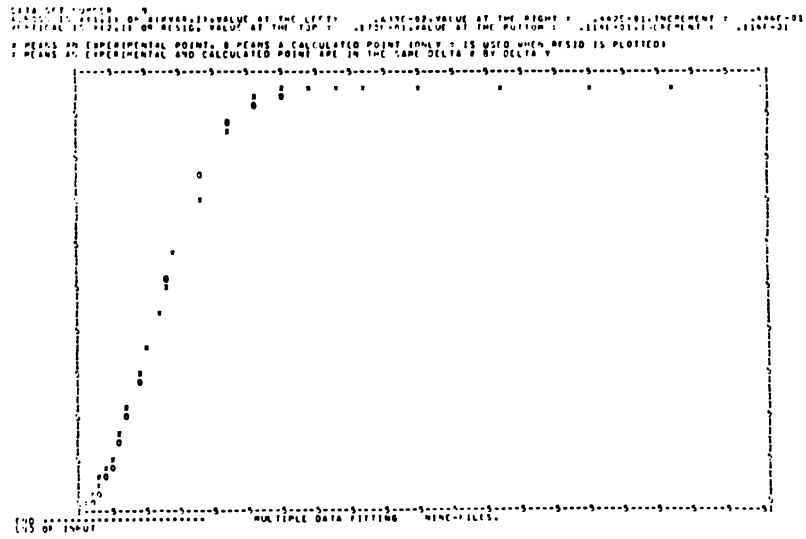

Figure 6.11

by K^+ or 5'-AMP, the final catalytically active conformation of AMP-aminohydrolase is the same.

Ellis and Sturtevant (28) reported that they were able to fit their experimental data, for activation of AMP-aminohydrolase by substrate, to the MWC model. However, as mentioned earlier, they assumed the enzyme to be composed of six subunits, and also neglected to account for substrate depletion in their analysis. In this present work, it was felt that the MWC model merited further investigation, but with the "correct" assumption that AMP-aminohydrolase is tetrameric, and that substrate depletion be accounted for during the entire course of the reaction.

The simplest MWC scheme with positive cooperativity involves one active, and one activator site per subunit. This was adopted here as the working model for AMP-aminohydrolase.

Therefore, a tetrameric enzyme such as AMP-aminohydrolase would have the MWC scheme shown in Figure 6.12 (page 109):

In Figure 6.12, k's represent rate constants; K's, dissociation equilibrium constants; E, inactive enzyme; E', active enzyme; S, substrate; ES_n, in active enzyme-substrate complex; E'Sn, active enzyme substrate complex, with n = 0,4.

It is assumed that only the active enzyme manifold can process substrate to product. The total "active" enzyme

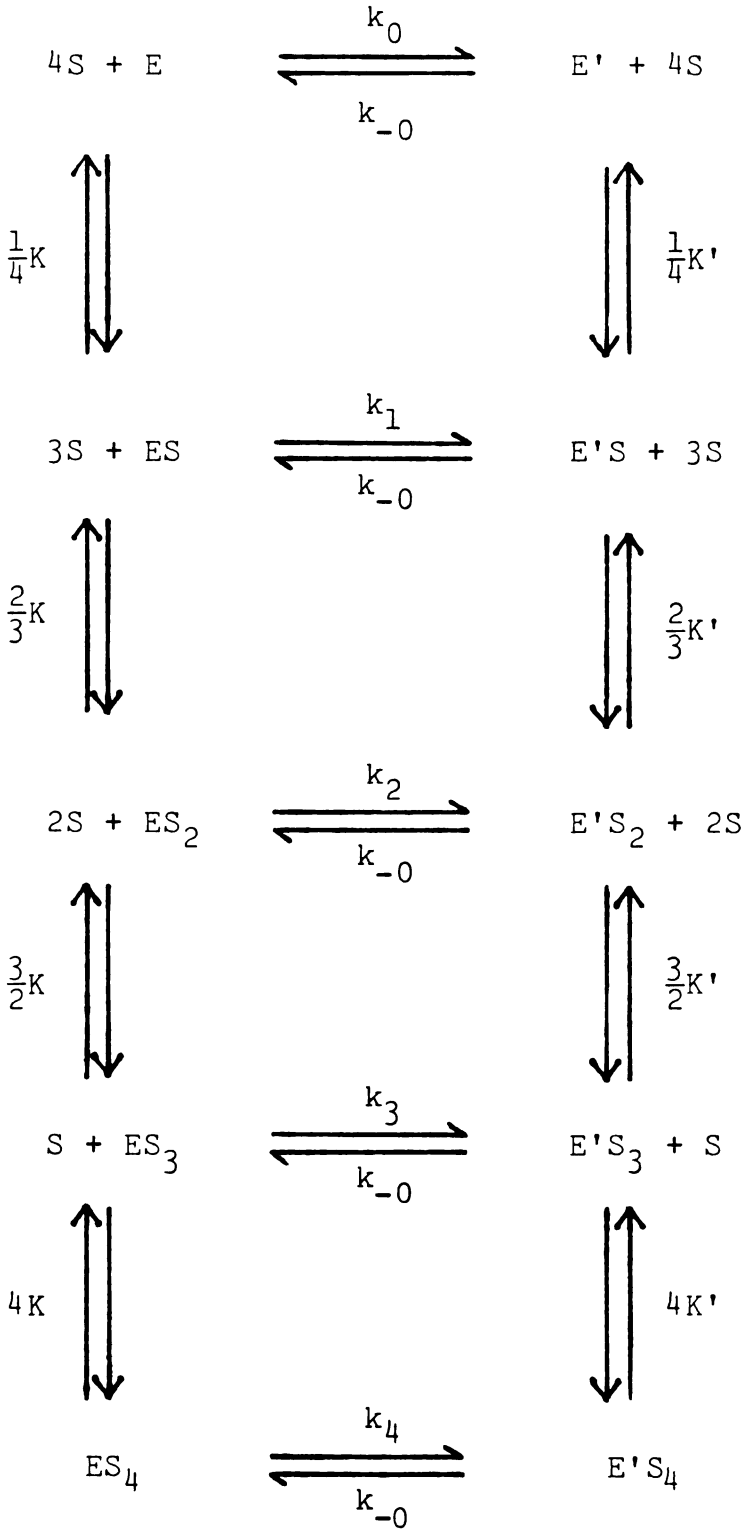

Figure 6.12. MWC Model for AMP-aminohydrolase.

concentration, E_0', is:

$$E_0' = E' + E'S + E'S_2 + E'S_3 + E'S_4 \qquad (1)$$

The total "inactive" enzyme concentration, E_0, is:

$$E_0 = E + ES + ES_2 + ES_3 + ES_4 \qquad (2)$$

Then, the initial enzyme concentration, $(E_0)_t$, is:

$$(E_0)_t = E_0 + E_0' \qquad (3)$$

Following enzyme activation by substrate is the Michaelis-Menten scheme:

$$E_0' + S \underset{}{\overset{K_m}{\rightleftharpoons}} E_0'S \xrightarrow{k_p} E_0' + P \qquad (4)$$

where (K_m) is the Michaelis-Menten constant; (k_p), the turnover number; (S), the substrate and (P), the product.

The rate of product formation is then

$$\frac{dP}{dt} = k_p \sum_{i=0}^{4} (E'S_i)(S) \qquad (5)$$

The working equation for KINFIT4 (see derivation in

Appendix C) is:

$$\frac{dP}{dt} = \frac{k_p(E_0')_\infty(1-e^{-k't})}{(1+K_m/S)} \tag{6}$$

where,

$$k' = B + k_{-0} \tag{7}$$

and

$$(E_0')_\infty = \frac{(B)(E_0)_t}{(B+k_{-0})} \tag{8}$$

with

$$B = k_0 \left[\frac{1+S/K'}{1+S/K}\right]^4 \tag{9}$$

and,

$$S = S_0 - P \tag{10}$$

Thus the familiar Michaelis-Menten equation for (dP/dt) is now modulated by $(E_0')_\infty$ and an exponential.

This model has six unknowns. To determine this many parameters, it was necessary to use the multiple data set

version of KINFIT4 from the start. Nine-data sets were thus simultaneously fitted to Equation (6), after the simulations, and the fittings of simulated data tests were carried out. The enzyme and substrate concentrations for these nine-data sets were the same ones used for Model A, and are listed in Table 6.1.

One set of initial estimates of the unknowns, for which convergence occurred in KINFIT4 were:

$k_0 = 1 \times 10^{-4}$ sec^{-1}

$k_{-0} = 0.1$ sec^{-1}

$K' = 0.1$ mM

$K = 1.0$ mM

$K_m = 0.1$ mM

$k_p = 1000$ sec^{-1}

Thus initially at equilibrium, when no substrate is present, the conformational change of the enzyme from inactive to active, was assumed to proceed at a very slow rate (k_0); whereas the reverse rate (k_{-0}) was assumed to be fast. The dissociation equilibrium constant for the active manifold (K') was calculated from the half-life of the activation, and was found to be about the same order of magnitude as K_m. The dissociation equilibrium constant for the inactive manifold (K) was initially set to be 10-fold greater than (K'). (K) must necessarily be greater than (K') in order

for activation to occur. Cooperativity occurs as a result of the statistics imposed by the model.

Results for the best convergence obtained were as follows:

$k_0 = 0.18 \times 10^{-3} \pm 0.26 \times 10^{-3}$ (sec^{-1})

$k_{-0} = 0.95 \times 10^{-1} \pm 0.20 \times 10^{-1}$ (sec^{-1})

$K' = 0.077 \pm 0.039$ (mM)

$K = 1.29 \pm 0.34$ (mM)

$K_m = 0.83 \pm 0.19$ (mM)

$k_p = 3066 \pm 162$ (sec^{-1})

Figures 6.13 through 6.21 show the KINFIT4 plots of the final results. As can be seen from the plots, the fits are not good for all the concentrations employed, indicating that while the (MWC) scheme used here is able to display the general trend of the experimental data, it is not acceptable overall. Still, the (K_m) value predicted by this model was in the same order of magnitude as the experimental (K_m), while the turnover number (k_p) predicted was the same as that obtained from experiment for the tetramer.

Some refinements for this MWC scheme were attempted. The primary ones involved using the product as an additional activator for the enzyme. However, the attempts proved inconclusive, and did not improve upon the original model.

Figure 6.13. MWC Model, Nine-Data Set Fitting; 0.225 μM AMP-Aminohydrolase with 0.3125 mM 5'-AMP, 22°C.

Figure 6.14. MWC Model, Nine-Data Set Fitting; 0.225 μM AMP-Aminohydrolase with 1.25 mM 5'-AMP, 22°C.

Figure 6.15. MWC Model, Nine-Data Set Fitting; 0.225 μM AMP-Aminohydrolase with 5.0 mM 5'-AMP, 22°C.

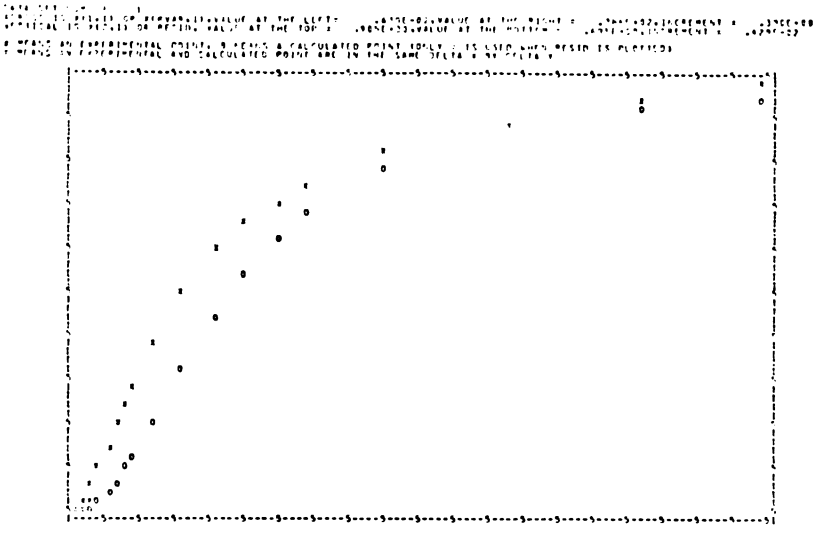

Figure 6.13

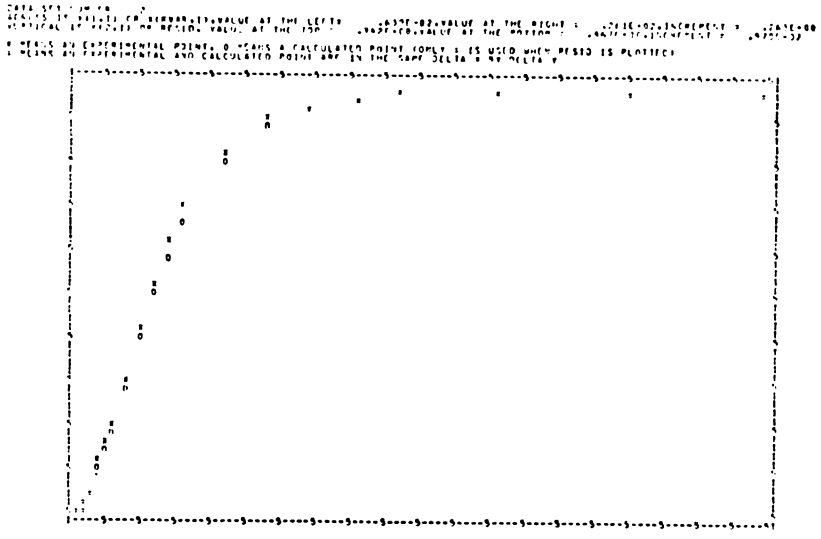

Figure 6.14

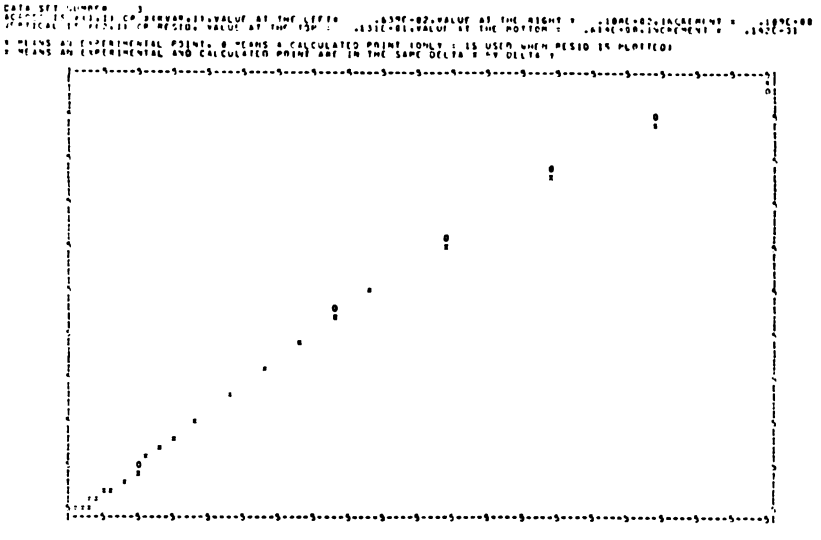

Figure 6.15

Figure 6.16. MWC Model, Nine-Data Set Fitting; 0.90 μM AMP-Aminohydrolase with 0.3125 mM 5'-AMP, 22°C.

Figure 6.17. MWC Model, Nine-Data Set Fitting; 0.90 μM AMP-Aminohydrolase with 1.25 mM 5'-AMP, 22°C.

Figure 6.18. MWC Model, Nine-Data Set Fitting; 0.90 μM AMP-Aminohydrolase with 5.0 mM 5'-AMP, 22°C.

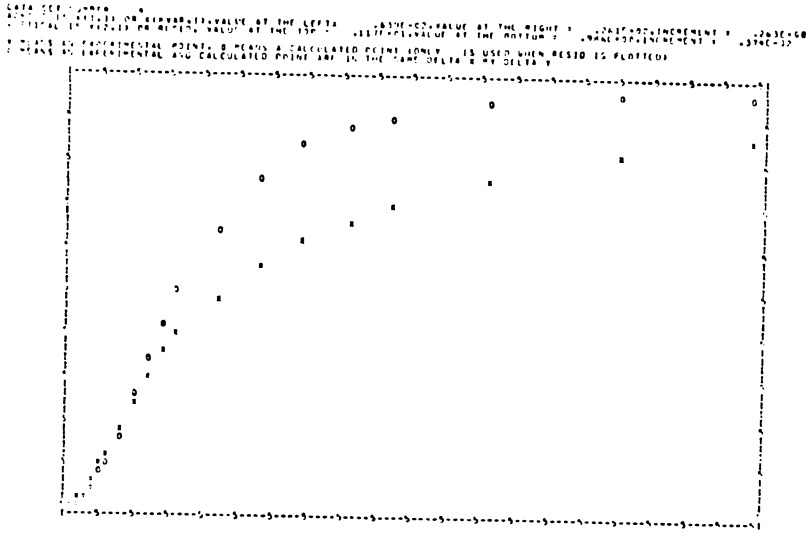

Figure 6.16

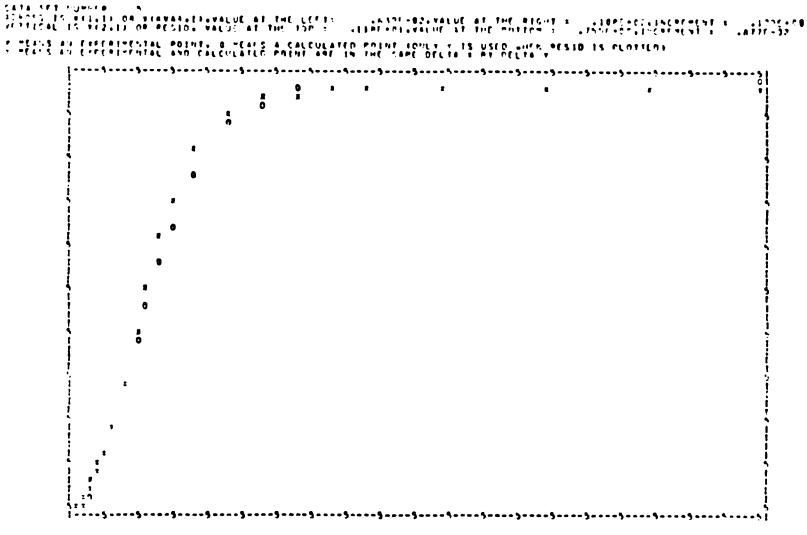

Figure 6.17

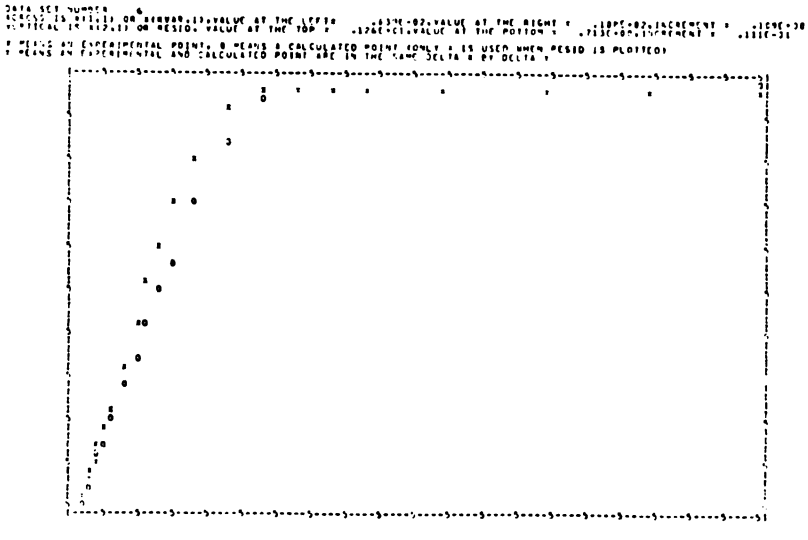

Figure 6.18

Figure 6.19. MWC Model, Nine-Data Set Fitting; 3.60 μM AMP-Aminohydrolase with 0.3125 mM 5'-AMP, 22°C.

Figure 6.20. MWC Model, Nine-Data Set Fitting; 3.60 μM AMP-Aminohydrolase with 1.25 mM 5'-AMP, 22°C.

Figure 6.21. MWC Model, Nine-Data Set Fitting; 3.60 μM AMP-Aminohydrolase with 5.0 mM 5'-AMP, 22°C.

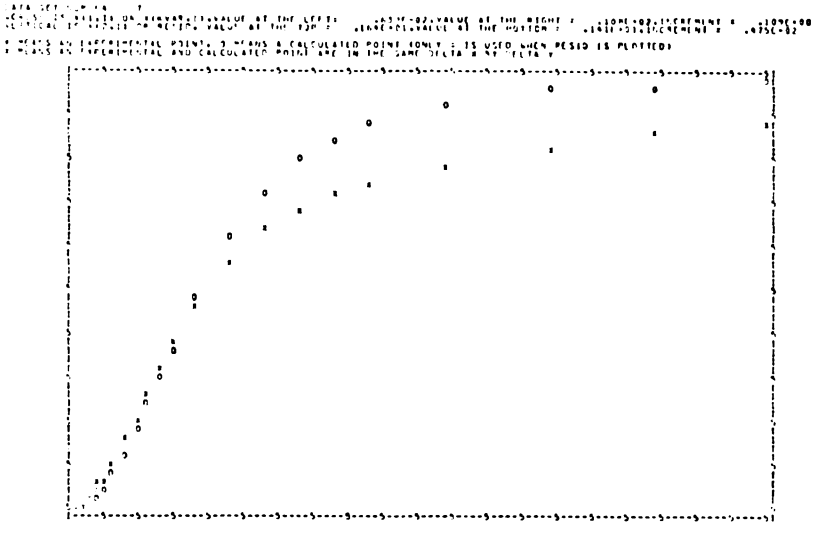

Figure 6.19

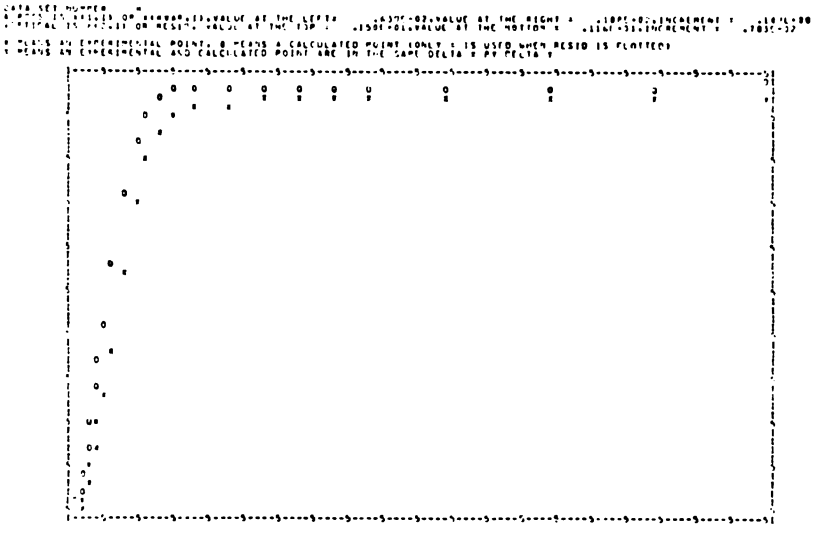

Figure 6.20

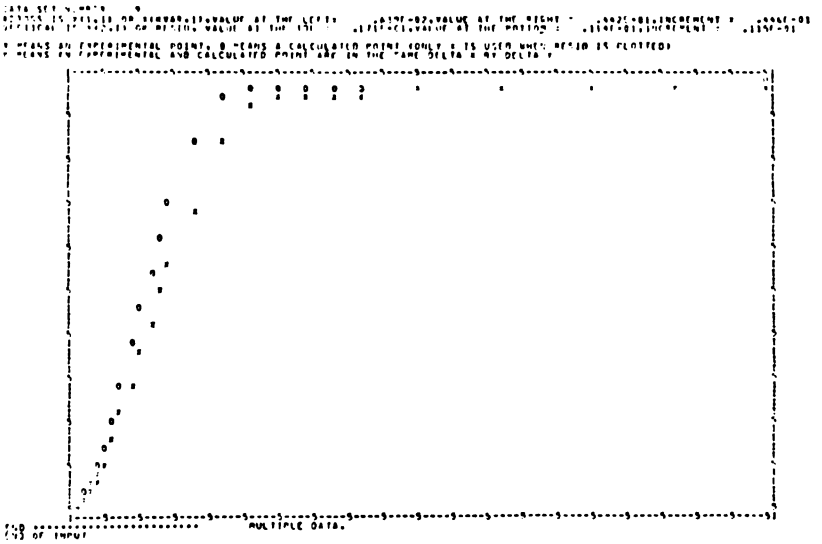

Figure 6.21

The difficulty one encounters in attempting to propose detailed models for enzymatic mechanisms is that the number of parameters (unknowns) to be determined becomes too large, even for relatively simple models. In addition, the assignment of proper initial values for these parameters is often difficult, due to the lack of experimental evidence to support such assignments.

Enzyme systems such as AMP-aminohydrolase present yet additional difficulties, since no detectable intermediates are available, from which additional information could then add some degree of certainty to a proposed mechanism.

C. Phenomenological Model (Model B)

Modelling thus far has included one model (Model A) whose scheme did not address cooperativity effects, and one which did (MWC Model). While both models were successful in describing the overall experimental behavior for the catalytic reaction of K^+-free AMP-aminohydrolase with 5'-AMP, they were not able to exactly fit all the individual reactions for the various enzyme and substrate concentrations employed.

The phenomenological model (Model B) which includes apparent cooperativity effects in its scheme, is a generalization of the Suelter *et al.* (27) model, with an exponential turn on. In this model, the enzyme is assumed to exist in two manifolds, inactive E_i, and active E_a.

Each manifold may exist in a number of enzyme forms, which may or may not have substrate bound to it.

The key to the first step (activation) is that substrate binds to inactive enzyme to activate it in a pseudo first order process, which may have a complex dependence on [S] and/or [E]. Likewise, the reverse process (deactivation) is assumed to occur in a similar fashion by a pseudo first order process.

Model (B) is represented schematically by:

Step 1 $$E_i + S \underset{k_2}{\overset{k_1}{\rightleftharpoons}} E_a$$

Step 2 $$E_a + S \overset{K_m}{\rightleftharpoons} E_aS \xrightarrow{k_p} E_a + P$$

in which k_1 and k_2 are phenomenological rate constants which may depend on [S] and [E], and where E_i is the inactive enzyme; S, the substrate; E_a the active enzyme; E_aS, the active enzyme-substrate complex; P, the product; K_m, the Michaelis-Menten constant; and k_p, the turnover number.

Hence, Step 1 involves the apparent cooperative activation of the enzyme, while Step 2 is the Michaelis-Menten scheme.

The initial enzyme concentration (E_0) is

$$E_0 = E_i + E_a + E_aS \qquad (1)$$

Let the total active enzyme concentration (E_a^t) be:

$$E_a^t = E_a + E_aS \tag{2}$$

then

$$E_0 = E_i + E_a^t \tag{3}$$

and

$$\frac{d(E_a^t)}{dt} = k_1 (E_i)(S) - k_2 (E_a^t) \tag{4}$$

Substituting the value of (E_i) from (3) into (4) yields:

$$\frac{d(E_a^t)}{dt} = k_1(E_0)(S) - [k_2 + k_1(S)](E_a^t) \tag{5}$$

Define,

$$k' = k_2 + k_1(S) \tag{6}$$

Then

$$\frac{d(E_a^t)}{dt} = k_1(E_0)(S) - k'(E_a^t) \tag{7}$$

The rate of product formation is:

$$\frac{dP}{dt} = \frac{k_p(E_a^t)}{(1 + K_m/S)} \qquad (8)$$

and

$$S = S_0 - P \qquad (9)$$

where (7), (8) and (9) are the working KINFIT4 equations.

Apparent cooperativity effects are thus embodied in the first order rate constant (k').

The behavior of Model B is described by the four parameters k_1, k_2, K_m and k_p. Values for these four parameters when employed in Equations (7), (8) and (9) should then map out the progress of product as a function of time, if the scheme is to successfully interpret the experimental data.

Experimental evidence presented earlier in this work has indicated that at 22°C, the Michaelis-Menten constant (K_m) is in the order of 0.35 mM, while that of the turnover number (k_p) is about 3000 sec^{-1}. The values of (k_p) at 12°C and 2°C were thus calculated from the Arrhenius relationship, by using the activation energy value of 16,500 calories per mole determined earlier. Thus the value of (k_p) at 12°C was calculated to be 1158 sec^{-1}, while at 2°C it was 379 sec^{-1}. These values were subsequently used in

fitting the experimental data. The value of the Michaelis-Menten constant (K_m) was not assumed to vary appreciably over the small range in temperature (2°C-22°C) at which the experiments were performed. This is because (K_m) is made up of a ratio of rate constants, and thus small changes in temperature should leave its overall value unchanged for the three temperatures.

Using the values of (K_m) and (k_p) shown above, it was then possible to reduce the number of unknowns in Model B to only two, namely (k_1) and (k_2). Individual files for all the pushes were fitted with KINFIT4. In all, twenty-five different AMP-aminohydrolase and 5'-AMP concentrations at each of the three temperatures (hence, a total of 75 combinations) were fitted to (k_1) and (k_2), while holding (K_m) and (k_p) at the levels indicated in the preceding paragraph.

Initial estimates were as follows:

$$k_1 = 1000 \text{ sec}^{-1}\text{M}^{-1}$$
$$k_2 = 2 \text{ sec}^{-1}$$

All the data fittings were successful. Tables 6.2, 6.3 and 6.4 show the results obtained. Figures 6.22, 6.23 and 6.24 are typical representations of KINFIT4 plots, for the fits obtained using Model B.

Results from Tables 6.2, 6.3 and 6.4 were used to

Table 6.2. Phenomenological Model, Data-Fitting Results at 2°C.

E_0	S_0	k_1	k_2	k'
	5.00	42.5(1.5)[a]	0.232(0.011)	0.445
	2.50	57.6(2.1)	0.226(0.013)	0.370
3.60	1.25	73.0(4.1)	0.309(0.022)	0.400
	0.625	56.3(2.8)	0.307(0.017)	0.342
	0.313	35.2(1.7)	0.374(0.019)	0.385
	5.00	49.6(2.0)	0.158(0.008)	0.407
	2.50	63.4(1.5)	0.151(0.006)	0.310
1.80	1.25	71.3(1.7)	0.118(0.006)	0.207
	0.625	78.3(3.2)	0.191(0.010)	0.240
	0.313	43.8(1.1)	0.216(0.006)	0.230
	5.00	18.2(0.7)	0.061(0.003)	0.151
	2.50	36.7(0.8)	0.099(0.003)	0.191
0.90	1.25	53.0(1.2)	0.114(0.003)	0.180
	0.625	72.9(2.7)	0.166(0.007)	0.211
	0.313	39.6(1.2)	0.257(0.008)	0.269
	5.00	16.8(0.9)	0.044(0.003)	0.128
	2.50	18.6(0.7)	0.035(0.002)	0.081
0.45	1.25	41.2(0.6)	0.065(0.001)	0.116
	0.625	62.1(1.0)	0.102(0.002)	0.141
	0.313	36.0(0.8)	0.161(0.004)	0.172
	5.00	5.6(0.3)	0.025(0.002)	0.053
	2.50	9.2(0.5)	0.025(0.002)	0.047
0.225	1.25	11.3(0.4)	0.021(0.001)	0.035
	0.625	39.6(0.4)	0.067(0.001)	0.092
	0.313	32.6(0.9)	0.095(0.003)	0.105

2°C; k_p = 379 sec^{-1}. K_m = 0.35 mM; E_0 (μM); S_0 (mM); k_1 ($sec^{-1}M^{-1}$); k_2 (sec^{-1}); k' (sec^{-1}).

[a]Numbers in parantheses are marginal standard deviation estimates.

Table 6.3. Phenomenological Model, Data-Fitting Results at 12°C.

E_0	S_0	k_1	k_2	k'
	5.00	417(16)[a]	1.061(0.051)	3.15
	2.50	614(12)	0.637(0.035)	2.17
3.60	1.25	711(19)	0.884(0.050)	1.77
	0.625	634(17)	1.439(0.047)	1.84
	0.313	462(27)	1.235(0.080)	1.38
	5.00	239(8)	0.602(0.026)	1.80
	2.50	338(8)	0.461(0.020)	1.31
1.80	1.25	512(9)	0.638(0.018)	1.28
	0.625	558(12)	0.796(0.022)	1.14
	0.313	435(20)	0.904(0.048)	1.04
	5.00	92(4)	0.300(0.016)	0.76
	2.50	165(4)	0.327(0.013)	0.74
0.90	1.25	298(5)	0.437(0.010)	0.81
	0.625	374(16)	0.697(0.033)	0.93
	0.313	151(24)	0.593(0.098)	0.64
	5.00	517(28)	0.247(0.016)	2.83
	2.50	112(2)	0.256(0.001)	0.54
0.45	1.25	161(3)	0.270(0.007)	0.47
	0.625	287(12)	0.435(0.020)	0.61
	5.00	542(26)	0.257(0.014)	2.97
	5.00	15(12)	0.100(0.074)	0.17
	2.50	26(2)	0.065(0.007)	0.13
0.225	1.25	64(2)	0.126(0.005)	0.21
	0.625	113(8)	0.191(0.014)	0.26
	0.313	62(5)	0.133(0.012)	0.15

12°C; k_p = 1158 sec^{-1}. K_m = 0.35 mM; E_0 (μM); S_0 (mM); k_1 ($sec^{-1}M^{-1}$); k_2 (sec^{-1}); k' (sec^{-1}).

[a]Numbers in parantheses are marginal standard deviation estimates.

Table 6.4. Phenomenological Model, Data-Fitting Results at 22°C.

E_0	S_0	k_1	k_2	k'
	5.00	941(50)[a]	1.93(0.17)	6.63
	2.50	906(86)	3.18(0.37)	5.45
3.60	1.25	513(26)	1.96(0.14)	2.60
	0.625	340(15)	1.93(0.10)	2.15
	0.313	179(5)	1.76(0.05)	1.82
	5.00	1298(44)	0.60(0.05)	7.09
	2.50	962(9)	0.80(0.02)	3.20
1.80	1.25	622(14)	1.07(0.05)	1.84
	0.625	375(10)	1.14(0.04)	1.37
	0.313	162(19)	1.40(0.17)	1.45
	5.00			
	2.50	1173(28)	0.55(0.03)	3.48
0.90	1.25	797(12)	0.68(0.02)	1.67
	0.625	526(10)	1.06(0.02)	1.39
	0.313	205(6)	1.58(0.05)	1.64
	5.00			
	2.50	1220(24)	0.47(0.02)	3.52
0.45	1.25	956(16)	0.58(0.02)	1.78
	0.625	745(14)	0.76(0.02)	1.22
	0.313	398(23)	1.08(0.06)	1.21
	5.00	1059(29)	0.47(0.01)	5.77
	2.50	748(19)	0.35(0.01)	2.22
0.225	1.25	725(14)	0.39(0.01)	1.30
	0.625	697(17)	0.65(0.02)	1.08
	0.313	458(158)	0.90(0.32)	1.04

22°C; k_p = 3000 sec^{-1}. K_m = 0.35 mM; E_0 (μM); S_0 (mM); k_1 ($sec^{-1}M^{-1}$); k_2 (sec^{-1}); k' (sec^{-1}).

[a]Numbers in parantheses are marginal standard deviation estimates.

Figure 6.22. Phenomenological Model, Single-Set Fitting; 1.8 μM AMP-Aminohydrolase with 2.5 mM 5'-AMP, 22°C.

Figure 6.23. Phenomenological Model, Single-Set Fitting; 3.6 μM AMP-Aminohydrolase with 2.5 mM 5'-AMP, 12°C.

Figure 6.24. Phenomenological Model, Single-Set Fitting; 0.9 μM AMP-Aminohydrolase with 1.25 mM 5'-AMP, 2°C.

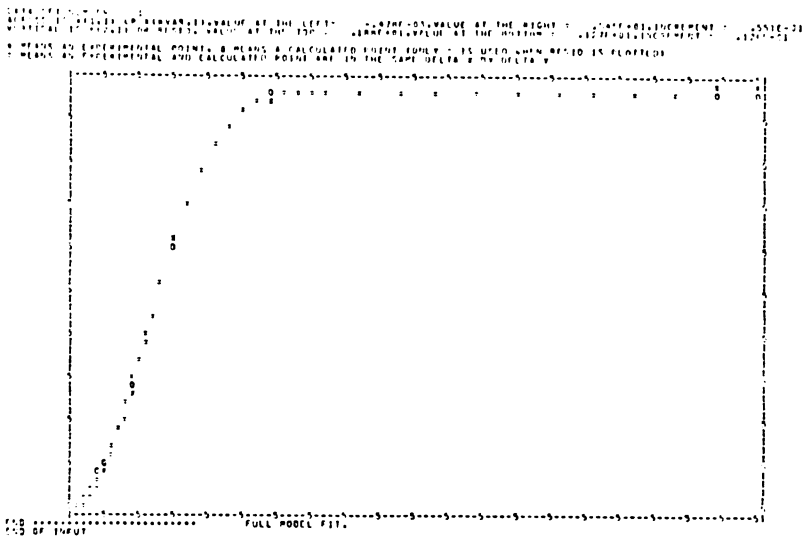

Figure 6.22

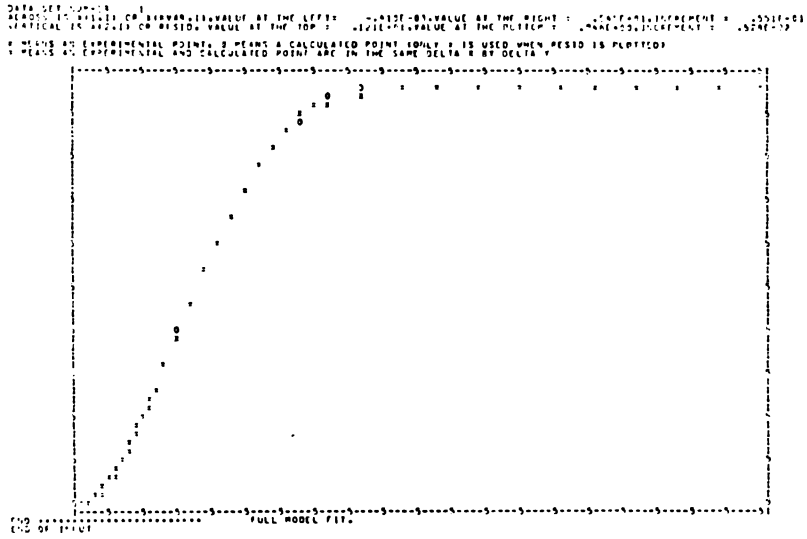

Figure 6.23

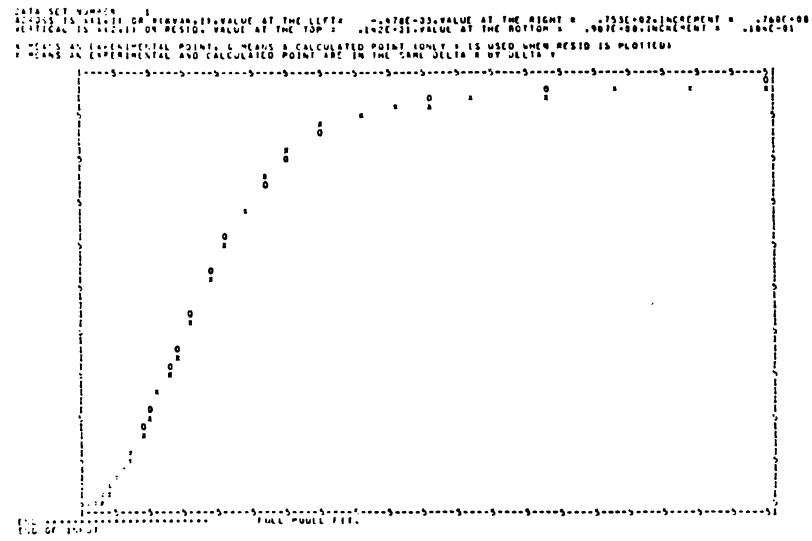

Figure 6.24

produce Figures 6.25, 6.26 and 6.27, which show plots of the initial substrate concentrations (S_0) versus [k_2 + $k_1(S)$] at 22°, 12° and 2°C, respectively. Figures 6.28, 6.29 and 6.30 show plots of the initial enzyme concentrations (E_0) versus [k_2 + $k_1(S)$] at 22°, 12° and 2°C, respectively.

It is clearly evident from Figure 6.25 that the pseudo first order rate constant (k') is dependent on (S_0) at 22°C, whereas it is independent of (S_0) at 12°C and 2°C, as shown in Figures 6.26 and 6.27 respectively. The reverse is true however, for the enzyme dependence. Figure 6.28 shows that (k') is independent of (E_0) at 22°C, but dependent on (E_0) at 12°C and 2°C, as shown in Figures 6.29 and 6.30 respectively.

Hence the apparent cooperativity effects embodied in (k') are manifested by their dependence on (S_0) but not (E_0) at the higher temperature (22°C); whereas these effects are completely reversed at the lower temperatures (12° and 2°C), where they are dependent on (E_0) but not (S_0).

The mechanistic interpretation of these phenomena can be ascribed to the constitution of the tetrameric enzyme - as related to the association-dissociation equilibria of its four subunits - as a function of temperature, where the independence of the rate on (E_0), at 22°C (Figure 6.28), indicates that the enzyme maintains its tetrameric

Symbols for Figures 6.25 - 6.27

Initial AMP-Aminohydrolase concentration (μM):

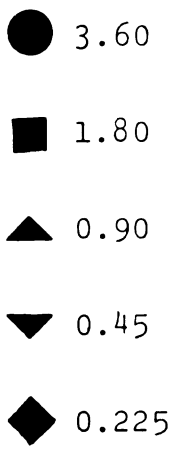

Symbols for Figures 6.28 - 6.30

Initial 5'-AMP concentration (mM):

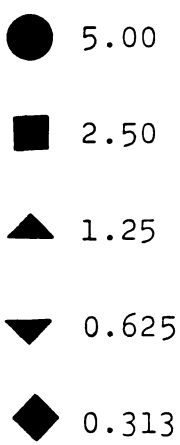

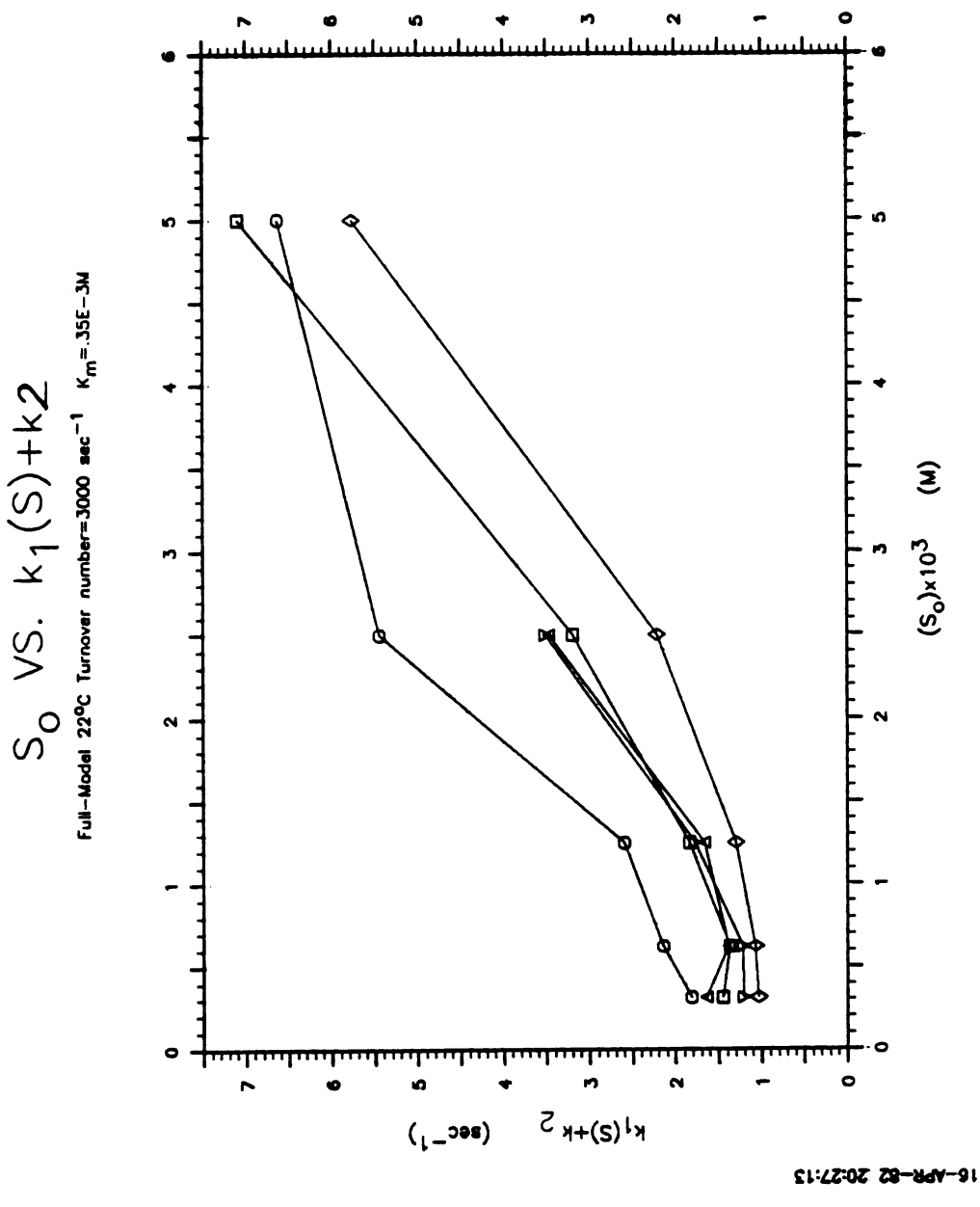

Figure 6.25. Phenomenological Model, $[k_2 + k_1(S)]$ versus (S_0) at 22°C.

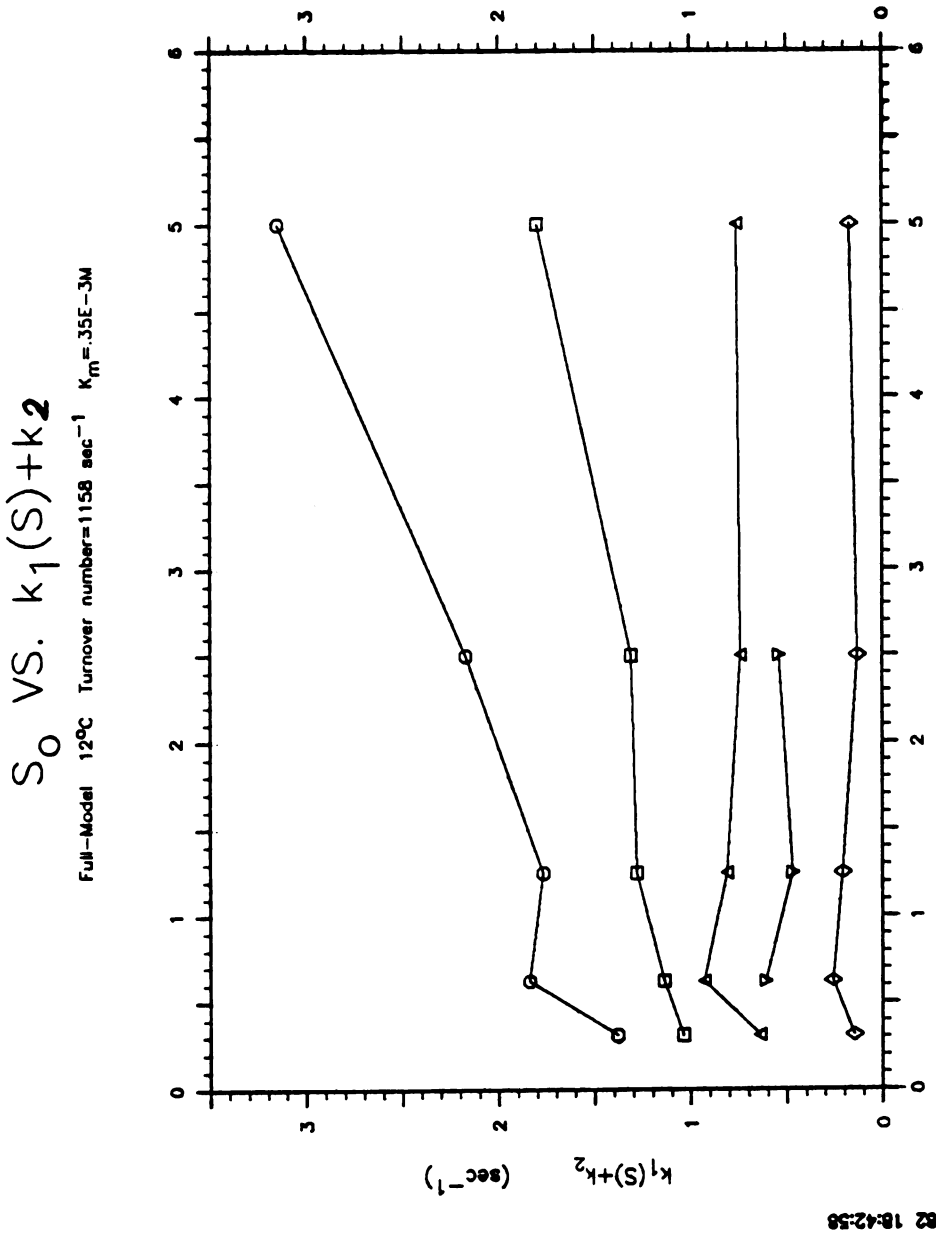

Figure 6.26. Phenomenological Model, $[k_2 + k_1(S)]$ versus (S_0) at 12°C.

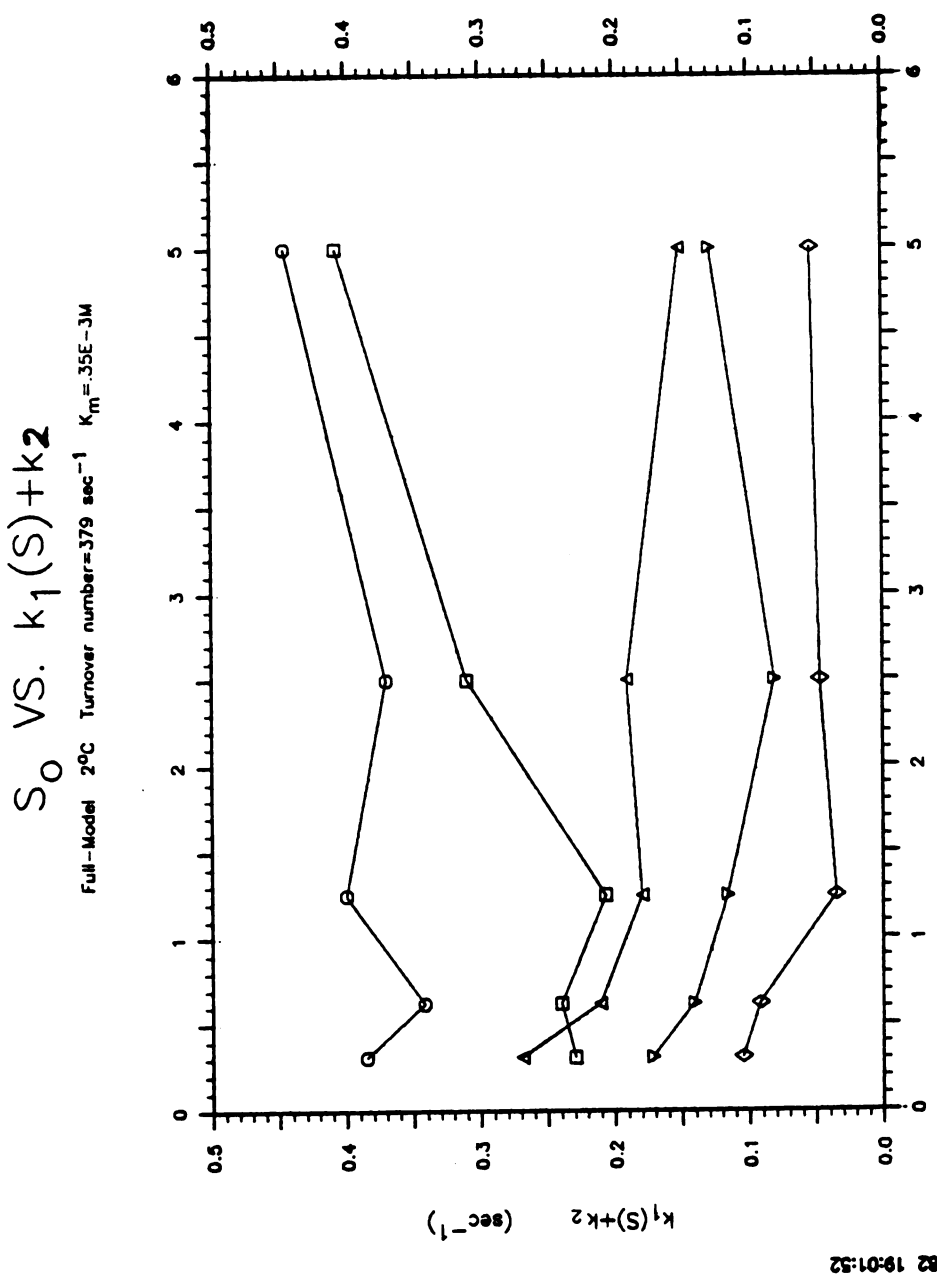

Figure 6.27. Phenomenological Model, $[k_2 + k_1(S)]$ versus (S_o) at 2°C.

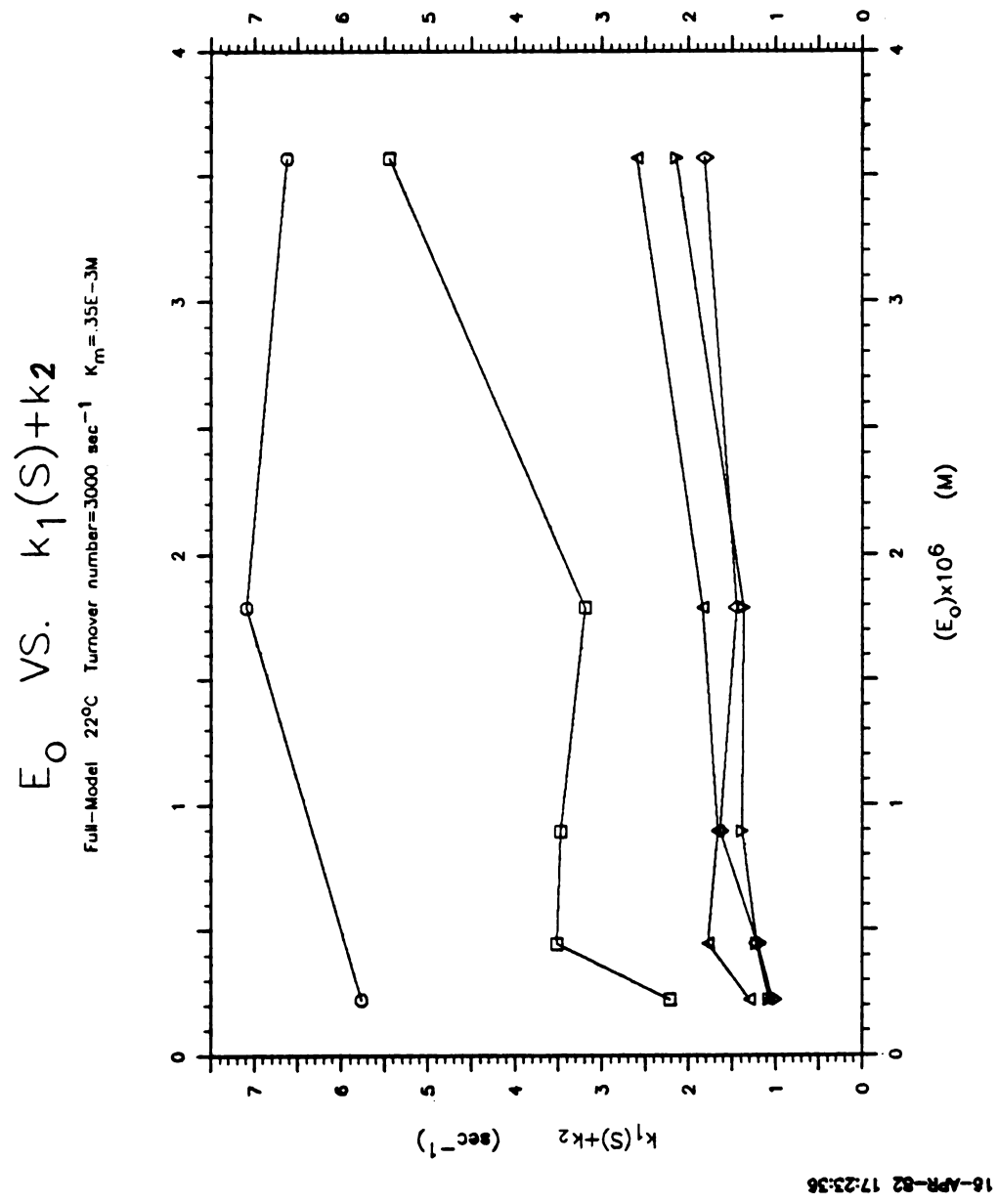

Figure 6.28. Phenomenological Model, $[k_2 + k_1(S)]$ versus (E_0) at 22°C.

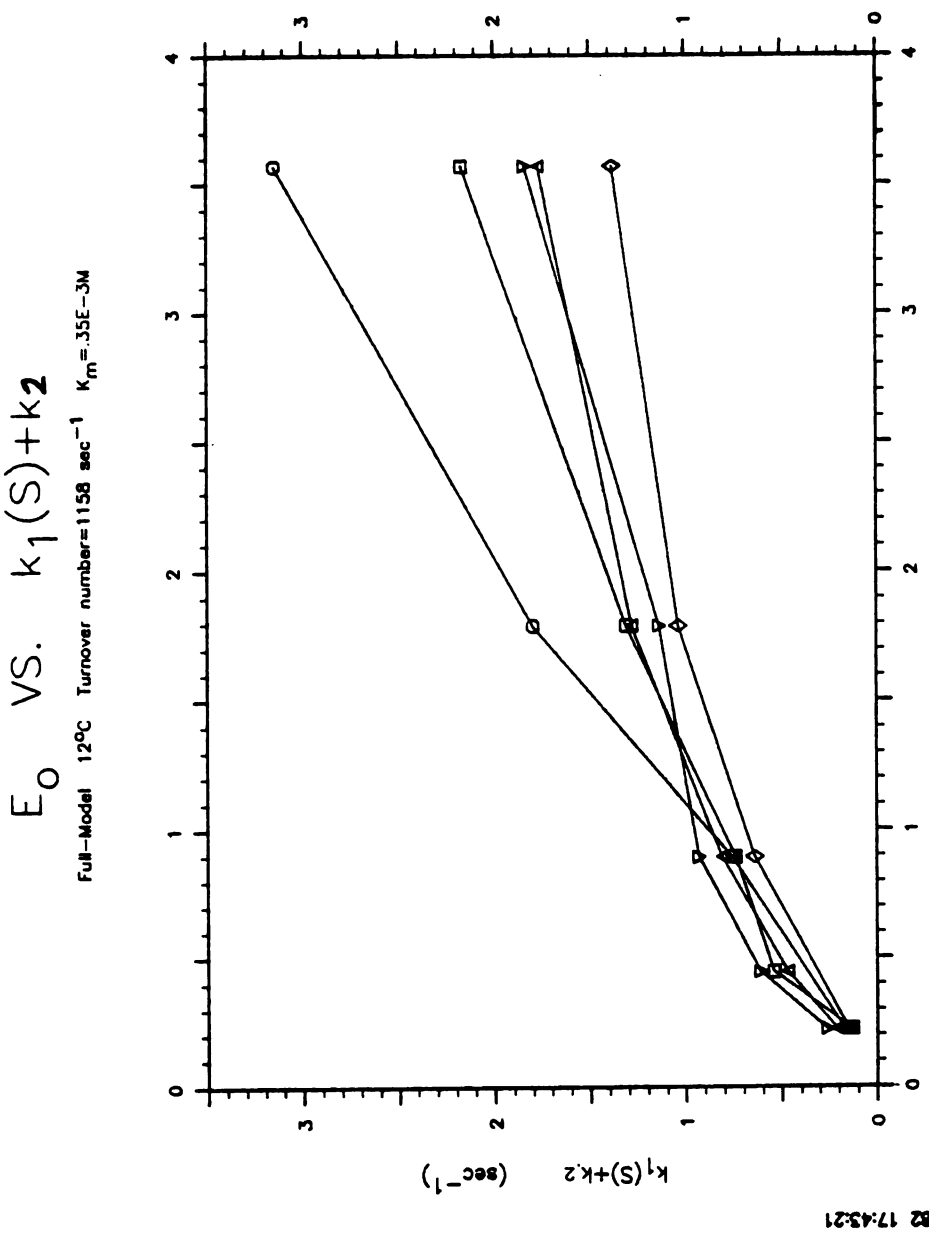

Figure 6.29. Phenomenological Model, $[k_2 + k_1(S)]$ versus (E_0) at 12°C.

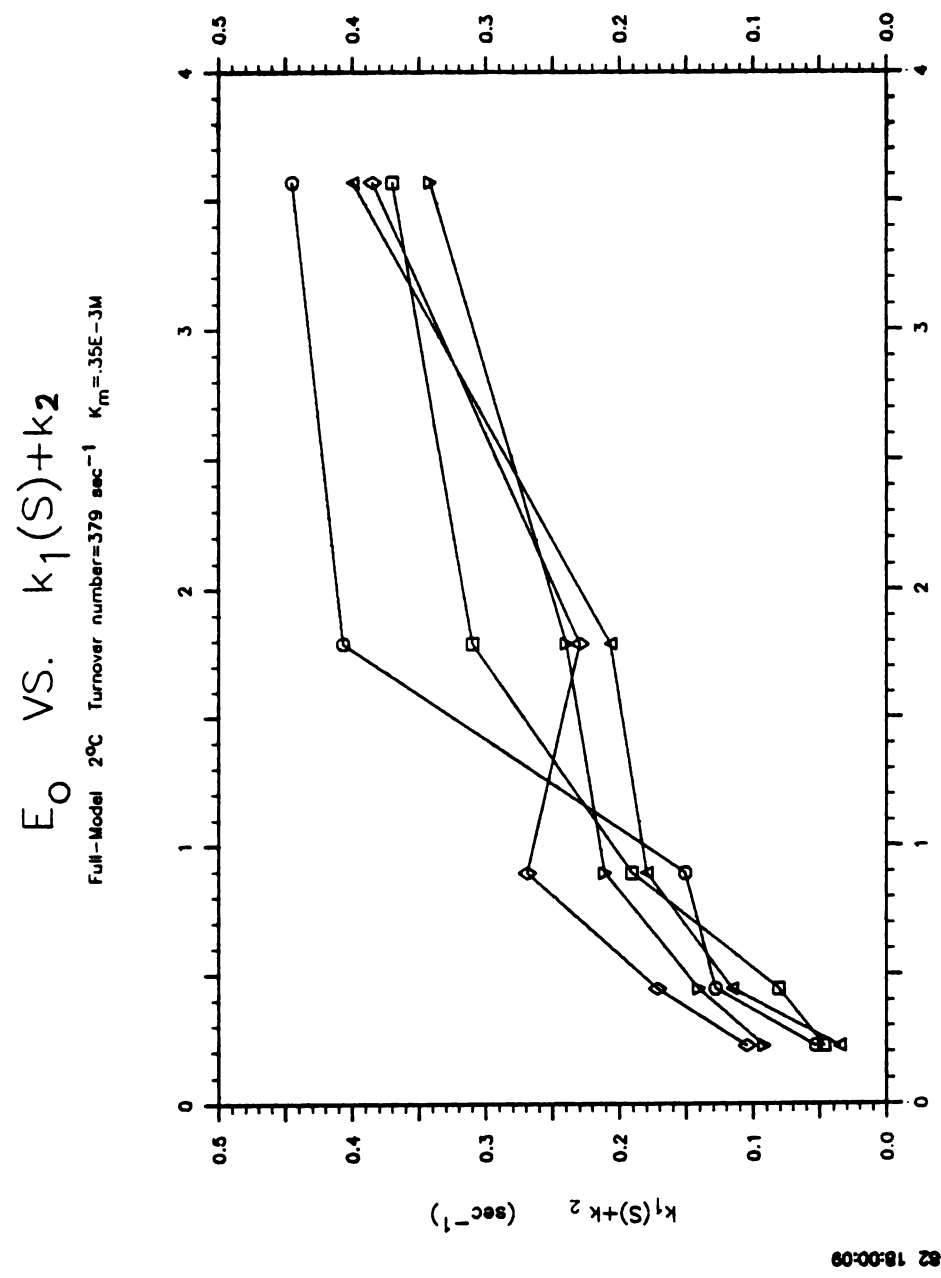

Figure 6.30. Phenomenological Model, $[k_2 + k_1(S)]$ versus (E_0) at 2°C.

configuration at this temperature even in the absence of monovalent cation activators. This is in agreement with the sedimentation velocity results presented earlier in this work. Dissociation to subunits occurs at the lower temperatures, as indicated by the dependence of the rate on the initial enzyme concentration, (E_0), at these temperatures (Figures 6.29 and 6.30).

PART B

STOPPED-FLOW STUDIES OF THE REACTION OF S-BENZYL-L-CYSTEINE WITH TRYPTOPHANASE

CHAPTER 7

TRYPTOPHANASE - AN INTRODUCTION

A. Historical

In 1875, Kühne (166) and Nencki (167) reported on the production of indole during putrefaction of protein. In 1903, Hopkins and Cole (168) showed that indole was formed by bacterial decomposition of the newly isolated (168,169) amino acid, tryptophan. Happold and Hoyle (170) in 1935 identified tryptophanase (EC4.1.99.1) as the enzyme responsible for the production of indole in bacterial cultures. Happold and Struyvenberg (171) demonstrated that tryptophanase action required the presence of NH_4^+, K^+ or Rb^+, and was inhibited by Na^+ or Li^+. Wood *et al.* (172) discovered that pyridoxal-P (PLP; pyridoxal 5'-phosphate), a coenzyme, was required for the activity of tryptophanase, and that indole, pyruvate and ammonia were formed in stoichiometric amounts from L-tryptophan. Thus by 1954, the reaction catalyzed by crude, cell-free preparations of tryptophanase could be summarized as follows:

$$\text{L-Tryptophan} + H_2O \xrightarrow[\text{PLP, } NH_4^+]{\text{Tryptophanase}} \text{Indole} + \text{Pyruvate} + NH_3$$

Reviews by Happold (173), Wada (174) and Snell (175) effectively cover what was known about tryptophanase up to 1975.

B. Enzyme Source

Snell (175) had suggested that the enzyme plays a catabolic role in animal metabolism, by regulating the intracellular concentrations of the essential amino acid tryptophan. Tryptophan is known to induce the formation of tryptophanase in a variety of bacterial cultures (175). However, the amount, physical and catalytic properties of the induced enzyme are dependent on the bacterial source (175).

In order to produce a consistently pure form of tryptophanase, free of a contaminating tryptophan synthetase, Newton and Snell (176) turned to Escherichia coli B/1t7 as a source of tryptophanase. This organism is auxotrophic* for tryptophanase, because it completely lacks the genes which code for tryptophan synthetase (177). It retains an inducible tryptophanase (175), and was made constitutive for this enzyme by selecting spontaneous mutants that grew on minimal medium lacking tryptophan but supplemented with indole (176,177).

*Auxotrophic mutants are defective in a biosynthetic pathway, but revert to normal growth when provided with the normal product of the pathway.

The resulting strain, designated E. coli B/lt7-A, produces large amounts of tryptophanase [up to 10% of the soluble intracellular protein (179)] under proper cultural conditions (179,180), and it was from this strain that crystalline tryptophanase, homogeneous by electrophoretic and ultracentrifugal criteria, was first obtained by Newton and Snell (179).

C. Structure and Properties

Isolated from Escherichi coli B/lt7-A (179), tryptophanase has a molecular weight of 220,000, and is composed of four subunits (179,181,182). Reversible association-dissociation processes are highly dependent on concentration, temperature, ionic environment, pH, and the presence or absence of the coenzyme, pyridoxal-P (169). In the absence of pyridoxal-P (PLP), the apo-enzyme is catalytically inactive, and has the spectrum of a simple protein with an absorption maximum at 278 nm.

Equilibrium dialysis studies showed that the apo-enzyme binds four molecules of PLP per molecule of the native tetrameric enzyme (181,183). The resulting holo-enzyme shows characteristic pH-dependent absorption maxima at 337 nm and 420 nm (184) in the presence of K^+ or NH_4^+ ions, which are essential for catalytic activity. At equivalent concentrations of Na^+ or imidazole (0.05-0.1 M), only the 420 nm band is formed, and the enzyme has little

or no catalytic activity. Suelter and Snell (188) however presented evidence which indicated that Na^+ was able to appreciably activate tryptophanase if employed in sufficient amounts. Their data showed ahat 0.5 M Na^+ elicited nearly 30% of the activity observed with 0.05 M NH_4^+.

Snell (175) suggests that PLP in holotryptophanase is apparently present in azomethine linkage with the ε-amino group of a particular lysine residue at the active site, as found for all other PLP dependent enzymes investigated (185), and that the four binding sites are equivalent (175, 186). Snell further proposes (175) that this equivalence is most simply explained by assuming the presence of one binding site on each of the four identical subunits of holotryptophanase. A large conformational change that results in a substantially more compact structure, accompanies the binding of PLP by apotryptophanase (182,187). Snell (175) points out that as a result of its more compact structure, holotryptophanase is more resistant than apotryptophanase to denaturation by sodium dodecyl sulfate (182), by heat (187), and by changes in pH.

D. Spectral Properties

Morino and Snell (184) reported that in the presence of K^+, holotryptophanase showed two pH dependent absorption bands with maxima at 337 nm and 420 nm, which they attributed to the active and inactive forms of the

enzyme respectively. Their conclusions were based on the following experimental evidence: (a) At acidic pH, the 420 nm band predominated, whereas the 337 nm band was more prominent at alkaline pH, where holotryptophanase displayed maximal catalytic activity (above pH 8.0). Similar spectral changes with pH were observed when K^+ was replaced by NH_4^+; (b) when 0.1 M K^+ was replaced by 0.1 M Na^+ or 0.1 M imidazole (neither of which replaces K^+ as an activator), there was a heightened absorption at 420 nm and little or no absorption at 337 nm, even at pH 8.0; and (c) the spectra of these enzymatically inactive forms of holotryptophanase resembled that obtained in the presence of K^+ at pH 6.1 where the inactive species predominated.

Later, and in contrast to the above conclusions of Morino and Snell (184), June et al. (197) presented experimental kinetic evidence from which they concluded that the 420 nm band corresponded to the active form of the enzyme, while the 337 nm band was attributed to the inactive form. Their analysis suggested that this kinetic interplay was manifested by complex pH and structural effects. Further discussion on their findings will be presented in the following section of this chapter.

It has been suggested from model studies (189) on pyridoxal-P aldimines that the band at 420 nm is due to the following structures:

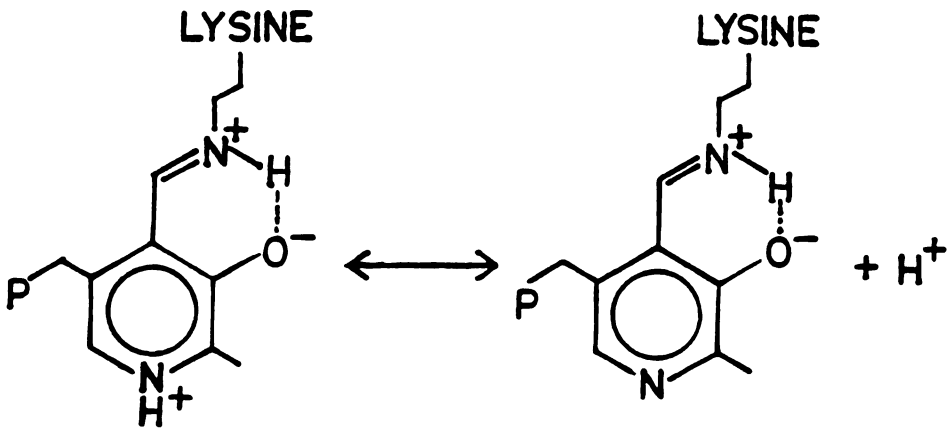

Johnson and Metzler (190) and Metzler et al. (192) have shown that the state of protonation at the pyridinium nitrogen does not greatly alter the position of the absorption maxima of pyridoxal-P Schiff bases although the extinction coefficients differ.

Davis and Metzler (191) and Snell (175) suggested the following as possible structures for the 337 nm band (page 145):

June et al. (193) reported that the interconversion of the 337 and 420 nm bands following a change in pH or K^+ concentration, occurs on the stopped-flow time scale. The authors analyzed results from three experiments performed

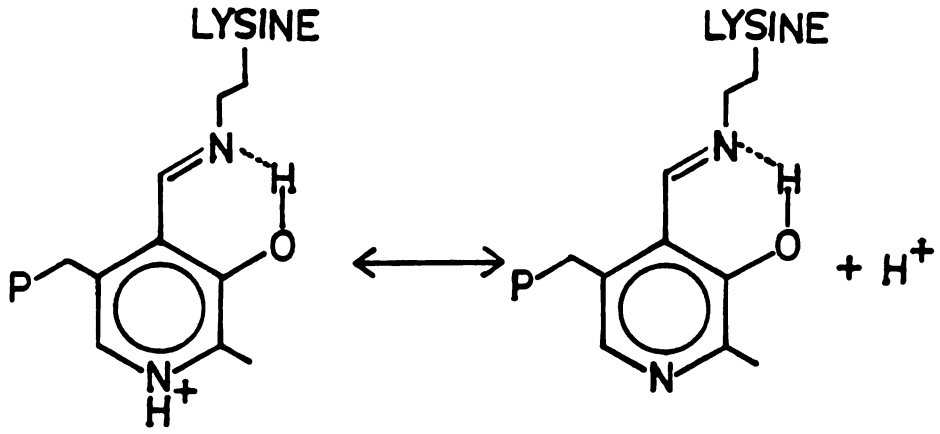

at 24°C: (a) a pH drop from 8.53 to 6.72; (b) a pH jump from 7.38 to 9.30 and (c) a sudden change (K^+-jump) from 0.1 M Na^+ to 0.05 M Na^+ and 0.05 M K^+ at pH 8.0. They presented the following scheme for the process:

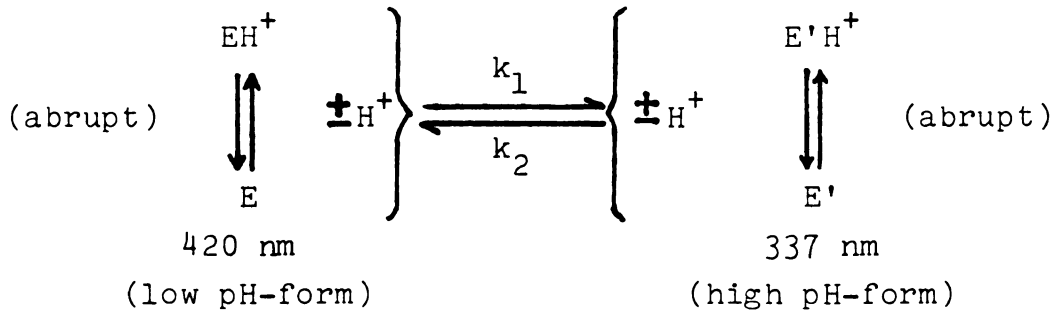

where $k_1 = 0.56 \pm 0.03$ sec^{-1}, and $k_2 = 0.43 \pm 0.03$ sec^{-1}.

The scheme assumes rapid protonation and deprotonation (involving one or more protons) of the two slowly interconvertible enzyme forms. The authors attributed the abrupt (<6.5 msec) spectral changes observed in their experiments, to reflect the rapid protonation and deprotonation of the E and E' forms, while the slow spectral changes (which required several seconds) reflected the interconversion of these forms. Their K^+-jump experiment also showed slow conversion of the 420 nm peak to the 337 nm absorption, but the kinetics were not clearly first order. An approximate first-order rate constant of 0.3-0.5 sec^{-1} could be obtained from their data at short times, but the analysis was complicated by continuing changes in absorbance. The authors concluded that their results indicated the occurrence of either enzyme conformational changes in the interconversion process or slow protonation-deprotonation steps.

Followup experiments on the pH-dependent interconversion of holotryptophanase spectral forms, studied by scanning stopped-flow spectrophotometry, were analyzed by June et al (194). The experiments which involved rapid incremental increase (jump) or decrease (drop) in pH over the range of enzyme stability in 0.2 M KCl at 24±0.3°C, showed three distinct time-dependent phases. They were: (1) an abrupt phase which is complete in less than 6.5 msec; (2) a fast first order interconversion of the 337 and 420 nm absorbances,

and (3) a slow first order process involving growth at 355 nm, coupled to two decays centered at 325 and 430 nm, in the incremental pH jumps and decay at 355 nm with concommitant growth at 430 and 290 nm in the incremental pH drop experiments.

The authors (194) analyzed the results of these experiments in terms of Scheme I (Figure 7.1), involving enzyme forms E_α, E_β, $E_\beta H^+$, E_γ, $E_\gamma H^+$ and E_δ. They proposed that the E_α form predominated in the absence of activating monovalent cations and absorbs at 420 nm. Those in the β-manifold, E_β and $E_\beta H^+$, also absorb at 420 nm, while those in the γ-manifold, E_γ and $E_\gamma H^+$, absorb at 337 nm. They assigned the changes at 355 nm to the E_δ form. $E_\beta H^+$ and $E_\gamma H^+$ represent the protonated form of the enzyme in each manifold. The points of entry for the α- and γ-forms in their proposed Scheme I are still unclear, and presently under study. Further details on the above work appear in the doctoral dissertation of David S. June (195).

E. Mechanism of Tryptophanase Catalysis

Morino and Snell (184) reported that on addition of substrates or of competitive inhibitors such as L-alanine, tryptophanase exhibited an absorption band with a maximum near 500 nm, which disappeared as the substrates decomposed, but remained unchanged in the presence of inhibitors.

Scheme I

Interconversion of Tryptophanase Spectral Forms (194)

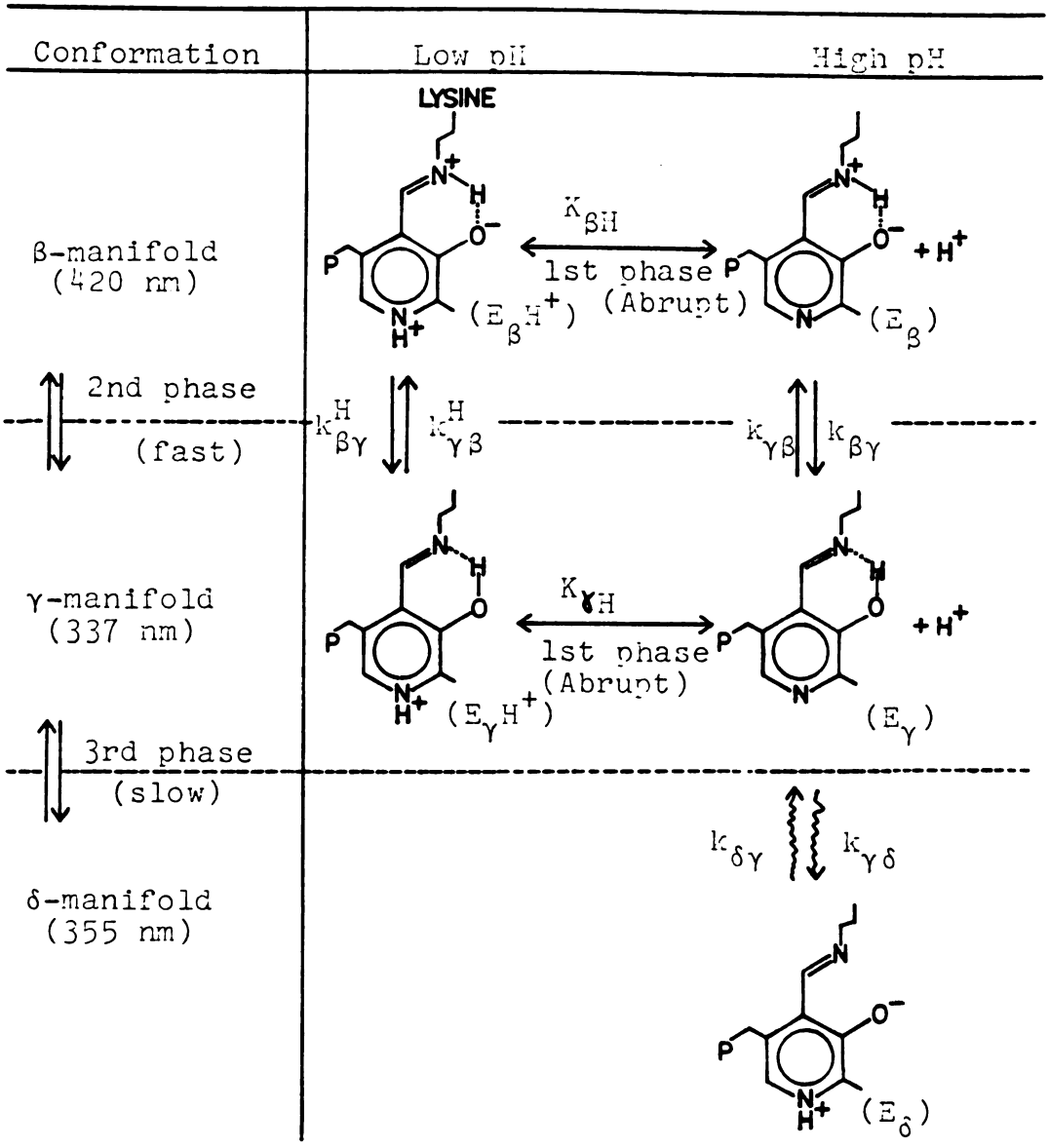

Figure 7.1. Interconversion of Tryptophanase Spectral Forms.

Their exchange experiments in the presence of D_2O and T_2O showed that the α-hydrogen of L-alanine was labilized under these conditions. On these and other grounds, they ascribed the 500 nm band to a quinonoid intermediate that lacks the α-proton of the bound amino acid.

Results of their experiments, and from previous kinetic data, prompted them to conclude that the β-elimination reaction *per se* was the rate limiting step. Later, Suelter and Snell (188) found that labilization of the α-proton was the rate limiting step in the reaction, when S-orthonitrophenyl-L-cysteine (SOPC) was employed as the substrate. Furthermore, Hillebrand *et al.* (196), also using SOPC as a substrate, reported that the enzyme-aminoacrylate complex decayed to yield either α-iminopropionate or the carbinolamine pyruvate as a transient intermediate, along with the regenerated active enzyme. The transient intermediate then decayed in a non-enzymatic reaction to yield pyruvate and ammonia.

June *et al.* (197) investigated the interaction of the amino acid inhibitors, ethionine and L-alanine, with tryptophanase. Their stopped-flow studies on the kinetics of quinonoid formation with ethionine led them to conclude that the 420 nm band of the enzyme was the active form. They supported this assignment by the following observations: (1) the rate constant for disappearance of the 420-nm absorbance, 18.0±2.2 sec^{-1}, was the same as that of the fast

phase of the observed biphasic growth of quinonoid at 508 nm, 15.0±1.2 sec^{-1}; (2) the rate of disappearance of the 337-nm absorbance, 0.56±0.08 sec^{-1}, was the same as the rate of the slow phase of quinonoid formation, 0.63±0.06 sec^{-1}, and was essentially unaffected by inhibitor concentration or the nature of the inhibitor, ethionine or L-alanine, and (3) the average rate constant for the slow phase obtained with ethionine, 0.51±0.14 sec^{-1}, and L-alanine, 0.47±0.15 sec^{-1}, agrees closely with the rate constant, 0.66±0.4 sec^{-1}, for the conversion of the 337-nm form, conformation γ, to the 420-nm form, conformation β, following a rapid decrease in pH (194). These and other results (193,194,197) prompted them to infer that the 337-nm form apparently does not form quinonoid directly, but is first converted to the 420-nm form before the α-proton of an amino acid inhibitor is removed to form quinonoid. Furthermore, deuterium isotope effects on the kinetics of formation of quinonoid with L-[α-^{1}H] alanine and L-[α-^{2}H] alanine led them to argue that the rate-limiting step of quinonoid formation is the abstraction of the α-proton. Based on their results, they proposed Scheme II (Figure 7.2) as a partial mechanism for quinonoid formation.

The authors (197) presented the following additional factors upon which they based their proposed scheme, Scheme II (Figure 7.2), for the reaction of ethionine with tryptophanase:

Scheme II

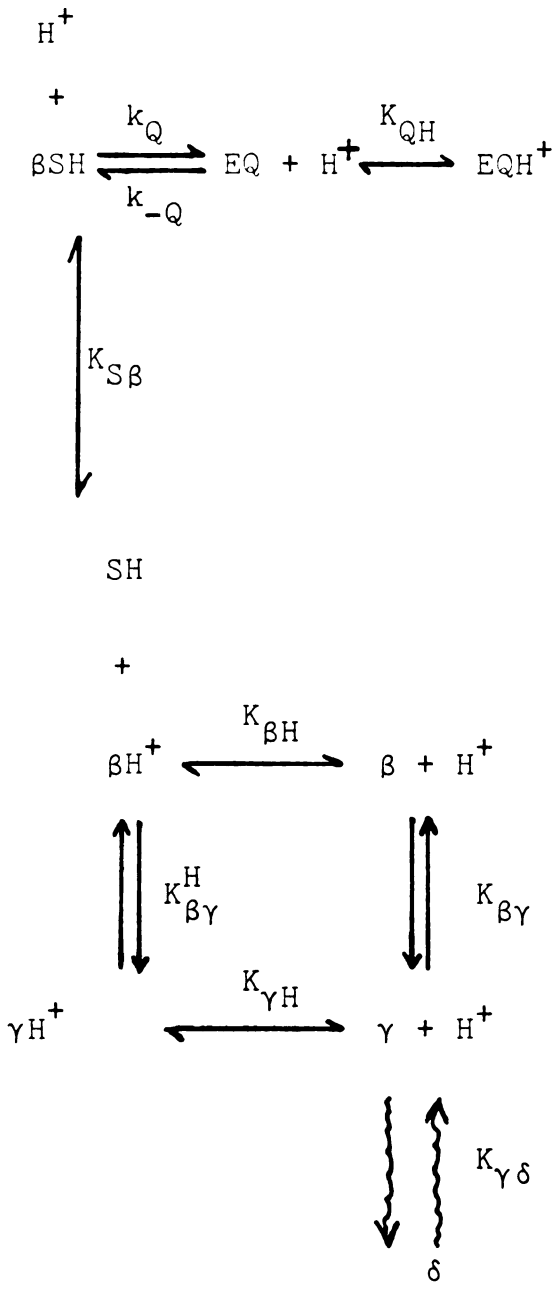

Figure 7.2. A Mechanism for the Interaction of a Competitive Inhibitor, Ethionine (SH), to Form a Quinonoid (EQ and EQH) (197).

(a) the 337-nm form of tryptophanase (γ-conformation) does not form quinonoid directly but is first converted to the 420-nm form (β-conformation), the active form of the enzyme, which forms a Schiff base from which the α-proton of the amino acid inhibitor is removed. Thus the β-conformation is the one poised for reaction. Furthermore, according to the scheme, the protonated form of the β-conformation is the one which proceeds to form the quinonoid. This is attractive because formation of the quinonoid requires a protonated pyridinium nitrogen,

(b) Values of the first order rate constant, k_1, for disappearance of the 420-nm absorbance (which were the same as those for the fast phase of the biphasic growth of the quinonoid at 508 nm) exhibited a hyperbolic dependence on ethionine concentration. This hyperbolic dependence is in accord with the results of previous investigators (175,182,184,188) who reported that the mechanism of interaction between holotryptophanase and a suitable amino acid substrate or inhibitor, involved the formation of a Michaelis complex via a transaldimination reaction,

(c) Values of the first order rate constant, k_2, for disappearance of the 337-nm absorbance (which were the same as those for the slow phase of the biphasic growth of the quinonoid at 508 nm) do not show a hyperbolic dependence with increasing ethionine concentration, but are essentially constant, suggesting that they reflect an

enzyme conformational change. This result conforms with the previous findings of June et al. (193,194),

(d) when the interaction of L-alanine with tryptophanase was examined under comparable conditions, values of k_1 were substantially smaller than those obtained with ethionine, whereas values for k_2 were essentially the same as those obtained with ethionine. Since k_2 values were comparable for both inhibitors, this presented further support to the authors previous suggestion (193,194) that k_2 reflects an enzyme conformational change,

(e) Examination of the effect of pH on quinonoid formation revealed that as the pH was increased, k_1 also increased, while the relative amplitude of the fast phase of the quinonoid diminished. This supports the proposal that the 420-nm form (β-conformation) is the one poised for reaction, i.e., the active form of the enzyme. In contrast, k_2 appeared to be less sensitive to pH. Since the rate of disappearance of the 337-nm form (γ-conformatin) corresponded to k_2 of the quinonoid, this added further reinforcement to the argument that the γ-form is not the active form of the enzyme, and finally

(f) Substitution of deuterium at the α-position of the inhibitor L-alanine, affected both the extent and rate of quinonoid formation. Thus, deuterium substitution slowed down the fast phase of the quinonoid growth, but left the slow phase virtually unchanged. This was interpreted as

additional evidence that the slower phase reflected an enzyme conformational change.

In order to render further validity to Scheme II (Figure 7.2), which was based on interaction of inhibitors with tryptophanase, rate studies with amino acid substrates should be performed and analyzed in terms of the same scheme. The following chapter will address some aspects of these studies; namely, the interaction of the substrate S-benzyl-L-cysteine with tryptophanase at pH 8.0.

CHAPTER 8

STOPPED-FLOW STUDIES OF THE REACTION OF S-BENZYL-L-CYSTEINE WITH TRYPTOPHANASE

A. Introduction

The study of the reaction of S-benzyl-L-cysteine with tryptophanase was undertaken in order to investigate the kinetics of the spectral forms at 337, 420 and 508 nm, and to determine the correlations which may exist between the time progress of these forms with this substrate, to the progress of the same forms observed with the inhibitors, ethionine and L-alanine, as investigated by June et al. (197). In particular, the objective was to analyze the fast decay at 420 nm, the slow decay at 337 nm, and their correlation to the biphasic (fast and slow) growth at 508 nm.

S-benzyl-L-cysteine (SBC) was chosen for two reasons: First; tryptophanase is able to catalyze this substrate to form products. Hence, if the time behavior in the progress of the curves at 337, 420 and 508 nm, for this substrate, can be interpreted in the same fashion as was done with the inhibitors, ethionine and L-alanine (197), then this

should confirm the earlier findings of June et al. (193, 194,197), and in particular the scheme (Scheme II, Figure 7.2) presented by June et al. (197), for the mechanism of quinonoid formation. Second; changes in the quinonoid band for the reaction of SBC with tryptophanase occur on the stopped-flow time scale, unlike those for SOPC and other substrates, where the rates of formation and decay of the quinonoid are faster than the stopped-flow time scale.

June et al. (193,194,197) also reported on slow absorbance changes at 355, 390 and 420 nm. They attributed (194) changes at 355 nm to the δ-form of the enzyme (Scheme I, Figure 7.1), whereas those at 390 nm were attributed to changes in the spectrum of free PLP (194). The slow growth of absorbance at 420 nm, following the fast phase was due to the nonenzymatic formation of a Schiff base between excess free ethionine and PLP (197).

B. Materials and Methods

B.1. Reagents

Pyridoxal 5'-phosphate (PLP); S-benzyl-L-cysteine (SBC); DL-dithiothreitol (DTT); potassium [ethylene diamine tetracetic acid] (KEDTA); and potassium N-(2-hydroxyethyl)-piperazinepropanesulfonic acid (Kepps), were all obtained from Sigma Chemical Company. All other reagents were

analytical grade.

B.2. Tryptophanase Preparation

Tryptophanase from Escherichia coli B/lt7-A was prepared by Iraj Behbahani Nejad as described by Watanabe and Snell (198) including the modification of Suelter et al. (199). Holoenzyme was prepared from stock apoenzyme by incubation in a dialysis buffer which consisted of 25 mM Kepps, 0.1 M KCl, pH 8.0, 1 mM KEDTA, 1 mM DTT, and 5 μM PLP, for one hour at 37°C. The enzyme had a specific activity of 45 μmole min^{-1} mg^{-1} when assayed with 0.6 mM S-(o-nitrophenyl)-L-cysteine (SOPC) in 50 mM potassium phosphate, pH 8.0, and 50 mM KCl, at 30°C (200). Protein concentration was determined spectrophotometrically by using $\varepsilon(278)=0.795$ mL mg^{-1} cm^{-1} (184).

B.3. Scanning Stopped-Flow Experiments

Activated holotryptophanase (5.04 mg mL^{-1}) was diluted to a concentration of 4.54 mg mL^{-1} with the dialysis buffer and pushed against five different concentrations (0.125, 0.25, 0.5, 1 and 2 mM) of SBC in the same buffer at 21.2°C. The final concentrations of the reactants, after mixing, were hence half the initial. All spectra were scanned over the wavelength range 326-491 nm.

Since absorbance over the wavelength range 475-540 nm

was shown (175,188) to represent only that due to quinonoid, scanning was limited up to 491 nm, due to the intense absorption of that band [ε_{max} (508) = 40400 M^{-1} cm^{-1} (197)] in order to simultaneously monitor changes at 337 nm [ε_{max} (337) = 3500 M^{-1} cm^{-1} (194)] and 420 nm [ε_{max} (420) = 4600 M^{-1} cm^{-1} (194)]. Analysis of the quinonoid band was performed at 478 nm (the left shoulder of the band); however, in order to avoid confusion in terminology, disscussion in this text shall continue to refer to the implicit 508 nm wavelength.

B.4. Data Analysis

Data were fitted by the appropriate mathematical function using the nonlinear curvefitting program KINFIT4 (18). Errors listed are marginal standard deviations, and therefore include the effects of coupling among the parameters.

The absorbance A, for single exponential growth or decay was fitted using the following equation:

$$A = A_{\infty} - \Delta A e^{k_1 t} \qquad (1)$$

The three adjustable parameters were: A_{∞}, the absorbance at infinite time; ΔA, the total change in absorbance, i.e., $A_{\infty} - A_0$, where A_0 equals the absorbance at zero time, and k_1, the apparent first order rate constant.

Biphasic data were analyzed as the sum of two exponentials according to the following equation:

$$A = A_\infty - \Delta A_1 e^{-k_1 t} - \Delta A_2 e^{-k_2 t} \qquad (2)$$

where A_∞ is the measured absorbance at infinite time; ΔA_1 and ΔA_2 are the changes in absorbance due to the fast and slow phases respectively and k_1 and k_2 are the apparent first-order rate constants for the fast and slow processes.

C. Results and Discussion

C.1. Absorbance Changes at 337 nm

The slow decay (Figure 8.1) observed at 337 nm was fitted to a single exponential (Equation 1), and the results appear in Tables 8.1, and 8.2.A. Total absorbance changes are shown in Table 8.2.B.

The rate constant, k_2, for the slow decay at 337 nm has an average value of 0.40±0.12 sec^{-1}, which compares favorably with 0.51±0.14 sec^{-1}, obtained by June *et al.* (197) with inhibitor ethionine. This slow decay is interpreted (194, 197) to reflect the enzyme conformational change from the γ to the β- form (Figure 7.1).

C.2. Absorbance Changes at 420 nm

A fast decay (up to about 200 msec) followed by a slow growth occurred at 420 nm (Figure 8.1). The fast decay

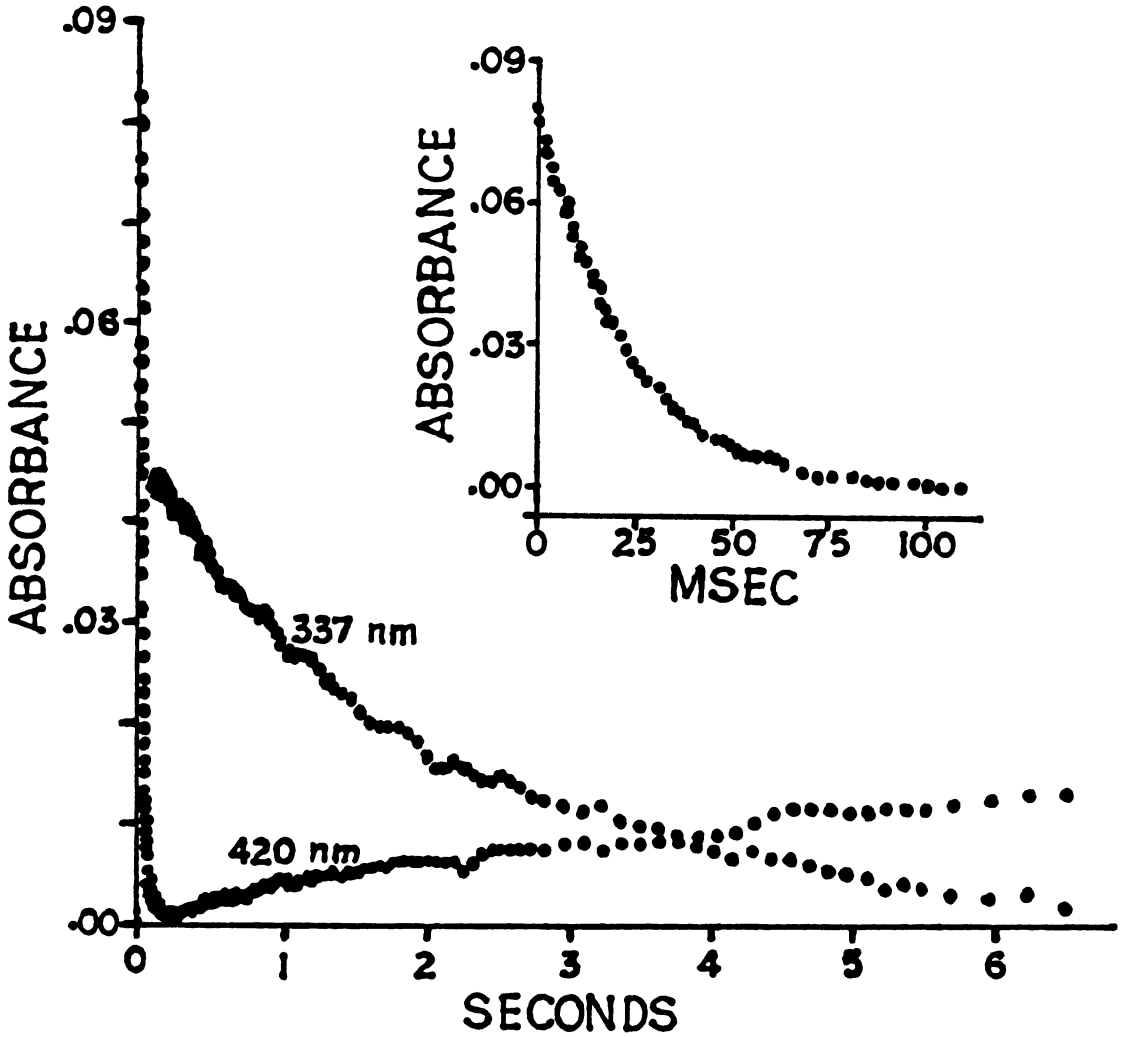

Figure 8.1. Changes in Tryptophanase Absorbance at 337 and 420 nm as a Function of Time After Mixing with S-Benzyl-L-Cysteine in 25 mM Kepps, 0.1 M KCl, pH 8.0, 1 mM KEDTA, 1 mM DTT and 5 μM PLP. After Mixing, Concentrations Were 1 mM S-Benzyl-L-Cysteine and 2.27 mg mL^{-1} Tryptophanase. (The rapid decrease in absorbance at 420 nm is expanded in the inset.)

Table 8.1. Rate Constants and Amplitudes[a] for Absorbance Changes at 337, 420 and 478 nm[d] When 2.27 mg mL^{-1} Tryptophanase is Mixed with 1 mM S-Benzyl-L-Cysteine.

Wavelength (nm)	k_1 (sec^{-1})	k_2 (sec^{-1})	Total A
337 (slow decay)		0.48 (1)[b]	0.042
420 (fast decay)	44.2 (3)		0.083
478[d] (biphasic growth)	42 (4)	0.68 (2)	0.75[c]

[a]The data at 337 and 420 nm were fitted with Equation 1. The data at 508 nm were fitted with Equation 2.

[b]Numbers in parentheses are the marginal standard deviation estimates for the last significant figure.

[c]56% fast phase; 44% slow phase.

[d]ε(478 nm)/ε(508 nm) = 0.54. Also see the second paragraph of Section (B.3) in this chapter.

Table 8.2.a. Rate Constants for 337, 420 and 478 nm[d] As a Function of S-Benzyl-L-Cysteine (SBC) Concentrations Determined with Scanning Stopped-Flow Spectrophotometry.[a] K_m and V_{max} Values were Determined by KINFIT4 (18) According to the Lineweaver-Burke Method.

SBC (mM)	337 nm (slow decay) $k_2(sec^{-1})$	420 nm (fast decay) k_1 (sec^{-1})	478 nm[d] (Biphasic Growth) (Fast) k_1 (sec^{-1})	(Slow) k_2 (sec^{-1})
0.0625	0.53(3)[b]	21.3(2)	21(1)	
0.125	0.35(3)	28.9(3)	30.1(5)	
0.25	0.21(2)	36.2(3)	38 (2)	
0.5	0.42(1)	43.6(4)	42.0(6)	0.70(1)
1.0	0.48(1)	44.2(3)	45 (2)	0.47(2)
K_m (mM)		0.080(9)	0.077(4)	
$V_{max}(sec^{-1})$[c]		48(1)	48.4(5)	

[a]The concentrations of the reaction components after mixing were 25 mM Kepps, 0.1 M KCl, pH 8.0, 1 mM KEDTA, 1 mM DTT, 5 μM PLP and 2.27 mg mL^{-1} tryptophanase. All data were fitted to a single exponential.

[b]Numbers in parantheses are the marginal standard deviation estimates for the last significant figure.

[c]The values of k_1 at infinite SBC concentration.

[d]$\varepsilon(478\ nm)/\varepsilon(508\ nm) = 0.54$. Also see the second paragraph of Section (B.3) in this chapter.

Table 8.2.B. Total Absorbance Changes at 337, 420 and 478 nm.[a] The Noise Level Was Approximately 0.001 A for All Absorbance Measurements.

SBC (mM)	337 nm (Slow Decay)	420 nm (Fast Decay)	478 nm (Biphasic Growth) (Fast)	478 nm (Biphasic Growth) (Slow)
0.0625	0.018	0.064	0.205	
0.125	0.020	0.073	0.240	
0.25	0.038	0.083	0.289	
0.5	0.043	0.079	0.39	0.18
1.0	0.043	0.083	0.42	0.33

[a] $\varepsilon(478\ nm)/\varepsilon(508\ nm) = 0.54$. Also see the second paragraph of Section (B.3) in this chapter.

was fitted to a single exponential (Equation 1), and the values for k_1 (Table 8.2) exhibited a hyperbolic dependence on SBC concentration, yielding a value of 0.081 mM for the Michaelis constant, and 48.5 sec^{-1} for k_1 at infinite SBC concentration.

June et al (197) reported that the slow growth of absorbance at 420 nm following the fast decay was due to the nonenzymatic formation of a Schiff base between excess free ethionine and PLP, and as such did not reflect directly on the mechanism of tryptophanase catalysis.

C.3. Absorbance Changes at 478 nm (508 nm)

Absorbance changes at 478 nm included a biphasic growth (Figure 8.2) followed by decay as substrate was depleted (Figure 8.3). The biphasic growth was initially fitted to the sum of two exponentials; however, due to substrate depletion, it was clearly evident that the slow phase of the biphasic growth was strongly coupled to the shutoff region of the reaction. Only the reaction with 1 mM SBC had a sufficiently long slow growth, free from interference by substrate depletion (i.e., decay of the quinonoid) that fitting to the sum of two exponentials was attempted. The values of k_1 (for the fast growth), and k_2 (for the slow growth) were 42±4 sec^{-1} and 0.68±0.02 sec^{-1}, respectively (Table 8.1). Later, the slow growth for the reaction of tryptophanase with 0.5 and 1.0 mM SBC was fitted to a

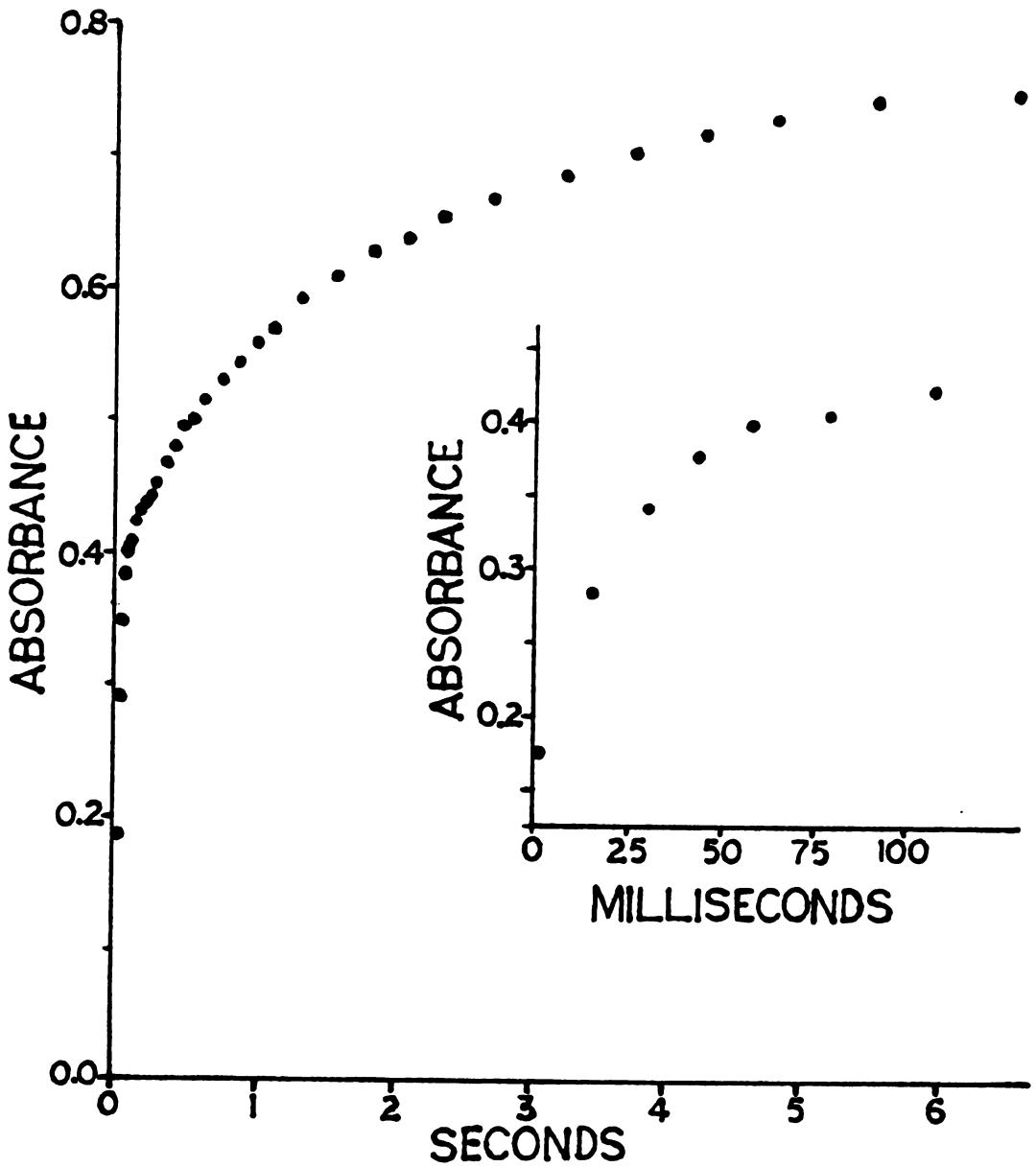

Figure 8.2. Biphasic Changes in Tryptophanase Absorbance at 478 nm as a Function of Time After Mixing with S-Benzyl-L-Cysteine in 25 mM Kepps, 0.1 M KCl, pH 8.0, 1 mM KEDTA, 1 mM DTT and 5 μM PLP. After Mixing Concentrations Were 1 mM S-Benzyl-L-Cysteine and 2.27 mg mL^{-1} Tryptophanase. (The data for the first 110 msec are expanded in the inset.)

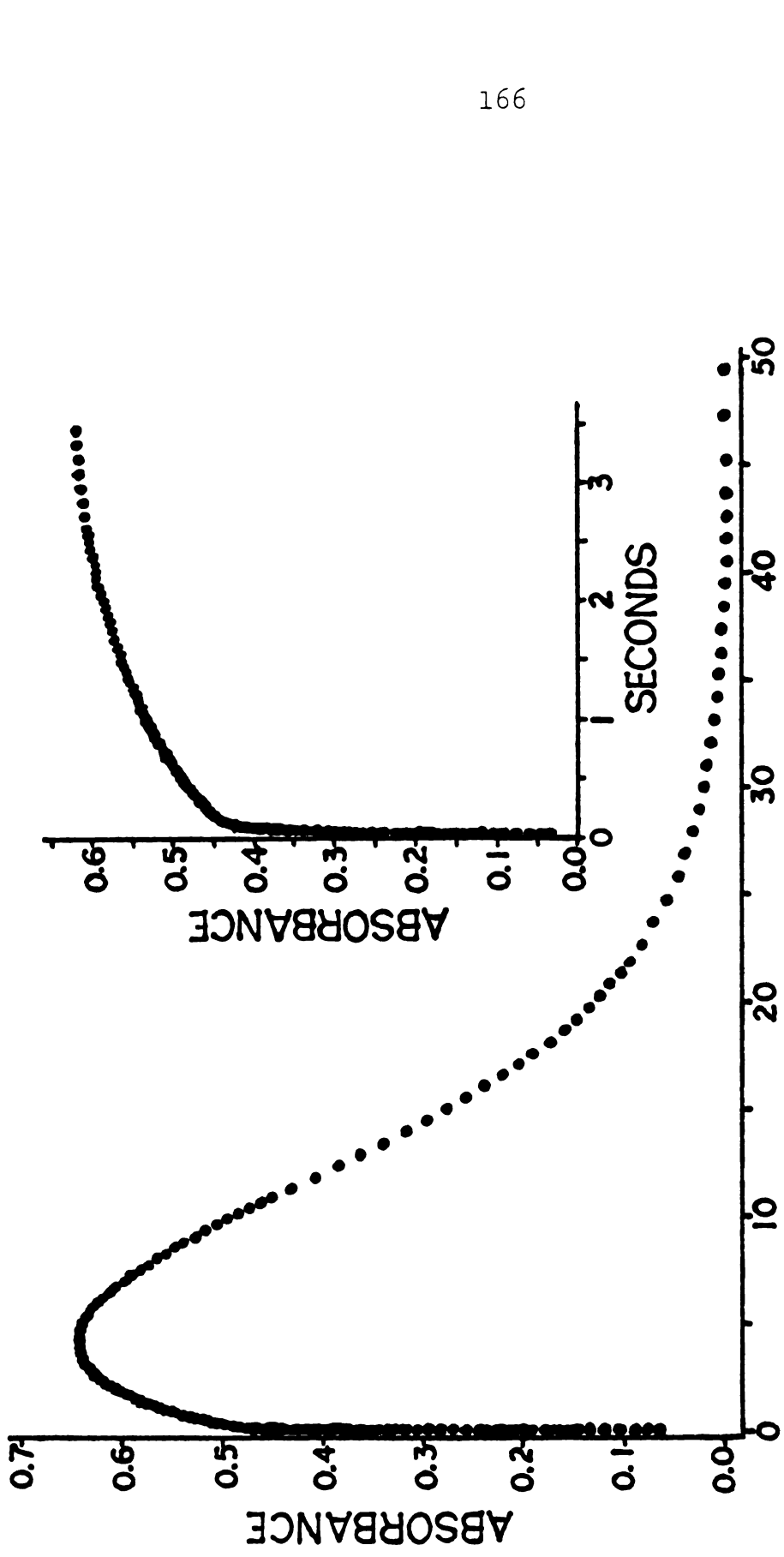

Figure 8.3. Overall Changes in Tryptophanase Absorbance at 478 nm as a Function of Time After Mixing with S-Benzyl-L-Cysteine in 25 mM Kepps, 0.1 M KCl, pH 8.0, 1 mM KEDTA, 1 mM DTT and 5 μM PLP. After Mixing Concentrations Were 0.5 mM S-Benzyl-L-Cysteine and 2.27 mg mL-1 Tryptophanase. (The inset shows the biphasic portion of the quinonoid.)

single exponential, and the corresponding values for k_2 are shown in Table 8.2.

The fast growth was fitted to a single exponential, and the k_1 values (Table 8.2) exhibited a hyperbolic dependence on SBC concentration yielding a value of 0.077 mM for the Michaelis constant, and 48.4 sec^{-1} for k_1 at infinite SBC concentration.

C.4. Absorbance Changes at 360 nm

A slow decay occurred at 360 nm with all SBC concentrations. Only scanning spectra were available at this wavelength, and it was not possible to reliably analyze the data due to the low total absorbance changes at this wavelength. June et al. (194) attributed changes at this wavelength to the δ-form of the enzyme (Scheme I; Figure 7.1).

C.5. Absorbance Changes at 397 nm

A fast decay (about 200 msec) followed by a slow decay occurred at 397 nm. Both phases had small total absorbance changes. The fast decay is due to the 420-nm form, since 397 nm is a shoulder of this band (188). The slow decay reflects changes in the spectrum of free PLP (194), and as such, it is not directly involved in the mechanism of tryptophanase catalysis.

C.6. Correlations Between the Fast Phases at 420 and 478 nm (508 nm)

The results obtained for k_1, along with the corresponding K_m and V_{max} values (Table 8.2) at 420 and 478 nm, clearly show the correspondence between the fast decay at 420 nm, and the simultaneous fast growth of the quinonoid at 478 nm (insets in Figures 8.1 and 8.2). This confirms the findings of June *et al.* (197) who reported that the 420-nm band (β-conformation) is the active form of the enzyme, i.e., the form directly preceding the quinonoid, and not the 327-nm band (γ-conformation) as previously reported by Marino and Snell (184) and Snell (175).

C.7. Correlations Between the Slow Phases at 337 and 478 nm (508 nm)

The rate of disappearance of the 337-nm absorbance is the same as the rate of the slow phase of quinonoid formation at 478 nm, and is essentially unaffected by SBC concentration (Table 8.2). The average rate constant for the slow decay at 337 nm obtained with SBC, 0.40 ± 0.12 sec^{-1}, compares favorably with 0.51 ± 0.14 sec^{-1}, obtained by June *et al.* (197) with the inhibitor ethionine, and agrees closely with the rate constant for the conversion of the 337-nm form, conformation γ, to the 420-nm form, conformation β, following a rapid decrease in pH (194). Thus the

337-nm form apparently does not form quinonoid directly but is first converted to the 420 nm form before the α-proton of an amino acid substrate, or inhibitor (197), is removed to form quinonoid.

D. Preliminary Principal Component Analysis of the Reaction of S-Benzyl-L-Cysteine with Tryptophanase

In this section, an attempt will be made to describe, in brief, some highlights of the principal component analysis of rapid scanning wavelength kinetic experiments. Later, some aspects of the method will be used in the analysis of the reaction of S-benzyl-L-cysteine (SBC) with tryptophanase. Details of the method are discussed in the doctoral dissertation of R. Cochran (17); see also, Cochran and Horne (201, 202) and Cochran et al. (203).

D.1. Introduction

A typical scanning stopped-flow kinetics experiment generates an absorbance-wavelength-time surface. This surface contains information about the static spectrum and concentration-time profile of each absorber in the reaction. The ultimate goal of such experiments is to identify one or more kinetic mechanisms that satisfactorily explain the concentration-time profiles of each of these absorbers. However, one must first extract these

concentration profiles from the experiments. Moreover, one needs to be able to extract the static spectra and concentration profiles before proposing a specific kinetic mechanism, since a kinetic mechanism presupposes that the concentration profiles are already known.

Prior to analysis of such kinetic experiments, the number of absorbers which occur in a reaction is not generally known. Although one usually knows which of the chemicals initially mixed are absorbers, and although one sometimes knows which products are absorbers, one usually does not know how many light absorbing transient intermediates occur in the reaction.

In a scanning stopped-flow experiment, absorbance is measured at $\underline{P}$ wavelength channels across a selected spectral region that is rapidly and repeatedly scanned as the reaction progresses. If the scanning rate is fast compared to the fastest absorbance change in the reaction, the resulting $\underline{N}$ consecutive spectra may be regarded as instantaneous, and the absorbance-wavelength-time surface may be represented by a PXN matrix $\underline{A}$, the actual experimental surface.

Cochran and Horne (201,202) developed the method of statistically weighted principal component analysis to determine the minimum number of absorbers required to explain each scanning experiment, and how many of these change concentration during a reaction. The authors describe

two kinds of principal component analysis (PCA) useful for kinetic experiments. Each requires only the matrix A from a scanning stopped-flow experiment, and each gives a lower bound estimate of the number of solutes in the reaction with a spectrophotometric response. Second moment matrix principal component analysis, called M analysis, gives a lower bounds estimate that is sensitive to the linear dependence of the concentrations of the detectable species. Sample covariance matrix principal component analysis, called S analysis, gives an estimate that is sensitive to the linear dependence of the time rates of the concentrations. These two estimates are not necessarily the same, and the authors show that application of both analyses enables discrimination between mechanistic alternatives that would be indistinguishable with either analysis alone.

The authors first develop rules for the application of M and S analyses to errorless data. With this simplification, the M and S estimates of the number of solutes are the ranks of respectively, the second moment matrix, M, and the sample covariance matrix, S. Later, they discuss the effects of random measurement errors, and in particular, the case in which the variance of the measurement errors, as a function of wavelength, is not constant throughout the experiment. The goal is to infer the essential ranks of the two matrices; i.e., the ranks that would be obtained if

measurement errors could be eliminated. The details of utilizing a general error variance model to develop a weighting scheme, are described in R. N. Cochran's doctoral dissertation (17). Cochran and Horne (201) used the variance model to weight the absorbance matrix $\underline{A}$, before performing the principal component calculations.

The applicability of PCA requires only that the response at each wavelength channel be a linear function of the concentrations of each detectable species, i.e., that Beer's Law holds.

The starting point for weighted M and S analyses is the properly weighted (201) experimental absorbance matrix, $\underline{A}_w$, obtained from a scanning stopped-flow experiment. Based on $\underline{A}_w$, M analysis reconstructs an absolute absorbance matrix, $\hat{\underline{A}}_r$. The essential rank m corresponds to the minimum number of linearly independent absorbers (eigenvectors) required to interpret the experiment, and is determined by finding the lowest value of r for which the reconstructed absorbance matrix $\hat{\underline{A}}_r$ fits the experimental matrix $\underline{A}$ to within its random errors. S analysis forms the experimentally weighted difference matrix ($\underline{A}_w - \overline{\underline{A}_w}$) [formed by subtracting the average of all the weighted N spectra, $\overline{\underline{A}_w}$, from each spectrum in $\underline{A}_w$] to reconstruct a difference absorbance matrix, ($\hat{\underline{A}}_r - \overline{\underline{A}}$). The essential rank s corresponds to the minimum number of linearly independent absorbers (eigenvectors) whose concentrations must have changed during the

experiment, and is determined by finding the lowest value of r for which ($\underline{\hat{A}}_r - \underline{\bar{A}}$) fits the experimental matrix ($\underline{A} - \underline{\bar{A}}$) to within its random errors.

Two criteria were used by Cochran et al. (203) to determine, via M analysis, how well the experimental surfaces were fit by reconstructed surfaces: (1) visual comparison of plots of the reconstructed absolute surface, $\underline{\hat{A}}_r$, and the experimental surface, $\underline{A}$, and (2) examination of the weighted residual surfaces, i.e., plots of the residuals ($\underline{\hat{A}}_r - \underline{A}$). The residuals should be random when plotted versus time and wavelength. The same protocol was followed with S analysis.

D.2. Data Analysis

In the present work, weighted M analysis was used to analyze the reaction of S-benzyl-L-cysteine with tryptophanase. Reconstructed absolute surfaces were plotted for $\underline{\hat{A}}_3$ through $\underline{\hat{A}}_7$, which correspond respectively to r=3 through 7 eigenvectors (absorbers). Residual surfaces, ($\underline{\hat{A}}_r - \underline{A}$) were also plotted for the same r values. Careful visual comparison of the reconstructed absolute surfaces revealed that $\underline{A}_6$ was the closest match to the experimental surface to within its random errors. Figure 8.4 shows the experimental surface $\underline{A}$ for the reaction of 0.125 mM SBC with tryptophanase. Figure 8.5 shows the reconstructed surface $\underline{\hat{A}}_6$. For comparison, $\underline{\hat{A}}_5$, shown in Figure 8.6 did not

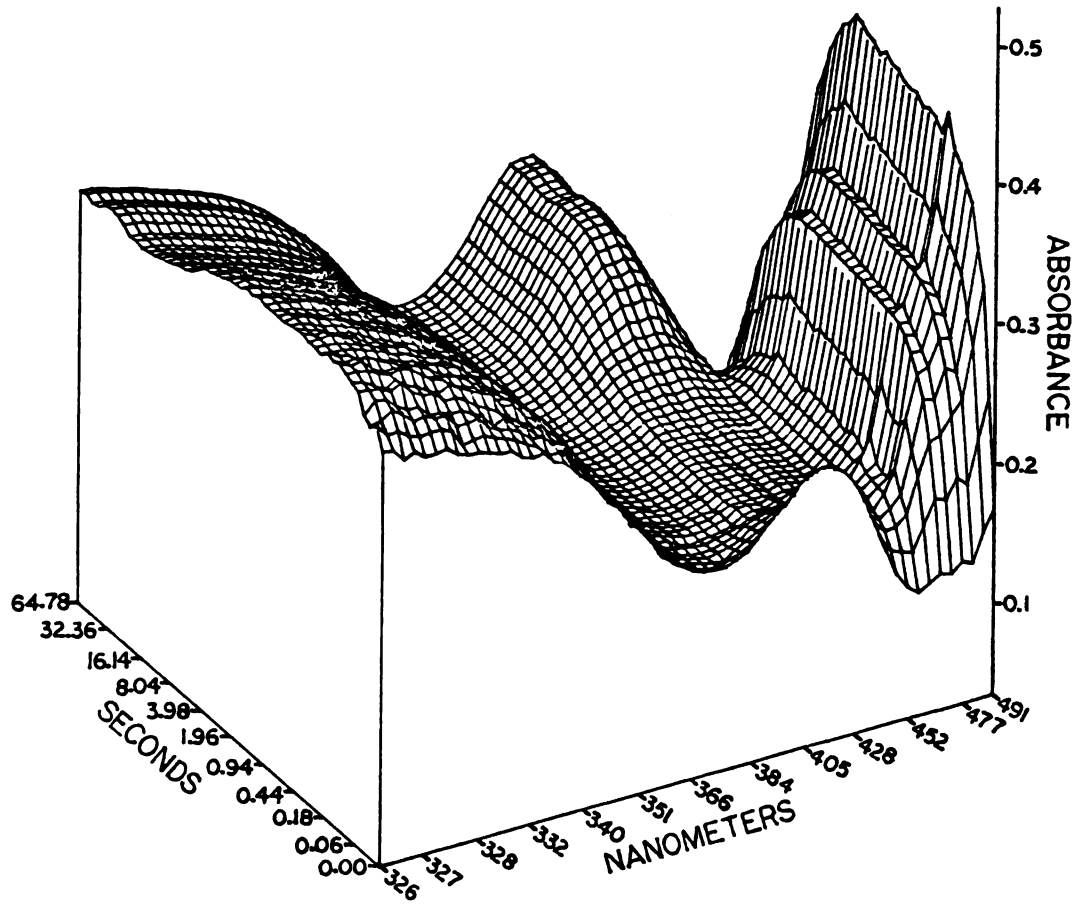

RESOLV1CCABAFSETAPE11 2.27MG/ML TRYPTOPHANASE + 0.125MM S-BENZYL-CYSTEINE

Figure 8.4. Experimental Surface, A, for the Reaction of 0.125 mM S-Benzyl-L-Cysteine with 2.27 mg mL^{-1} Tryptophanase.

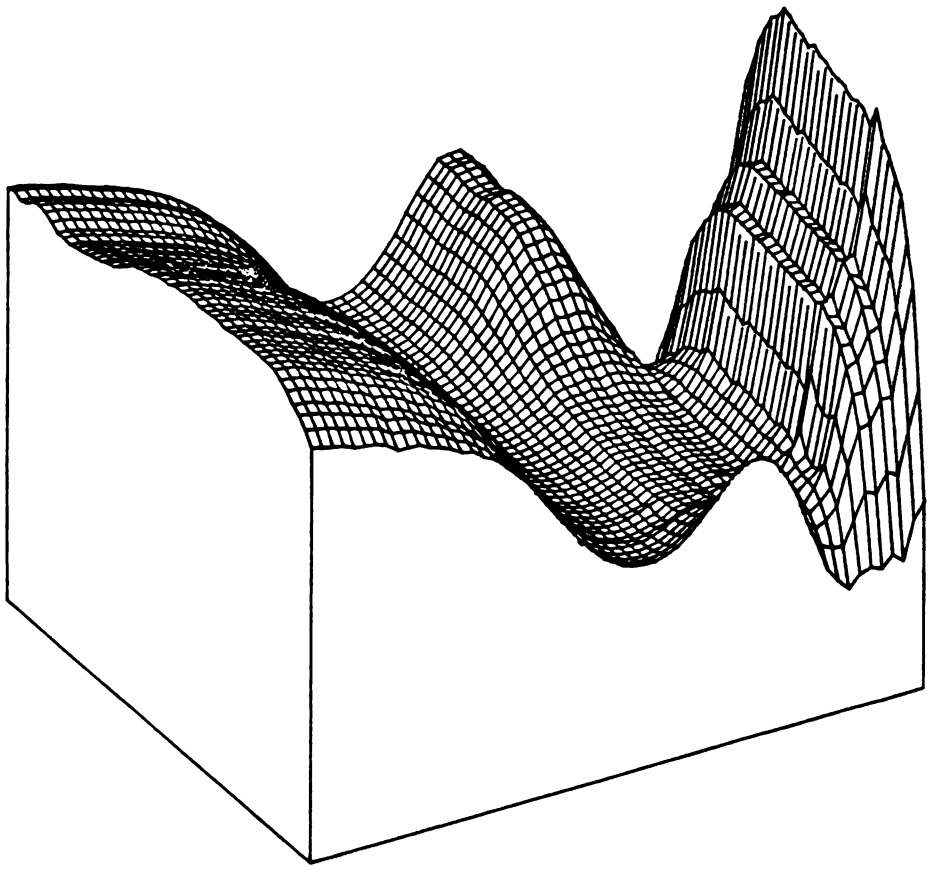

Figure 8.5. Reconstructed Absolute Surface, $\underline{\hat{A}}_6$, for the Reaction of 0.125 mM S-Benzyl-L-Cysteine with 2.27 mg mL^{-1} Tryptophanase.

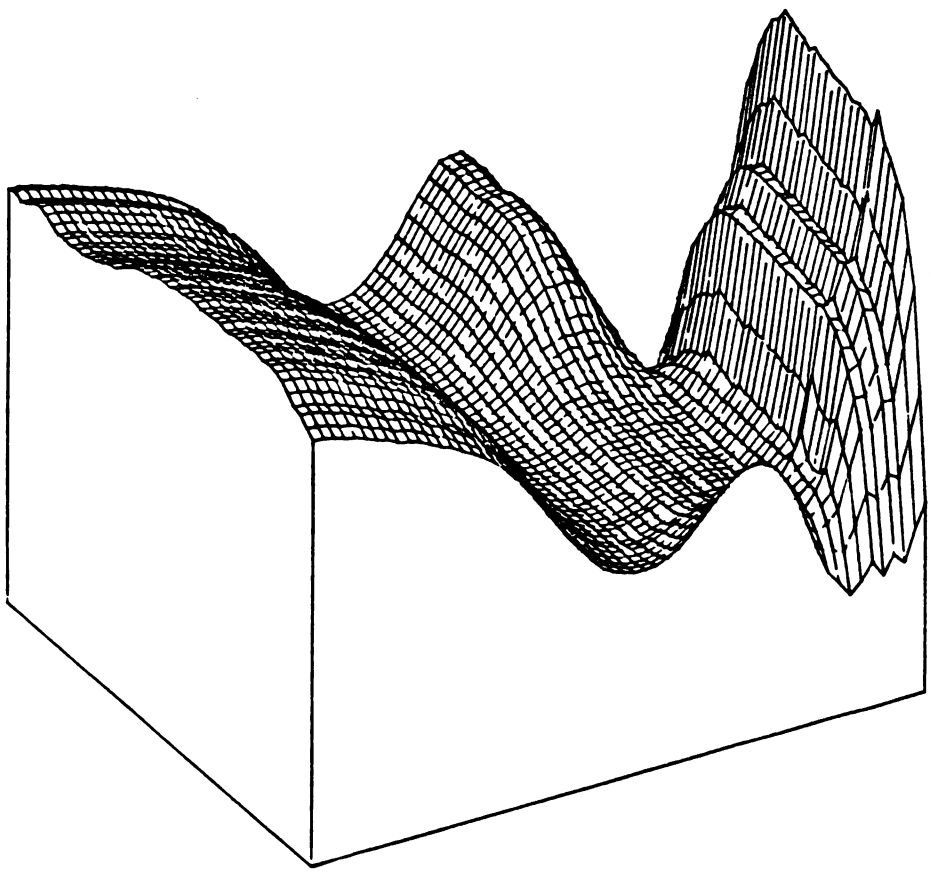

RESOLV3CCABAFSE5EVABSSURF. 0.125 mM S-BENZYL-CYSTEINE.

Figure 8.6. Reconstructed Absolute Surface, $\hat{\underline{A}}_5$, for the Reaction of 0.125 mM S-Benzyl-L-Cysteine with 2.27 mg mL^{-1} Tryptophanase.

reproduce the experimental surface. Inspection of the residual surfaces provided better visual comparison of the fit, and for ($\underline{\hat{A}}_6$ - $\underline{A}$) shown in Figure 8.7, the randomness is clearly evident. Figure 8.8 shows the residual surface for r=5, which clearly shows non-randomized residuals. The same results were obtained in the M analysis of the reaction of 0.0625, 0.25, 0.5 and 1.0 mM SBC with tryptophanase.

Hence, M analysis indicates that a minimum of six absorbers, with a spectrophotometric response, are present in the reaction of SBC with tryptophanase, since a minimum of six eigenvectors, (r=6), are required to reconstruct the surfaces to within the random errors of the experimental surfaces.

Three of these absorbers, namely, the 337, 420 and 508-nm forms have already been analyzed in this study. The fourth absorber is the 360-nm form (δ-conformation). The fifth is the nonenzymatic PLP absorber with a maximum at 397 nm, and the sixth is the independent slow growth at 420 nm (following the fast phase), which is probably due to the nonenzymatic formation of a Schiff base between excess free SBC and PLP.

As described earlier, application of M analysis yields the minimum number of linearly independent absorbers required to reconstruct the experimental surface. However, according to the results obtained earlier (Section B),

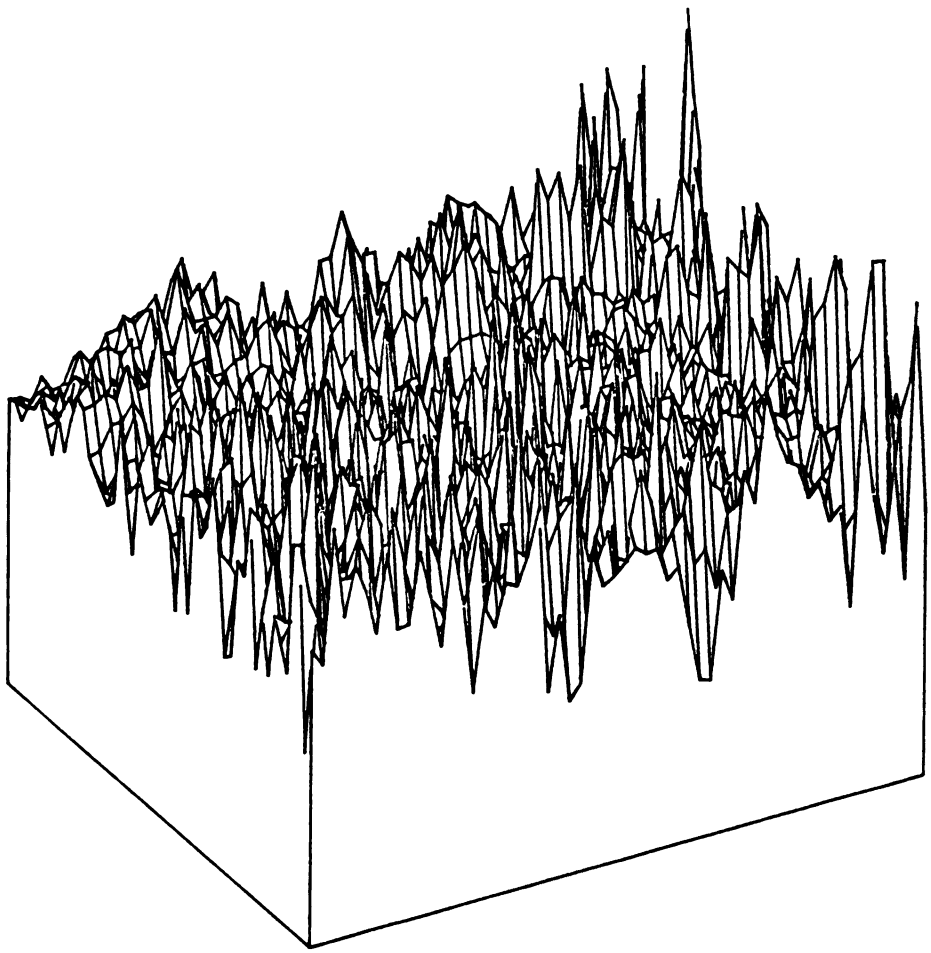

Figure 8.7. Reconstructed Residual Surface, ($\hat{\underline{A}}_6$ - $\underline{A}$) for the Reaction of 0.125 mM S-Benzyl-L-Cyesteine with 2.27 mg mL^{-1} Tryptophanase.

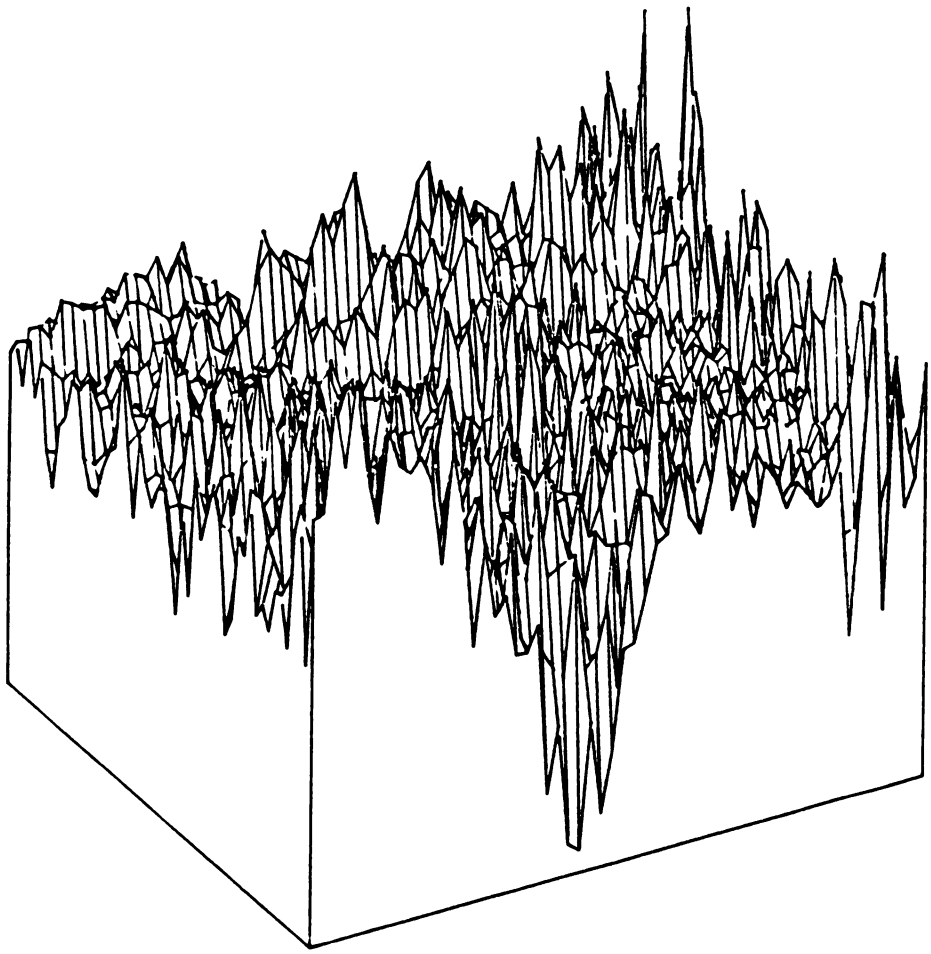

Figure 8.8. Reconstructed Residual Surface, ($\hat{\underline{A}}_5$ - $\underline{A}$), for the Reaction of 0.125 mM S-Benzyl-L-Cysteine with 2.27 mg mL^{-1} Tryptophanase.

concentration changes of some of these absorbers should not be linearly independent in time. In particular, the coupling of the fast decay at 420 nm to the fast growth of the quinonoid at 508 nm, and the slow decay at 337 nm to the slow growth of the quinonoid. S analysis must be performed in order to verify these findings.

CHAPTER 9

SUGGESTIONS FOR FUTURE WORK

A. AMP-Aminohydrolase

Four modes of action are suggested. The first involves a systematic study of product (IMP) effects on the catalytic reaction, which may yield information helpful in clarifying the role of product on the enzyme activation. The second involves studies on the activation of enzyme by (H^+) ion. This would constitute a follow up of the work done by Campbell and Suelter (147), in which they reported on the activation of AMP-aminohydrolase (from rabbit skeletal muscle) by (H^+). Stopped-flow studies on the uptake and release of (H^+) may provide information on the conformational changes in the enzyme following interaction of K^+. The third suggestion would be to conduct sedimentation velocity studies on K^+-free AMP-aminohydrolase, as a function of temperature, to verify the conclusions made about the dissociation of the tetrameric enzyme at low temperatures. The fourth should involve stopped-flow studies on the effects of ADP, ATP and GDP, on the catalytic reaction of the enzyme, as a function of pH. This should

help clarify the present ambiguities as to the effect of these nucleotides on the regulatory role of AMP-amino-hydrolase at, and below physiological pH levels.

B. Tryptophanase

Since the equilibrium concentrations of the spectral forms of tryptophanase are pH dependent (193,194), the reaction of S-benzyl-L-cysteine with tryptophanase should be performed as a function of pH. One important point that could be resolved from such an experiment is whether the δ-form can also form a Schiff base directly with S-benzyl-L-cysteine, which would then form the quinonoid. The other would be to study the pH dependence of the quinonoid formed between this substrate, and to compare such results to those obtained with the inhibitor ethionine (197).

Fixed wavelength pushes should be done with S-benzyl-L-cysteine at 360 nm in order to reliably analyze the mechanistic role of the δ-form.

Finally, complete principal component analysis of the reaction of S-benzyl-L-cysteine with tryptophanase is suggested.

APPENDICES

APPENDIX A

Uncomplicated "Clean" Reaction and Its Independence of Wavelength

For an uncomplicated "clean" reaction, where only the reactant and product absorbances change with time, the absolute absorbance (A_t) at any time (t), and at any wavelength is:

$$A_t = (\varepsilon_B)(b)(B) + (\varepsilon_E)(b)(E) + (\varepsilon_S)(b)(S) + (\varepsilon_P)(b)(P) \quad (1)$$

where (A_t) is the absorbance at any time (t); (ε_B), the sum total of the background absorptivity; (b), the path length of the cell; (B), the sum total of the background absorbance; (ε_E), the absorptivity of the enzyme; (E), the enzyme concentration; (ε_S), the substrate absorptivity; (S), the substrate concentration; (ε_P), the product absorptivity; and (P), the product concentration.

Furthermore, if (S_0) >> (E_0), where (S_0) is the initial substrate concentration, and (E_0) the initial enzyme concentration, then

$$(S_0) = (S) + (P) \tag{2}$$

Substitution of (2) into (1) yields:

$$A_t = (b)[(\varepsilon_B)(B) + (\varepsilon_E)(E) + (\Delta\varepsilon)(P) + (\varepsilon_S)(S_0)] \tag{3}$$

where

$$\Delta\varepsilon = \varepsilon_p - \varepsilon_s \tag{4}$$

The absorbance at infinity (A_∞) is:

$$A_\infty = (b)[(\varepsilon_B)(B) + (\varepsilon_E)(E) + (\varepsilon_P)(S_0)] \tag{5}$$

The absorbance at zero time (A_0) is:

$$A_0 = (b)[(\varepsilon_B)(B) + (\varepsilon_E)(E) + (\varepsilon_P)(S_0)] \tag{6}$$

Subtraction of (6) from (1) yields:

$$A_t - A_0 = (\Delta\varepsilon)(b)(P) \tag{7}$$

Subtraction of (6) from (5) yields:

$$A_\infty - A_0 = (\Delta\varepsilon)(b)(S_0) \tag{8}$$

Dividing (7) by (8) yields:

$$\frac{A_t - A_0}{A_\infty - A_0} = \frac{(P)}{(S_0)} \qquad (9)$$

Rearranging equation (9) yields:

$$A_t = A_0 + \frac{(P)(A_\infty - A_0)}{(S_0)} \qquad (10)$$

Equation (10) is independent of the wavelength (λ).

APPENDIX B

MODEL A

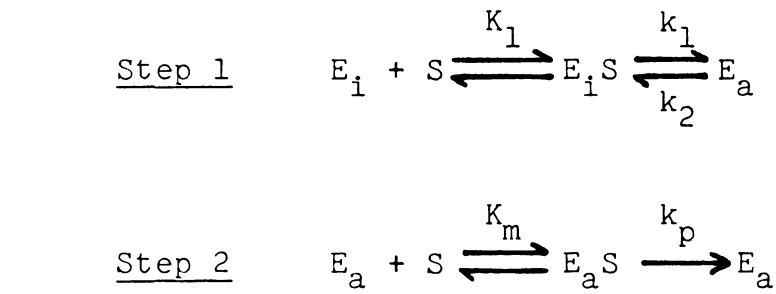

where (E_i) is the inactive enzyme; (S), the substrate; (E_a), the active enzyme, (P) the product; capital (K)'s, are equilibrium constants and small (k)'s are rate constants.

The initial enzyme concentration (E_0) is:

$$E_0 = E_i + E_iS + E_a + E_aS \qquad (1)$$

The initial substrate concentration (S_0) is:

$$S_0 = S + E_iS + E_a + 2E_aS + P \qquad (3)$$

From the equilibria in Steps (1) and (2) above:

$$E_iS = \frac{(E_i)(S)}{K_1} \tag{3}$$

and

$$E_aS = \frac{(E_a)(S)}{K_m} \tag{4}$$

Substituting (3) and (4) into (1), and solving for (E_i) yields:

$$E_i = \frac{E_0 - E_a(1 + S/K_m)}{(1 + S/K_1)} \tag{5}$$

Define (E), as the total concentration of <u>active enzyme</u>; then

$$E = E_a + E_aS \tag{6}$$

Substituting (4) into (6), and solving for (E_a) yields:

$$E_a = \frac{E}{(1 + S/K_m)} \tag{7}$$

Substitution of (7) into (5) yields:

$$E_i = \frac{(E_0 - E)}{(1 + S/K_1)} \tag{8}$$

Substitution of (8) into (3) yields:

$$E_iS = \frac{(S)(E_0 - E)}{(S + K_1)} \tag{9}$$

Substitution of (8) into (4) yields

$$E_aS = \frac{(E)(S)}{S + K_m} \tag{10}$$

Subtraction of (1) from (2), using (8) and (9) for the values of (E_i) and (E_iS), respectively; and finally solving for (S) yields:

$$S = S_0 - P - E_0 = \frac{(S)(E)}{(S+K_m)} + \frac{K_1(E_0 - E)}{(S + K_1)} \tag{11}$$

Since,

$$\frac{dP}{dt} = k_p\ (E_aS) \tag{12}$$

then substitution of (10) into (12) yields:

$$\frac{dP}{dt} = \frac{k_p(E)(S)}{(S + K_m)} \tag{13}$$

and since

$$\frac{dE}{dt} = k_1(E_iS) - k_2(E_a) \tag{14}$$

then substituting values for (E_iS) and (E_a) from (9) and (7) respectively, into (14) yields:

$$\frac{dE}{dt} = \frac{k_1(S)(E_0 - E)}{(S + K_1)} - \frac{k_2(E)}{(1 + S/K_m)} \tag{15}$$

The working equations for KINFIT4 are then (11), (13) and (15)

APPENDIX C

THE MONOD WYMAN AND CHANGEUX MODEL (MWC) - Concerted Model

The model represents a tetrameric enzyme with one active, and one activator site per subunit.

In the scheme shown below, only rate constants are represented. For comparison, see Figure 6.12

In the MWC Scheme the (k)'s represent rate constants; (E), the inactive enzyme; (E'), the active enzyme; (A), the activator species; (EA_n), the inactive enzyme-activator complex; and ($E'A_n$), the active enzyme-activator complex, with (n) = 0,4.

Also (k_f)'s represent the forward rate constants, and (k_r)'s the reverse rate constants.

Then

$$K = k_r/k_f$$

and

$$K' = k'_r/k'_f$$

MWC Scheme

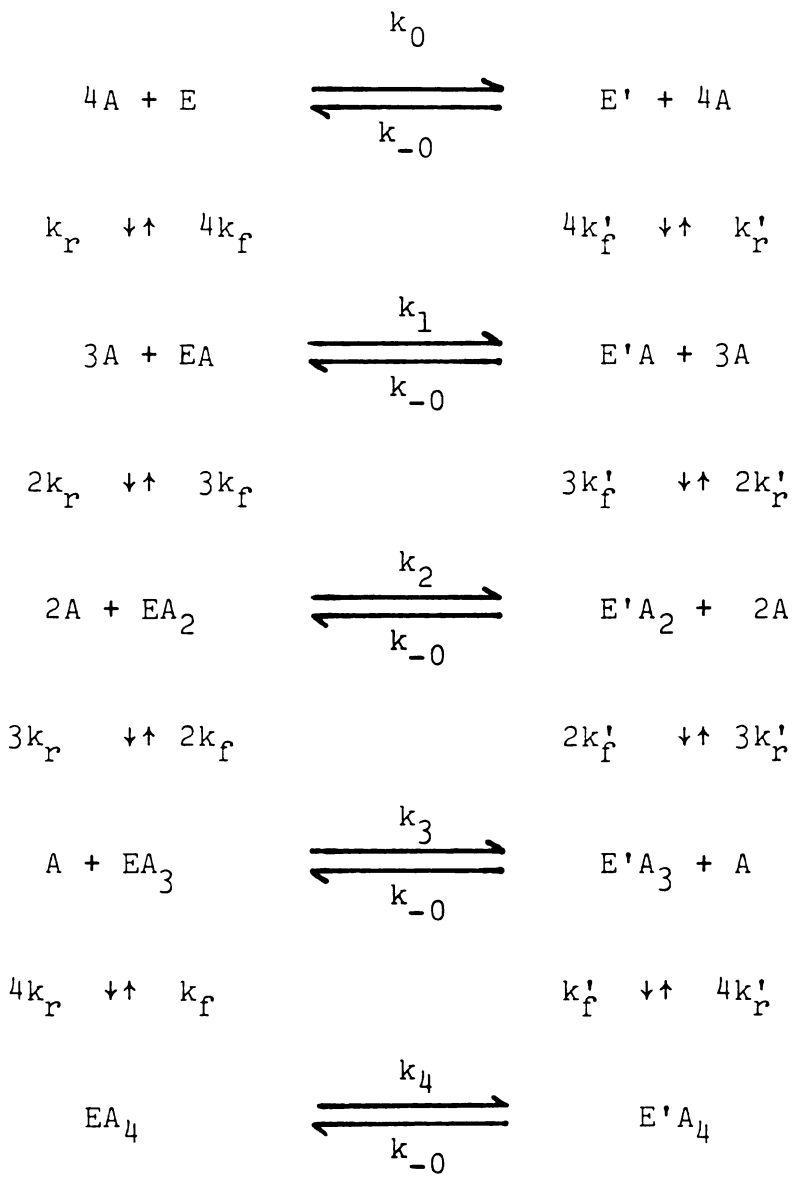

For a "tractable" model, four assumptions were further made, without which the solution to this scheme would become too complicated to resolve, as the number of unknowns (parameters) would become too large to be determined reliably for purposes of data fittings.

The assumptions made were as follows:

(1) While changes from inactive to active conformations proceed at different rates, (k)'s (governed by thermodynamical constraints) for the various E → E' forms; the reverse deactivation rate (k_{-0}) is the same for all forms. Thus,

$$EA_i \overset{\rightarrow}{\leftarrow} E'A_i; \quad i = 0,4$$

is independent as to whether or not substrate is bound to the enzyme. This means that (K_m) for the active site on (E) and (E') is the same. Therefore substrate can equally bind to the active and inactive conformations; however, only the active conformation is able to successfully process the substrate to form product,

(2) substrate depletion, and activation by product, during activation of the enzyme is assumed to be negligible,

(3) the rate for (E_0'), the total concentration of active enzyme, is assumed to reach a steadv state; i.e.,

$$\frac{d(E_0')}{dt} = 0$$

(4) The (E_0) forms are all in equilibrium, governed by the same equilibrium constant (K), and the addition or

removal of an activator is governed only by statistical probabilities of the occupied and unoccupied sites. In other words, since

$$K = \frac{k_r}{k_f}$$

it is assumed that the forward and reverse rate constants (k_f) and (k_r), respectively, are the same for the different forms. But depending on the number of occupied and unoccupied sites, in any one of the (E_0) species, each (k_r) and (k_f) is then multiplied by the appropriate (whole integer) statistical factor.

Thus cooperativity occurs simply as a result of the statistics imposed by the model.

The same assumption was made for the (E_0') forms and their associated (K')s.

Finally, for activation to occur, (K) must be greater than (K').

Using thermodynamical constraints about each of the four loops in the scheme:

$$k_1 = k_0(K/K'),$$

$$k_2 = k_0(K/K')^2,$$

$$k_3 = k_0(K/K')^3, \text{ and}$$

$$k_4 = k_0(K/K')^4$$

Let the total active enzyme concentration (E'_0) be:

$$E'_0 = E' + E'A + E'A_2 + E'A_3 + E'A_4 \tag{1}$$

the total inactive enzyme concentration (E_0):

$$E_0 = E + EA + EA_2 + EA_3 + EA_4 \tag{2}$$

Then, the initial enzyme concentration $(E_0)_T$ is:

$$(E_0)_T = E_0 + E'_0 \tag{3}$$

After activation of the enzyme, the Michaelis-Menten scheme is followed, thus the rate of product formation is

$$\frac{dP}{dt} = \frac{k_p(E'_0)}{(1 + K_m/S)} \tag{4}$$

The (E) forms represent:

$$\begin{aligned} E &= E + ES + \ldots + ES_4 \\ EA &= EA + EAS + \ldots + EAS_4 \\ &\vdots \qquad\qquad\qquad\qquad \vdots \\ EA_4 &= EA_4 + EA_4S + \ldots + EA_4S_4 \end{aligned} \tag{5}$$

The (E') forms are similarly represented.

Then from the equilibria in the scheme:

$$EA = 4(E)(A/K); \qquad EA_2 = 6(E)(A/K)^2$$
$$EA_3 = 4(E)(A/K)^3; \qquad EA_4 = (E)(A/K)^4 \tag{6}$$

and also:

$$E'A = 4(E')(A/K') ; \qquad E'A_2 = 6(E')(A/K')^2$$
$$E'A_3 = 4(E')(A/K')^3; \qquad E'A_4 = (E')(A/K')^4 \tag{7}$$

Then,

$$\frac{d(E'_0)}{dt} = ([k_0(E) + k_1(EA) + k_2(EA_2) + k_3(EA_3) + k_4(EA_4)]$$
$$- k_{-0}[E' + E'A + E'A_2 + E'A_3 + E'A_4]) \tag{8}$$

Substitution of (6) into (8) yields:

$$\frac{d(E'_0)}{dt} = [k_0(E)[1 + 4(A/K') + 6(A/K')^2 + 4(A/K')^3$$
$$+ (A/K')^4] - k_{-0}(E'_0)] \tag{9}$$

Combining terms from (9) results in:

$$\frac{d(E'_0)}{dt} = k_0(E)[1 + (A/K')]^4 - k_{-0}(E'_0) \qquad (10)$$

Substitution of (7) into (1) yields:

$$(E'_0) = (E')[1 + (A/K')]^4 \qquad (11)$$

Substitution of (6) into (2) yields:

$$(E_0) = (E)[1 + (A/K)]^4 \qquad (12)$$

Substitution of (12) into (10) yields:

$$\frac{d(E'_0)}{dt} = \frac{k_0(E_0)[1 + (A/K')]^4}{[1 + (A/K)]^4} - k_{-0}(E'_0) \qquad (13)$$

But from (3),

$$E_0 = (E_0)_T - E'_0 \qquad (14)$$

Then substitution of (14) into (13) gives

$$\frac{d(E'_0)}{dt} = k_0(E_0)_T \frac{(1+A/K')^4}{(1+A/K)^4} - (E'_0)[k_0 \frac{(1+A/K')^4}{(1+A/K)^4} + k_{-0}] \qquad (15)$$

let

$$Q = \frac{(1 + A/K')^4}{(1 + A/K)^4} \tag{16}$$

and

$$B = k_0(Q) \tag{17}$$

then

$$\frac{d(E'_0)}{dt} = (E_0)_T(B) - (E'_0)(B + k_{-0}) \tag{18}$$

Equation (18) is in the form:

$$\frac{dy}{dt} = M - N_y \tag{19}$$

Equation (19) can be rearranged to

$$\frac{d(M - Ny)}{(M - Ny)} = - N\, dt \tag{20}$$

Thus, rearranging equation (18) in the same fashion and integrating yields:

$$(E_0') = (E_0') \qquad t=t$$

$$\int \frac{d[(B)(E_0)_T-(B+k_{-0})(E_0')]}{[(B)(E_0)_T-(B+k_{-0})(E_0')]} = \int -(B+k_{-0})dt$$

$$(E_0') = (E_0')_0 \qquad t=0$$

(21)

let

$$k' = B + k_{-0} \tag{22}$$

then

$$\frac{(B)(E_0)_T - (k')(E_0')}{(B)(E_0)_T - (k')(E_0')_0} = e^{-k't} \tag{23}$$

Solving for (E_0') yields:

$$(E_0') = \frac{(B)(E_0)_T}{k'}(1-e^{-k't}) + (E_0')_0\, e^{-k't} \tag{24}$$

$$\text{at large (t), } (E_0') = \frac{(B)(E_0)_T}{k'} \tag{25}$$

let

$$(E_0')_\infty = \frac{(B)(E_0)_T}{k'} \quad , \quad \text{for large (t)} \tag{26}$$

Substitution of (26) into (24) yields:

$$(E_0') = (E_0')_\infty(1-e^{-k't}) + (E_0')_0 e^{-k't} \tag{27}$$

$(E_0')_0$ is the concentration of (E_0') at zero time; i.e., prior to the addition of activator. Thus $(E_0')_0$ is assumed to be close to zero, since at zero time, (E') the active enzyme concentration, prior to the addition of activators is itself very small.

Therefore,

$$(E_0') = (E_0')_\infty(1-e^{-k't}) \tag{28}$$

Substitution of (28) into (4) yields the final working equation:

$$\frac{dP}{dt} = \frac{k_p(E_0')_\infty(1-e^{-k't})}{(1 + K_m/S)} \tag{29}$$

REFERENCES

REFERENCES

1. Roughton, F. J. W., Proc. R. Soc., B115, 475 (1934).

2. Chance, B., J. Franklin Inst., 229, 455, 613, 637 (1940).

3. Gibson, Q., J. Physiol., 117, 49P (1952).

4. Sturtevant, J. M., Rapid Mixing and Sampling Techniques in Biochemistry, Editors: Chance, B., Eisenhardt, R. H., Gibson, Q. H., and Lonberg-Hohn, K. K., Academic Press, New York (1964), p. 89.

5. Dye, J. L., Acc. Chem. Res., 1, 306 (1968).

6. Dye, J. L., and Feldman, L. H., Rev. Sci. Instrum., 37, 154 (1966).

7. Dewald, R. R., Dye, J. L., Eigen, M., and deMaeyer, L., J. Chem. Phys., 39, 2388 (1963).

8. Feldman, L. H., Dewald, R. R., and Dye, J. L., in "Solvated Electron, Adv. Chem. Ser., 50, 163 (1964).

9. Ho, G.-H., Dye, J. L., and Suelter, C. H., J. Biochem. and Biophys. Methods, 4, 287 (1981).

10. DeBacker, M. G., and Dye, J. L., J. Phy. Chem., 75, 3092 (1971).

11. Minnich, E. R., Long, L. D., Ceraso, J. M., and Dye, J. L., J. Am. Chem. Soc., 95, 1061 (1973).

12. Hansen, E. M., Ph.D. Dissertation, Michigan State University, East Lansing, Michigan (1970).

13. Coolen, R. B., Papadakis, N., Avery, J., Enke, C. G., and Dye, J. L., Anal. Chem., 47, 1649 (1975).

14. Ho, G.-H., Ph.D. Dissertation, Michigan State University, East Lansing, Michigan (1976).

15. Papadakis, N., Ph.D. Dissertation, Michigan State University, East Lansing, Michigan (1974).

16. Coolen, R. B., Ph.D. Dissertation, Michigan State University, East Lansing, Michigan (1974).

17. Cochran, R. N., Ph.D. Dissertation, Michigan State University, East Lansing, Michigan (1977).

18. Dye, J. L., and Nicely, V., J. Chem. Educ., 48, 443 (1971).

19. Hill, R., Proc. R. Soc., B100, 419 (1925).

20. Monod, J., Wyman, J., and Changeux, J.-P., J. Mol. Biol., 12, 88 (1965).

21. Adair, G. S., J. Biol. Chem., 63, 529 (1925).

22. Adair, G. S., Proc. Roy. Soc. London Ser., A109, 292 (1925).

23. Koshland, D. E., Nemethy, G., and Filmer, D., Biochemistry, 5, 365 (1966).

24. Eigen, M., Nobel Symposium, 5, 333 (1967).

25. Hammes, G. G., and Wu, C.-W., Science, 172, 1205 (1971).

26. Herzfield, J., and Stanley, H. E., J. Mol. Biol., 82, 231 (1974).

27. Suelter, C. H., Kovacs, A. L., and Antonini, E., FEBS Letters, 2, 65 (1968).

28. Ellis, K. J., Kuntz, K., and Sturtevant, J. M., J. Biol. Chem., 246, 6631 (1971).

29. Frieden, C., J. Biol. Chem., 245, 5788 (1970).

30. Ainslie, Jr., G. R., Schill, J. P., and Neet, K. E., J. Biol. Chem., 247, 7088 (1972).

31. Frieden, C., Ann. Rev. Biochem., 48, 471 (1979).

32. Pierce, T. H., Ph.D. Dissertation, Michigan State University, East Lansing, Michigan (1981).

33. Cukier, R. I., Levine, H. B., Shuler, K. E., J. Comput. Phys., 26, 1 (1978).

34. Blum, J. J., Arch. Biochem. Biophys., 55, 486 (1955).

35. Aust, A. E., Ph.D. Dissertation, Michigan State University, East Lansing, Michigan (1975).

36. Badwey, J. A., and Westhead, E. W., J. Biol. Chem., 251, 5600 (1976).

37. Spivey, H. O., Flory, W., Peczon, B. D., Chandler, J. P., and Koeppe, R. E., Biochem. J., 141, 119 (1974).

38. Rodriguez, H. B., and Halloway, M. R., Biochem. Soc. Trans., 4, 83 (1976).

39. Kirschner, K., Gallego, E., Schuster, I., and Goodall, D., J. Mol. Biol., 58, 29 (1971).

40. Shill, J. P., and Neet, K. E., Biochem. J., 123, 283 (1971).

41. Hatfield, G. W., Ray, Jr., W. J., and Umbarger, H. E., J. Biol. Chem., 245, 1748 (1970).

42. Mankovitz, R., and Segal, H. L., Biochemistry, 8, 3757 (1969).

43. Vagelos, P. R., Alberts, A. W., and Martin, D. B. J. Biol. Chem., 238, 533 (1963).

44. Rabin, B. R., Biochem. J., 102, 22c (1967)

45. Whitehead, E., Prog. in Biophys. and Mol. Biol., 21, 321 (1970).

46. Schmidt, G., Hoppe-Seyler's Z. Physiol. Chem., 179, 243 (1928).

47. Schmidt, G., Hoppe-Seyler's Z. Physiol. Chem., 208, 185 (1932).

48. Schmidt, G., Hoppe-Seyler's Z. Physiol. Chem., 219, 191 (1933).

49. Conway, E. J., and Cooke, R., Biochem. J., 33, 479 (1939).

50. Zielke, C. L., and Suelter, C. H., The Enzymes, 4, ed. Boyer, 3rd, ed., Academic Press, New York (1971).

51. Brams, J., J. Am. Chem. Soc., 81, 4997 (1959).

52. Atkinson, M. R., and Murray, A. W., Biochem. J., 104, 10c (1967).

53. Burger, R., and Lowenstein, J. M., J. Biol. Chem., 242, 5281 (1967).

54. Chapman, A. G., and Atkinson, D. E., J. Biol. Chem., 248, 8309 (1973).

55. Lee, Y., J. Biol. Chem., 227, 987 (1957).

56. Suelter, C. H., Byrnes, E. W., Berry, A., and Winely, C. L., Fed. Proc., 25, 756 (1966).

57. Kalckar, H. M., J. Biol. Chem., 167, 461 (1947).

58. Byrnes, E. W., and Suelter, C. H., Biochem. Biophys. Res. Commun., 20, 422 (1965).

59. Su, J.-C., Li, C.-C, and Ting, C. C., Biochemistry, 5, 536 (1966).

60. Wolfenden, R., Tomozawa, Y., and Bamman, B., Biochemistry, 7, 3965 (1968).

61. Setlow, B., Burger, R., and Lowenstein, J. M., J. Biol. Chem., 241, 1244 (1966).

62. Coffee, C. J., and Kofke, W. A., J. Biol. Chem., 250, 6653 (1975).

63. Lee, Y., The Enzymes, 4, Academic Press, New York (1959).

64. Ashby, B., and Frieden, C., J. Biol. Chem., 253, 8728 (1978).

65. Setlow, B., and Lowenstein, J. M., J. Biol. Chem., 242, 607 (1967).

66. Matsuo, I, Ohkido, M., Kizaki, H., and Sakurada, T., Biochem. Cutaneous Epidermal Differ., Proc. Jpn.-U.S. Semin. (1976); Edited by Seiji, M., and Bernstein, I. A., Univ. Park Press, Baltimore, Md. (1977).

67. Prus, E., Purzycha-Preis, J., Wozniak, M., and Zydowo, M., Acta Biochem. Pol., 27, 241 (1980).

68. Murakami, K., J. Biochem. (Tokyo), 86, 1331 (1979).

69. Niven, D. F., Collins, P. A., and Knowles, C. J., J. Gen. Microbiol., 100, 5 (1977).

70. Nathans, G. R., Chang, D., and Deuel, T. F., Methods Enzymol., 51 (Purine Pyrimidine Nucleotide Metab.), 497 (1978)

71. Barsacchi, R., Ranieri-Raggi, M., Bergamini, C., and Raggi, A., Biochem. J., 182, 361 (1979).

72. Lowenstein, J. M., Physiol. Rev., 52, 382 (1972).

73. Ogasawara, N., Goto, H., Yamada, Y., Biochim., Biophys. Acta, 524, 442 (1978).

74. Shiraki, H., Ogawa, H., Matsuda, Y., and Nakagawa, H., Biochim. Biophys. Acta, 566, 345 (1979).

75. Shiraki, H., Ogawa, H., Matsuda, Y., and Nakagawa, H., Biochim. Biophys. Acta, 566, 335 (1979).

76. Ashby, B., and Frieden, C., J. Biol. Chem., 252, 1869 (1977).

77. Koretz, J., and Frieden, C., Proc. Natl. Acad. Sci., U.S.A., 77, 7186 (1980).

78. Embden, G., and Wassermeyer, H., Z. Physiol. Chem., 179, 226 (1928).

79. Parnas, J. K., Biochem. Z., 206, 16 (1929).

80. Parnas, J. K., Mozolowski, W., and Lewinski, W., Biochem. Z., 188, 15 (1927).

81. Pennington, R. J., Nature, 192, 884 (1961).

82. Suelter, C. H., Thompson, D., Oakley, G., Pearce, M., Husic, H. D., and Brody, M. S., Biochem. Med., 21, 352 (1979).

83. Young, R. B., McConnell, D. G., Suelter, C. H., Philip, T. A., Muscle Nerve, 4, 117 (1981).

84. Husic, H. D., and Suelter, C. H., Biochem. Biophys. Res., Commun., 95, 228 (1980).

85. Brody, M. S., Diss. Abstr. Int. B (1978).

86. Raggi, A., Ronca-Testoni, S., and Ronca, G., Biochim Biophys. Acta, 178, 619 (1969).

87. Raggi, A., Bergamini, C., and Ronca, G., FEBS Lett., 58, 19 (1975).

88. Rahim, Z. H. A., Lutaya, G., and Griffiths, J. R., Biochem. J., 184, 173 (1979).

89. Sabina, R. L., Swain, J. L., Patten, B. M., Ashizawa, T., O'Brien, W. E., and Holmes, E. W., J. Clin. Invest. 66, 1419 (1980).

90. Rajendra, W., Chetty, C. S., Indira, K., and Swami, K. S., Arch. Int. Physiol. Biochim., 88, 379 (1980).

91. Rajendra, W., Indira, K., and Swami, K. S., Indian J. Exp. Biol., 18, 1487 (1980).

92. Lagerkvist, U., J. Biol. Chem., 233, 138 (1958).

93. Abrams, R., and Bentley, M., Arch. Biochem. Biophys., 79, 91 (1959).

94. Davey, C. L., Arch. Biochem. Biophys., 95, 296 (1961).

95. Lieberman, I., J. Biol. Chem., 223, 327 (1956).

96. Tornheim, K., and Lowenstein, J. M., J. Biol. Chem., 249, 3241 (1974).

97. Lehninger, A. L., Biochemistry, 2nd. ed., Worth Publishers, Inc., N.Y. (1977), p. 733.

98. Kelley, W. N., Rosenbloom, F. M., Henderson, J. F., and Seegmiller, J. E., Proc. Natl. Acad. Sci. U.S., 57, 1735 (1967).

99. Dagley, S., and Nicholson, D. E., An Introduction to Metabolic Pathways, Wiley, New York (1970).

100. Greenberg, D. M. (ed.), Metabolic Pathways, 4, Academic Press, New York (1970).

101. Henderson, J. F., and Paterson, A. R. P., Nucleotide Metabolism, Academic Press, New York (1972).

102. Mahler, H. R., and Cordes, E. H., Biological Chemistry (2nd ed.), Harper and Row, New York (1971).

103. Hers, H. G., and Van den Berghe, G., Lancet, 1, 585 (1979).

104. Ranieri-Raggi, M., Bergamini, C., and Raggi, A., Ital. J. Biochem., 29, 238 (1980).

105. Ronca-Testoni, S., Raggi, A., and Ronca, G., Biochim Biophys. Acta, 198, 101 (1970).

106. Raggi, A., and Raineri-Raggi, M., Biochim. Biophys. Acta, 566, 353 (1979).

107. Wheeler, T. J., and Lowenstein, J. M., J. Biol. Chem., 254, 8994 (1979).

108. Ronca, G., Raggi, A., and Ronca-Testoni, S., Ital. J. Biochem., 21, 305 (1972).

109. Cohen, P., Control of Enzyme Activity, ed., Chapman and Hall, London (1976).

110. Parnas, J. K., and Lewinsky, W., Biochem. Z., 276, 398 (1935).

111. Coffee, C. J., and Solano, C., J. Biol. Chem., 252, 1606 (1977).

112. Chung, L., and Bridger, W. A., FEBS Lett., 64, 338 (1976).

113. Tornheim, K., and Lowenstein, J. M., J. Biol. Chem., 247, 162 (1972).

114. Mockrin, S. C., Byers, L. D., and Koshland, D. E., Jr., Biochemistry, 14, 5428 (1975).

115. Smiley, K. L., Berry, A. J., and Suelter, C. H., J. Biol. Chem., 242, 2502 (1967).

116. Zielke, C. L., and Suelter, C. H., J. Biol. Chem., 246, 2179 (1971).

117. Boosman, A., and Chilson, O. P., J. Biol. Chem., 251, 1847 (1976).

118. Ranieri-Raggi, M., and Raggi, A., Biochem. J., 189, 367 (1980).

119. Stankiewicz, A., Spychala, J., Skladanowski, A., and Zydowo, M., Comp. Biochem. Physiol. B, 62B, 363 (1979).

120. O'Driscoll, D., Roring, N. P., and Ross, C. A., Biochem. Soc. Trans., 4, 928 (1976).

121. Ogasawara, N., Goto, H., Yamada, Y., and Yoshino, M., Biochem. Biophys. Res. Commun., 79, 671 (1977).

122. Shiraki, H., Ogawa, H., Matsuda, Y., and Nakagawa, H., Biochim. et Biophysica Acta, 566, 335 (1979).

123. Yoshino, M., Kawamura, Y., and Ogasawara, N., J. Biochem., 80, 299 (1976).

124. Skladanowski, A., Kaletha, K., and Zydowo, M., Int. J. Biochem., 13, 865 (1981).

125. Stankiewicz, A., and Spychala, Y., Comp. Biochem. Physiol. B, 69B, 5 (1981).

126. Weber, G., in: Molecular Biophysics, eds. B. Pullman and M. Weissbluth (Academic Press, New York) p. 369 (1965).

127. Kurganov, B. I., Dorozhko, A. I., Kagan, Z. S., and Yakovlev, V. A., J. Theor. Biol., 60, 247 (1976).

128. Fersht, A., Enzyme Structure and Mechanism, Freeman, New York (1977).

129. Raggi, A., Ranieri, M., Taponeco, G., Ronca-Testoni, S., Ronca, G., and Rossi, C. A., FEBS Lett., 10, 101 (1970).

130. Ogasawara, N., Goto, H., and Yamada, Y., Adv. Exp. Med. Biol., 122B, 169 (1980). [Purine Metabolism. Man. - 3:Biochem., Immunol. Cancer Res.].

131. Sammons, D. W., Diss. Abstr. Int. B (1977).

132. Sammons, D. W., and Chilson, O. P., Arch. Biochem. Biophys., 191, 561 (1978).

133. Hampton, A., Sasaki, T., Perini, F., Slotin, L. A., and Kappler, F., J. Med. Chem., 19, 1029 (1976).

134. Lazarus, R. A., Benkovic, P. A., Benkovic, S. J., Arch. Biochem. Biophys., 197, 218 (1979).

135. Dudycz, L., and Shugar, D., FEBS Lett., 107, 365 (1979).

136. Stankiewicz, A., Spychala, J., Makarewicz, W., Comp. Biochem. Physiol. B., 66B, 529 (1980).

137. Doree, M., and Terrine, C., Compt. Rend. Acad. Sci. Ser. D, 275, 1503 (1972).

138. Zielke, C. L., and Suelter, C. H., J. Biol. Chem., 246, 1313 (1971).

139. Ashman, L. K., and Atwell, J. L., Biochim. Biophys. Acta, 258, 618 (1972).

140. Setlow, B., and Lowenstein, J. M., J. Biol. Chem., 243, 6216 (1968).

141. Citri, N., Adv. Enzymol., 37, 397 (1973).

142. Nachod, F. C., and Wood, J., J. Am. Chem. Soc., 67, 629 (1945).

143. Pauling, L., The Nature of the Chemical Bond, Cornell University Press, Ithaca, New York (1960), p. 514.

144. Suelter, C. H., Science, 168, 789 (1970).

145. Suelter, C. H., Metal Ions in Biological Systems, 3, High M-lecular Complexes. Editor - Helmut Sigel; Marcel Dekker, Inc., New York (1974).

146. Smiley, K. L., Jr., and Suelter, C. H., J. Biol. Chem., 242, 1980 (1967).

147. Campbell, J. C. W., and Suelter, C. H., Biochemistry, 16, 4836 (1977).

148. Lee, Y.-P., J. Biol. Chem., 227, 999 (1957).

149. Nikiforuk, G., and Colowick, S. P., J. Biol. Chem., 219, 119 (1956).

150. Kaletha, K., Stankiewicz, A., Makarewicz, W., and Zydowo, M., Int. J. Biochem., 7, 67 (1976).

151. Henry, H., Chilson, O. P., Comp. Biochem. Physiol., 29, 301 (1969).

152. Kizer, D. E., Cox, B., Lovig, C. A., and DeEstrugo, S. F., J. Biol. Chem., 238, 3048 (1963).

153. Lee, Y.-P., and Wang, M. H., J. Biol. Chem., 243, 2260 (1968).

154. Askari, A., Mol. Pharmacol., 2, 518 (1966).

155. Setlow, B., and Lowenstein, J. M., J. Biol. Chem., 243, 3409 (1968).

156. Turner, D. H., and Turner, J. F., Biochem. J., 79, 143 (1961).

157. Makarewicz, W., Comp. Biochem. Physiol., 29, 1 (1969).

158. Nara, S., Siekagaku, 32, 204 (1960); CA 60, 5815 (1964).

159. Tomozowa, Y., and Wolfenden, R., Biochemistry, 9, 3400 (1970).

160. Skladanowski, A., Kaletha, K., and Zydowo, M., Int. J. Biochem., 10, 177 (1979).

161. Melander, W. R., Arch. Biochem. and Biophys., 164, 90 (1974).

162. Zielke, C. L., Ph.D. Dissertation, Michigan State University, East Lansing, Michigan (1970).

163. Askari, A., Nature, 202, 185 (1964).

164. Brown, W. E. L., and Hill, A. V., Proc. Roy. Soc. (London), Ser. B., 94, 297 (1922-1923).

165. Zielke, C. L., and Suelter, C. H., Fed. Proc., 28, 728 (1969).

166. Kuhne, W., Ber., 206 (1875).

167. Nencki, M., Ber., 336 (1875).

168. Hopkins, F. G., and Cole, W. S., J. Physiol., 29, 451 (1903).

169. Hopkins, F. G., and Cole, W. S., J. Physiol., 27, 418 (1901).

170. Happold, F. C., and Hoyle, L., Biochem. J., 29, 1218 (1935).

171. Happold, F. C., and Struyvenberg, A., Biochem. J., 58, 379 (1954).

172. Wood, W. A., Gunsalus, I. C., and Umbreit, W. W., J. Biol. Chem., 170, 313 (1947).

173. Happold, F. C., Adv. Enzymol. Relat. Subj. Biochem., 10, 51 (1950).

174. Wada, H., Tryptophan Metabolism Vol. 1, Sekai, Hoken Tsushinsha, Ltd., Osaka, Japan, 77-92 (1964).

175. Snell, E. E., Adv. Enzymol. Relat. Areas Mol. Biol., 42, 287 (1975).

176. Newton, W. A., and Snell, E. E., Proc. Natl. Acad. Sci. U.S.A., 48, 1431 (1962).

177. Yanofsky, C., and Crawford, I. P., Proc. Nat. Acad. Sci. U.S.A., 45, 1016 (1959).

178. Newton, W. A., and Snell, E. E., J. Bact., 89, 355 (1965).

179. Newton, W. A., and Snell, E. E., Proc. Natl. Acad. Sci. U.S.A., 51, 382 (1964).

180. Kagamiyama, H., Wada, H., Matsubara, H., and Snell, E. E., J. Biol. Chem., 247, 1571 (1972).

181. Newton, W. A., Morino, Y., and Snell, E. E., J. Biol. Chem., 240, 1211 (1965).

182. Morino, Y., and Snell, E. E., J. Biol. Chem., 242, 5591 (1967).

183. Hogberg-Raibaud, A., Raibaud, O., and Goldberg, M. E., J. Biol. Chem., 250, 3352 (1975).

184. Morino, Y., and Snell, E. E., J. Biol. Chem., 242, 2800 (1967).

185. Snell, E. E., and DiMari, S. J., in The Enzymes, Vol 2, 3rd ed., P. D. Boyer, Ed., Academic Press, New York, p. 335 (1970).

186. Kagamiyama, H., Morino, Y., and Snell, E. E., J. Biol. Chem., 245, 2819 (1970).

187. Raibaud, O., and Goldberg, M. E., J. Biol. Chem., 248, 3451 (1973).

188. Suelter, C. H., and Snell, E. E., J. Biol. Chem., 252, 1852 (1977).

189. Heinert, D., and Martell, A. E., J. Am. Chem. Soc. 84, 3257 (1962).

190. Johnson, R. J., and Metzler, D. E., Methods in Enzymology, 18A, 443 (1970).

191. Davis, L., and Metzler, D. E., in The Enzymes (Boyer, P. D., ed.) Vol. 7, pp. 33-74 (1972).

192. Metzler, C. M., Cahill, A., and Metzler, D. E., J. Am. Chem. Soc., 102, 6075 (1980).

193. June, D. S., Kennedy, B., Pierce, T. H., Elias, S. V., Halaka, F., Behbahani-Nejad, I., El-Bayoumi, A., Suelter, C. H., and Dye, J. L., J. Am. Chem. Soc., 101, 2218 (1979).

194. June, D. S., Suelter, C. H., and Dye, J. L., Biochemistry, 20, 2707 (1981).

195. June, D. S., Ph.D. Dissertation, Michigan State University, East Lansing, Michigan (1979).

196. Hillebrand, G. G., Dye, J. L., and Suelter, C. H., Biochemistry, 18, 1751 (1979).

197. June, D. S., Suelter, C. H., and Dye, J. L., Biochemistry, 20, 2714 (1981).

198. Watanabe, T., and Snell, E. E., J. Biochem. (Tokyo), 82, 733 (1977).

199. Suelter, C. H., Wang, J., and Snell, E. E., Anal. Biochem., 76, 221 (1977).

200. Suelter, C. H., Wang, J., and Snell, E. E., FEBS Lett., 66, 230 (1976).

201. Cochran, R. N., and Horne, F. H., Anal. Chem., 49, 846 (1977).

202. Cochran, R. N., and Horne, F. H., J. Phys. Chem., 84, 2561 (1980).

203. Cochran, R. N., Horne, F. H., Dye, J. L., Ceraso, J. and Suelter, C. H., J. Phys. Chem., 84, 2567 (1980).

204. Ivanov, V. I., and Karpeisky, M. Y., Adv. Enzymol. Relat. Areas Mol. Biol., 32, 21 (1969).

205. Coetzee, W. F., and Pollard, E. C., Photochem. Photobiol., 22, 29 (1975).